Universidad Europea de Madrid

Escuela de Arquitectura, Ingeniería y Diseño
Degree in Aerospace Engineering

Final Project Report

Design of a Multirole Jet Transport Tanker Aircraft

Diego Catalá Clemente

Year 2023-2024

TITLE: DESIGN OF A MULTIROLE JET TRANSPORT TANKER AIRCRAFT

AUTHOR: DIEGO CATALÁ CLEMENTE

SUPERVISOR: RAFAEL PAX

DEGREE OR COURSE: DEGREE IN AEROSPACE ENGINEERING

DATE: JUNE, 2024

Abstract

Tanker aircraft are one of the most important pillars of every nation's air force, supporting remote operations and allowing a fast deployment and operation of different type of military aircraft which perform aerial refueling. Airbus A330 MRTT and Boeing KC-46A Pegasus are the current leading tanker aircraft in service, which are manufactured from commercial aircraft conversion processes.

This project describes the complete preliminary design and analysis of a new multirole jet transport tanker aircraft which aims to be highly versatile and efficient, combining the best attributes from modern airliners and military tanker aircraft including some of the latest techniques, technological means, engineering solutions and state-of-the-art systems which are used in aviation industry.

Modern tools are used in the elaboration of this project, making use of advanced engineering software to support the design, optimization and analysis process of this tanker aircraft, called "LT-018 Archangel".

Keywords: aerial refueling, aircraft design, tanker aircraft.

Resumen

Los aviones cisterna son uno de los pilares más importantes de la fuerza aérea de las naciones más relevantes, apoyando operaciones remotas y permitiendo un rápido despliegue y operación de diferentes tipos de aviones militares capaces de realizar reabastecimiento en vuelo. El Airbus A330 MRTT y el Boeing KC-46A Pegasus son los actuales líderes en esta categoría y son fabricados a partir de procesos de conversión de aviones comerciales.

Este proyecto describe el diseño preliminar y el análisis de un aeronave de ala fija que tiene como propósito reabastecer en vuelo y transportar una gran variedad de cargas de pago, siendo altamente versátil y eficiente combinando algunas de las mejores características de los aviones militares y comerciales más modernos, incluyendo técnicas, medios tecnológicos, soluciones de diseño y sistemas que se utilizan en la industria aeronáutica actualmente.

Para la elaboración de este proyecto, se han empleado y combinado tanto herramientas y técnicas clásicas como herramientas de diseño y análisis avanzados (libros, dibujos, datos operacionales y software de ingeniería) para realizar el diseño, la optimización y el análisis de este avión cisterna, llamado “LT-018 Arcángel”.

Palabras clave: reabastecimiento en vuelo, diseño de aeronaves, avión cisterna.

Figure Index

Symbols and Abbreviations

2D *— Two-dimensional*
3D *— Three-dimensional*
AC *— Aerodynamic Center*
APU *— Auxiliary Power Unit*
AR *— Aspect Ratio*
ARBS *— Aerial Refueling Boom System*
BDA *— Boom-Drogue Adaptor*
CAD *— Computer-Aided Design*
c *— Speed of sound*
CFRP *— Carbon Fiber Reinforced Plastic*
CFD *— Computational Fluid Dynamics*
CG *— Center of gravity*
C_L *— Lift Coefficient*
C_{LAC} *— Aircraft Lift Coefficient*
C_L/C_D *— Aerodynamic efficiency (finesse)*
C_{Lh} *— Horizontal stabilizer Lift Coefficient*
C_{Lmax} *— Maximum Lift Coefficient*
C_M *— Moment Coefficient*
CO_2 *— Carbon Dioxide*
CS *— Certification Specifications*
D_{AC} *— Aircraft Drag*
DME *— Distance Measurement Equipment*
e *— Oswald Efficiency Factor*
EASA *— European Aviation Safety Agency*
FAA *— Federal Aviation Administration*
FC *— Fuel Capacity*
ft *— Feet*
g *— Grams*
GPS *— Global Positioning System*
HUMVEE *— High Mobility Multipurpose Wheeled Vehicles*
ICAO *— International Civil Aviation Organization*
kt *— Knots (nautical miles per hour)*
K *— Kelvin*
kg *— Kilograms*
kgf *— Kilogram of force*
km *— Kilometers*
L *— Liters*
L_{AC} *— Aircraft Lift*
LCD *— Liquid Crystal Display*
L/D *— Aerodynamic efficiency (finesse)*
L_{FC}/d_F *— Fuselage tail length and diameter ratio*
L_h *— Horizontal stabilizer Lift force*
$\Lambda_{c/4}$ *— Quarter chord sweep angle*
M *— Mach Number*
M_{ac} *— Wing's pitching moment about the aerodynamic center*
m *— Meters*
m *— Moment*
MRTT *— Multi Role Tanker Transport*
MTOW *— Maximum Take-Off Weight*
NASA *— National Aeronautics and Space Administration*
NACA *— National Advisory Committee for Aeronautics*
NATO *— North Atlantic Treaty Organization*
nmi *— Nautical Miles*
N *— Newtons*
π *— Pi (3'14159265)*
P *— Pressure*
Pa *— Pascals*
PTU *— Power Transfer Unit*
R *— Ideal gas constant*
R *— Range*
R *— Resultant force*
RAF *— Royal Air Force*
RAT *— Ram Air Turbine*
Re *— Reynolds number*
RTM *— Resin Transfer Moulding*
ρ_∞ *— Fluid density*
SATCOM *— Satellite Communication*
S *— Wing Area*
SAF *— Sustainable Aviation Fuel*
SFC *— Specific Fuel Consumption*
S_h *— Horizontal Stabilizer Area*
T *— Temperature*
T *— Thrust*
T_∞ *— Fluid temperature*
T_{req} *— Required*
T_{TO} *— Take-Off Thrust*
TSFC *— Thrust Specific Fuel Consumption*
t/c *— Thickness-to-chord ratio*
u_∞ *— Fluid velocity*
ULD *— Unit Load Devices*
USAF *— United States Air Force*
V *— Velocity*
$\tilde{V}_h$ *— Horizontal stabilizer Volume Coefficient*
$\tilde{V}_v$ *— Horizontal stabilizer Volume Coefficient*
VHF *— Very High Frequency*
W *— Weight*
x_{CG} *— Location of the Center of Gravity*
x_h *— Horizontal tail lever arm's length*
x_w *— Wing lever arm's length*
x_v *— Vertical tail lever arm's length*
´´ *— Inches*
γ *— Specific heat*
Γ *— Dihedral angle*
Δ *— Increment*
$\sum$ *— Summatory*
μ *— Dynamic viscosity*

Acknowledgements

I thank God for giving me life, for his infinite kindness and for guiding my steps every day — Agradezco a Dios por darme la vida, por su bondad infinita y por guiar mis pasos día a día.

To my parents, for making everything possible, for instilling in me the culture of effort and for guiding and supporting me in all my decisions — A mis padres, por hacer todo posible, por inculcarme la cultura del esfuerzo y por guiarme y apoyarme en todas mis decisiones.

To my grandparents, may they rest in peace, for encouraging me to strive for my goals and for always believing in me — A mis abuelos, que en paz descansen, por animarme siempre a perseguir mis metas y creer en mí.

To my best friends, Marcos and Gonzalo, for supporting and helping me in every possible way throughout the process of developing this project — A mis mejores amigos, Marcos y Gonzalo, por animarme y apoyarme de todas las maneras posibles durante el proceso de elaboración de este proyecto.

To my degree professors and my tutor, for sharing their wisdom, teaching with heart, and further igniting my passion for aviation — A mis profesores del grado y mi tutor, por compartir su sabiduría, enseñar con el corazón y por avivar en mí más aún la pasión por la aviación.

Table of Contents

Introduction

I.1 Problem approach

Tanker aircraft have been operating almost since aircraft started to be used for military purposes, performing aerial refueling mainly to military aircraft belonging to the air forces of different nations. However, tankers which operate nowadays rely on commercial airliners which were developed several decades ago and do not benefit from several state-of-the-art technological advancements, design solutions and revolutionary engineering systems which have been developed in the modern aircraft industry.

The motivation of this project is to develop the preliminary design of a multirole jet transport tanker aircraft which is solely designed for this specific purpose, developing design solutions to adapt optimally to the missions that it may perform combining and equipping some of the state-of-the-art materials, systems, techniques and designs which make the latest aircraft almost perfect.

I.2 Historical and technical background

It has been more than 100 years since in June 1923, the first successful aerial refueling operation was carried out by the USAF (United States Air Force). This important milestone allowed historical aircraft of that time, such as the Fokker C-2, to complete flights with world-record durations of up to 151 hours. Important engineering advancements were made during the following years, in the Second World War, modifying large-scale bombers to perform aerial refueling tests. In fact, the British RAF (Royal Air Force) started to use this technique in those years using the “Looped Hose” system on their bombers. Moreover, after several tests and developments on the Consolidated B-24 Liberator and the Boeing B-17 Flying Fortress, the first official American aerial refueling squadrons started to operate in the year 1948 in Arizona and New Mexico, which used modified versions of the Boeing B-29 Superfortress equipping the British mentioned system to carry out their air-refueling task. These aircraft were called KB-29M ([1], United States Air Force, 2023) ([2], AirTanker, 2023) ([3], US Centennial of flight commission, 2023).

Some years later, in the 1950s, the NATO (North Atlantic Treaty Organization) allies developed the “probe and drogue” system to provide more versatility and efficiency. The system mainly consists in a flexible hose which is deployed from the tanker aircraft, equipped with a special “basket” at the end, the drogue; which main functions are to stabilize the hose during flight and to serve as a funnel to facilitate the insertion of the probe, which commonly would be located at the front of the fuselage of the receiver aircraft ([2], AirTanker, 2023).

General Curtis LeMay (US Air Force) recognized the major drawbacks in the existing aerial refueling systems, mainly with the amount of fuel that could be transferred through the hoses and the speed limitations that the system imposed ([3], US Centennial of flight commission, 2023). In parallel, the Boeing Company tested the “flying boom” system, which consisted in a large-diameter pipe which was equipped with small wings at its end; making it possible to be maneuvered by an operator in the tanker to connect it to the fuel-receiving aircraft and which permitted the delivery of large amounts of fuel at high speeds. ([3], US Centennial of flight commission, 2023).

Important American tanker aircraft were developed in the following years, such as Boeing KC-97 Stratotanker or Boeing KC-135 (similar to the civil jet-powered Boeing 707) ([3], US Centennial of flight commission, 2023).

There were problems regarding the compatibility of both refueling systems which were described, mainly because the probe and drogue system was not compatible with the flying boom refueling technology, increasing the difficulty of military operations and compromising the versatility of the fleet. That is the main reason why Boom-Drogue Adapter (BDA) kits were developed to allow the functioning of the flying boom system with the Probe and Drogue one ([4], ARSAG, 2018, p. 10).

Figures I.1 and I.2 show both systems, the probe and drogue and the flying boom.

Figure I.1: Probe and drogue refueling system (USA Marines, 2016)

Figure I.2: Flying Boom refueling system (Aviation Stack Exchange, 2018)

I.3 Modern jet tankers and recent technologies

Significant developments and achievements were made in the 1980s, resulting in some tanker aircraft using turbofan propulsion systems, some of which are already retired but do not differ significantly from the ones which operate currently. Some examples are Lockheed TriStar used by the Royal Air Force (converted from the civil variant, already retired) or McDonell Douglas KC-10 Extender, an advanced tanker at that time which had the purpose to enhance the mobility of the United States Armed Forces ([5], United States Air Force, 2023). Conversions of modern civil turbofan-powered aircraft kept on happening during the next decades, resulting in the majority of tankers which operate nowadays in important armed forces and organizations. The main actual representatives are Boeing KC-46A Pegasus in the case of the United States and Airbus A310MRTT and Airbus A330MRTT (Multi Role Tanker Transport) in the case of Europe and Canada.

Boeing KC-46A Pegasus was developed with the main purpose of modernizing the tanker fleet of the US Air Force. To mention some of its operational capabilities, it provides a receiver envelope 3 times larger than the previous KC-135 and is able to load 96,162 kg of fuel, which can be delivered through a flying boom, a central hose (with a drogue system) and wing aerial refueling pods (which are equipped with the probe and drogue system) ([6], Boeing, 2023) ([8], United States Air Force, 2023). The aircraft can load up to 29,484 kg of cargo or 18 pallets (463 L military standard), is certified for 58 passengers by the FAA and on its aeromedical evacuation configuration, it has the capacity of accommodating 54 patients with their respective patient support pallets ([6], Boeing, 2023) ([7], Boeing, 2023).

Airbus A330 MRTT is another advanced-multirole turbofan-powered tanker aircraft based on the civil version Airbus A330-200 and which is mainly operated by NATO and other European and Asian countries. Being the main competitor of the previous mentioned Boeing KC-46A Pegasus, this aircraft carries on as well aerial refueling, payload transport, deployment and cargo and aeromedical evacuation transport missions. When it comes to fuel capacity, it can carry up to 111,000 kg of fuel, being the tanker aircraft with the highest capacity among all its competitors. In different configurations (combining the upper and lower deck), the aircraft is able to transport 45,000 kg of payload: 300 passengers and 37,000 kg of cargo in the lower deck which can be organized in 27 standard LD3 ULD (Unit Load Devices) containers or 8 military pallets. The configuration used for aeromedical evacuation can transport up to 40 patients, 20 people from the medical staff and 100 additional passengers ([10], Airbus, 2023) (([11], Airbus, 2023). Aerial refueling tasks can be carried out by both a flying boom (named ARBS by Airbus [Aerial Refueling Boom System]) or by wing pods. It also became the first tanker in the world which received certification for automatic air-to-air refueling boom operations, which is part of the SMART MRTT program developed by Airbus ([10], Airbus, 2023).

Both aircraft described previously are shown in Figures I.3 and I.4:

Figure I.3: Boeing KC-46A Pegasus (Infodefensa, 2024)

Figure I.4: Airbus A330 MRTT (Flynews, 2023)

I.4 Objectives of the project

The main objective of this project is to elaborate a **preliminary design** of a new **high-capacity multirole tanker aircraft** for military use, which will be called LT-018 Archangel. It will be employed actual techniques, resources and engineering technological advancements which are used currently in the aircraft industry. The goal is to develop the mentioned preliminary design of a high-versatile tanker and transport aircraft which combines some of the best capabilities and performance features of modern civil and military aircraft.

To achieve this, the knowledge acquired throughout all the courses of the degree will be applied, making additional research and use of the information and sources learned mainly in Aircraft Design, Mechanics of Flight, Aeronautical Structures, Aircraft Production Systems, Aircraft Propulsion, Aerodynamics and Navigation Systems.

I.5 Methodology

To elaborate this project, it is made a combination of different iterative processes and techniques which make use and combine traditional engineering design data sources (mainly books and research documents) with state-of-the-art tools, such as advanced design and analysis software.

The aircraft is designed progressively separating each chapter in all the different major components which form the tanker aircraft (fuselage, wings, empennage, engines, etc). Each chapter contains three main sections: the description of the main requirements and the preliminary analysis on all the consequences and decisions which need to be taken to develop each respective component, the design of 2D drawings to describe each design solution and indicate the most relevant design parameters of each one and the last one; where the design solution is modeled and assembled in a 3D CAD modeling software, which is developed throughout all the project until the aircraft is completely finished.

As mentioned previously, for the development of this project, some of the best resources available to an engineering student up to date are used, combining information from books, technical documents from official sources, class notes, and various software tools to design, analyze, optimize and study the tanker aircraft, including Catia V5, XFLR5, Ansys, Aeolus ASP and Adobe Procreate.

Chapter 1: Fuselage Design

The first step to begin with the design process of LT-018 is the fuselage, as it is crucial to ensure that the aircraft is able to accommodate on its interior the different types of payloads for which it is being designed. The cross-section design and the overall length define the most important dimensions of the fuselage.

1.1 Cross section design and aircraft configurations

The cross-section is designed to comply with the necessary requirements that each configuration needs. To provide the maximum possible interior space and to carry a significant amount of payload, a wide-body fuselage is selected.

To define the dimensions of the fuselage's width and height, a research process is carried out on the dimensions of actual wide-body jet transport aircraft in service (Boeing 777-300, 787-8, Airbus A340-600 and A350-900). Basing on this data, it is concluded that the fuselage's width and height dimensions will be located in the range of 5'6 - 6'2 m approximately ([14], Boeing, 2022) ([15], Boeing, 2023) ([16], Airbus, 2021) ([17], Airbus, 2021).

As the fuselage is pressurized due to the high altitude at which the aircraft will operate, a circular cross section is selected, which is the most efficient sectional shape for a pressurized fuselage ([26], T.H.G. Megson, 2007, p. 380). This decision will also remove difficulty from the design and manufacturing processes.

It must be studied too the different payloads which are intended to be transported by the aircraft to ensure a proper space dimensioning and distribution (military pallets, troops, medical stretchers, etc):

- **Standard military pallets (463L HCU-6/E)**: developed in the 1950s, it is one of the most important pillars of current military air transport, especially for the United States Air Force, the main responsible of its development. Throughout the years, it has become an adopted standard for transporting air cargo, especially in the military field, as it enhances the efficiency of ground transport, loading and unloading processes. The majority of modern military aircraft are compatible with 463L master pallets (Airbus A400M Atlas, Boeing KC-46A Pegasus or McDonell Douglas KC-10 Extender, to mention a few). The handling system (located inside the aircraft) consists in lines of metal rollers on the floor which allow the smooth movement of cargo into the aircraft. Side rails are responsible of guiding the 463L pallet and restraining lateral and vertical movement. Detent locks secure the pallet to prevent forward or aft movement during flight. The main dimensions of these rectangular pallets (108 x 88" = 274 x 223 cm) are illustrated in Figure 1.1 ([18], Globid Inc, 2023).

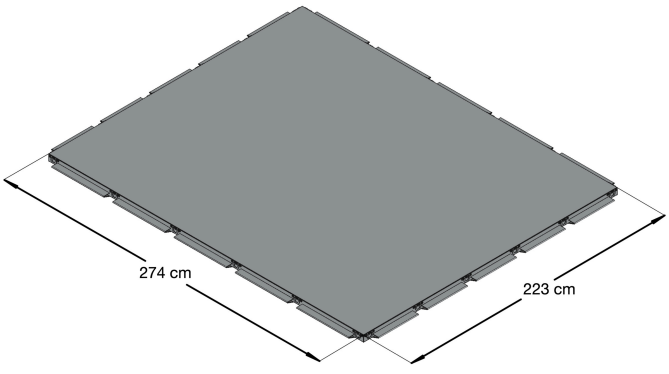

Figure 1.1: 463L Standard Military Pallet dimensions

- **Passenger seats**: to have a reference and to approach the size of the average passenger seats used in commercial aviation, it is selected one similar to those which a renowned airline (Air Europa) uses in wide-body aircraft for the economy class. On Boeing 787 for Economy Class, for example, Air Europa uses a seat pitch of 79 cm (31 ”) and a seat width of 43 cm (17 ”) ([19], Air Europa, 2023). Similar dimensions are used for this project.

  The seats are mounted over standard 463L master pallets, modified with seat tracks to allow the easy installation and removal of them. A total number of 9 seats are mounted in each pallet (which is the maximum possible number of seats to maintain a minimum level of safety and comfort taking into consideration the size of the pallets), to result in 6 seats per row with a single-aisle configuration. The main dimensions and the seat arrangement are illustrated in Figure 1.2:

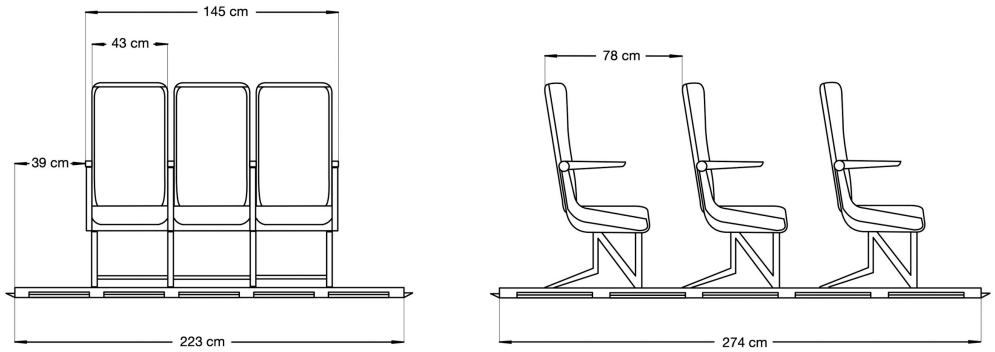

Figure 1.2: 463L pallet with passenger seats installed

- **Medical stretchers** are also mounted over 463L master pallets, making use of the typical ones used in current aircraft which operate as aeromedical evacuation transporters. 463L pallets for aeromedical evacuation missions are illustrated in Figure 1.3:

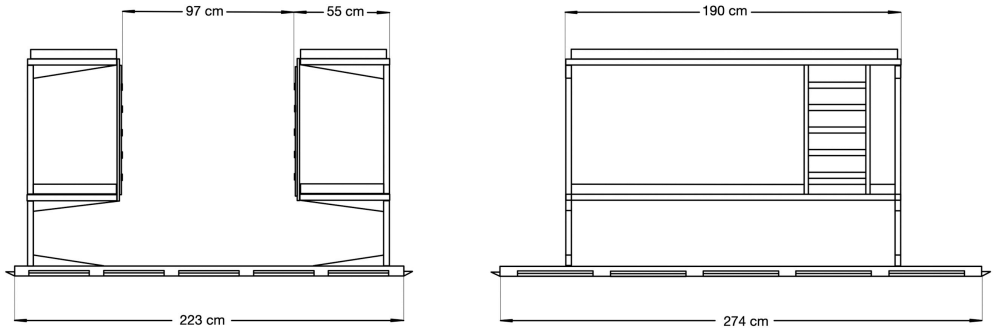

Figure 1.3: 463L pallet with medical stretchers

Considering all dimensions, the cross section of the aircraft can be already defined. Basing on the dimensions of similar aircraft which were mentioned before and already knowing the different types of payloads that the aircraft will transport, the fuselage outer diameter selected has a value of 590 cm, resulting in an interior maximum width of 565 cm, dimension which allows the installation of 2 standard pallets per row, to result in 6 seats per row in a single-aisle configuration (certifiable and with a reasonable degree of comfort). This configuration is illustrated in Figure 1.4.

Additionally, a second exceptional case of passenger transport configuration is considered for this aircraft which could be highly useful in the military context. For extreme evacuation circumstances (for example, the complete evacuation of a unit/squad of troops from an area that is going to be attacked imminently), the maximum number of passengers would be increased by using 463L pallets with 4 seats abreast in the upper deck of the aircraft.

Note that this specific extreme-evacuation configuration would not be certifiable in any possible manner and is intended only for specific, extreme and urgent evacuation or humanitarian aid missions. This configuration is illustrated in Figure 1.5.

The last configuration regarding passenger transport is the aeromedical evacuation transport, where 463L pallets are mounted with medical stretchers for the transport of inured troops or civilians. A total number of 4 medical stretchers are mounted per row in the aircraft (two per pallet), as it is illustrated in Figure 1.6.

Standard passenger configuration (certifiable) cross section design:

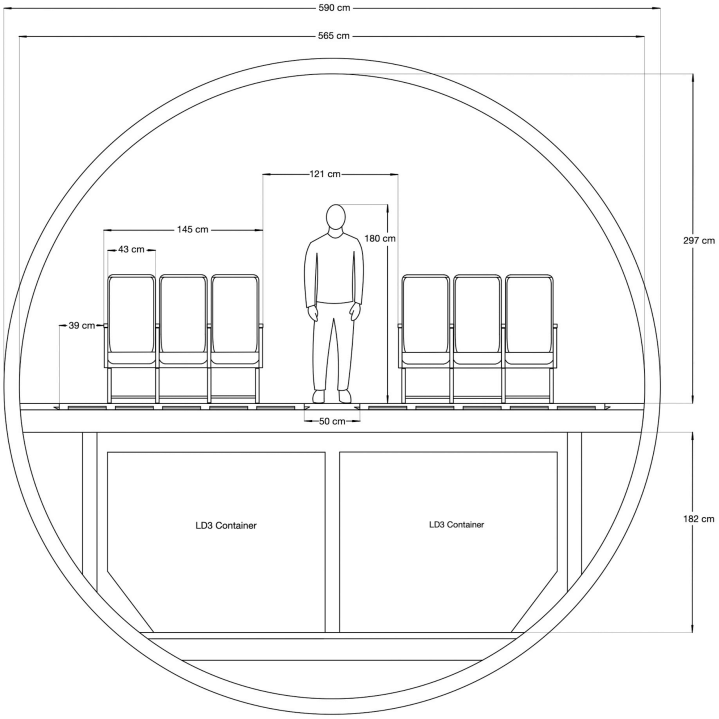

Figure 1.4: Aircraft cross section in passenger transport configuration (463L pallets with seats installed)

Extreme-evacuation passenger configuration (non-certifiable) cross section design:

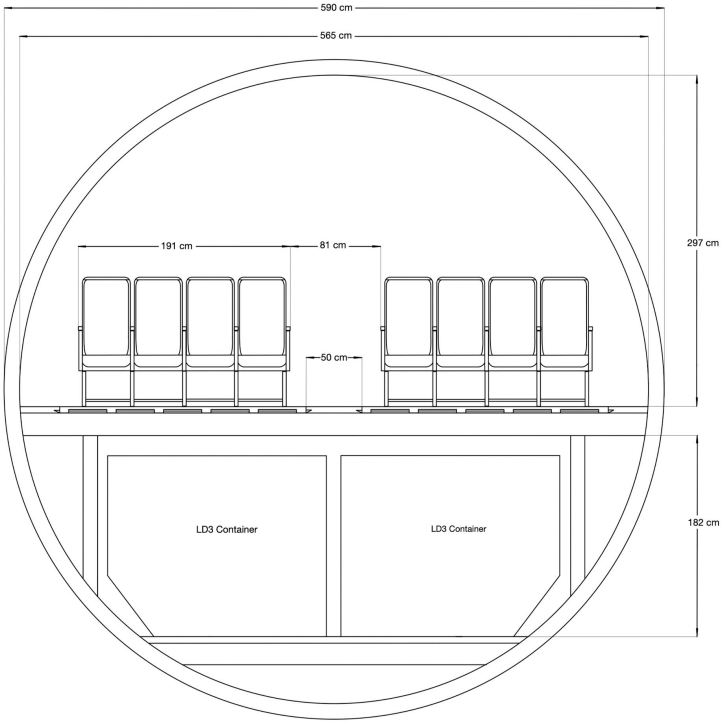

Figure 1.5: Aircraft cross section in extreme-evacuation passenger configuration (463L pallets with 4 seats installed)

Aeromedical evacuation transport configuration cross section design:

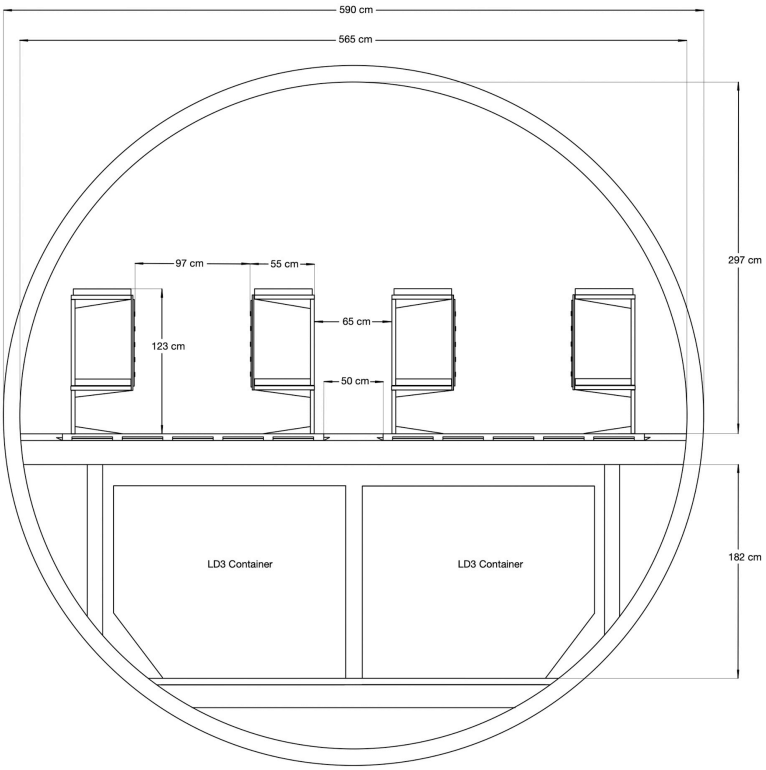

Figure 1.6: Aircraft cross section in aeromedical evacuation configuration (463L pallets with stretchers installed)

Different examples showing cargo transport scenarios are described and shown in the next illustrations. Note that the lower deck also equips the 463L master pallet handling system.

Some examples of useful cargo devices, weapons or vehicles which the armed forces may need to transport are described below:

- **Weapons, armament and ammunition**: firearms and different weapons are usually transported by means of reinforced boxes which usually are able to accommodate between 4 and 5 long firearms. The dimensions depend on the size of the firearms, but to serve as a reference, M4 carbines are about 80 cm long. Ammunition is transported as well in special metallic boxes, which size depends on the specific type. Artillery cannons and its respective ammunition also belong to this category.
- **Supplies and food**: depending on the size of the different elements which need to be transported (tactical clothes, food, equipment, medical supplies, etc), usually rectangular wooden or cardboard boxes are used.
- **Ground vehicles**: besides small ground vehicles such as light cars or motorbikes, heavier vehicles prepared for harder combat scenarios need to be transported to conflict areas by means of aircraft. One of the most common military ground vehicles are High Mobility Multipurpose Wheeled Vehicles (Humvees), which are used by many armed forces globally.

Two different cases of cargo transport scenarios carrying these mentioned payloads are represented in the following figures:

Cargo transport configuration example (1) cross section design:

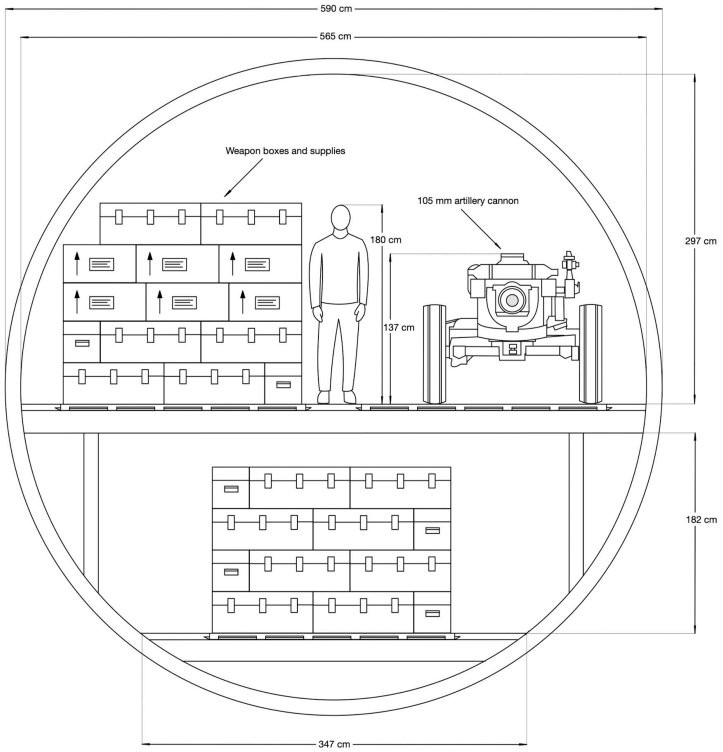

Figure 1.7: Aircraft cross section in cargo transport configuration (463L pallets with supplies and weapon boxes and 105 mm artillery cannon)

Cargo transport configuration example (2) cross section design:

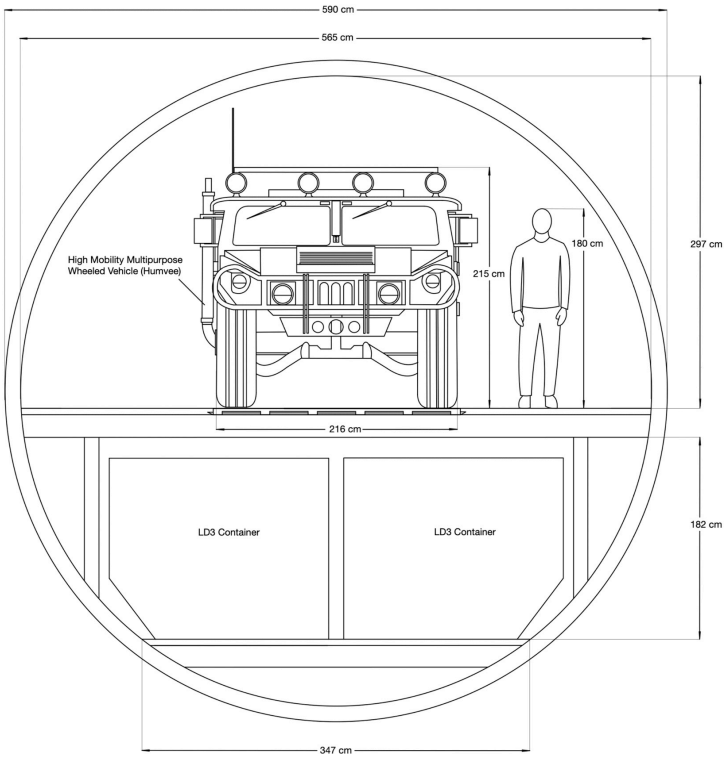

Figure 1.8: Aircraft cross section in cargo transport configuration (463L pallet with High mobility Multipurpose Wheeled Vehicle and standard LD3 Containers in the lower deck

Figure 1.9 shows the most relevant distances, dimensions and tolerances in the pallet handling system inside the aircraft fuselage.

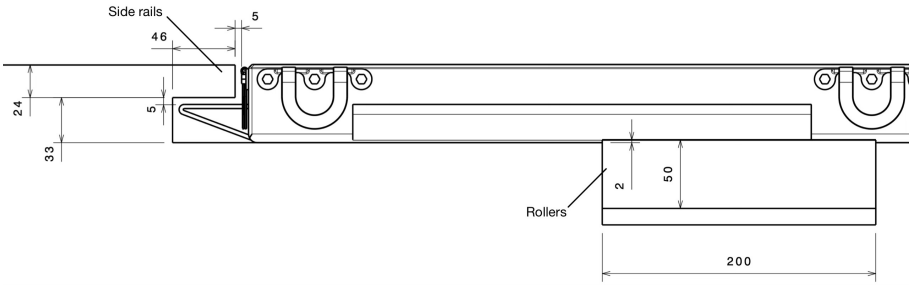

Figure 1.9: Aircraft's handling system dimensions (in mm)

1.2 Upper deck layout

The upper deck is designed to transport a total number of 26 standard 463L military pallets in a double-line configuration. With 26 pallets, a significant cargo and passenger transport capacity is ensured while maintaining a moderate fuselage length (in comparison to similar wide-body military aircraft), as the fuselage length will be directly proportional to the number of pallets that the aircraft can accommodate.

Regarding the centerline pallet configuration, designed for the transport of large cargo elements (as exemplified by the Humvee illustrated in Figure 1.8), a total number of 13 pallets can be accommodated in the upper deck of the aircraft.

26 pallets with passenger seats provide a maximum certifiable capacity of 234 passengers (9 seats per pallet) and in the case of the extreme-evacuation configuration, 312 passengers (12 seats per pallet). In the case of aeromedical evacuation transport configuration, 104 stretchers can be accommodated (4 stretchers per pallet).

Lastly, it is worth mentioning that 6 seats will be fixed at the forward part of the fuselage for crew members (including air-refueling operator, reserve pilots, cargo-handling personnel, etc). Additional necessary space is left at the rear part of the fuselage for the boom-operators station, a lavatory and additional consoles and/or computer stations.

If a maximum number of 234 passengers are accommodated, adding 2 pilots, 2 air refueling operators and 4 additional air crew members, the resultant number of people which the aircraft will be able to transport is 242. According to EASA Certification Specification for Large Aeroplanes (CS-25), the maximum number of passenger seats permitted for each Type A door is 110, and for Type I doors, 45 ([20], EASA, 2024). By installing two Type A and two Type I doors, it is ensured compliance with regulations, as the resultant maximum number of passenger seats would be 310, which is higher than the maximum passenger capacity of the aircraft.

Another important aspect to consider for certification compliance is the distance between exit doors, as no passenger emergency exit shall be located at a distance higher than 18’3 m (60 ft) from any adjacent passenger emergency exit on the same side of the same deck of the fuselage ([21], EASA, 2024).

In Figure 1.10, it is illustrated the aircraft’s upper deck pallet layout in the double-line configuration. Relevant cabin monuments are indicated.

In Figure 1.11, compliance with regulations regarding the distance between adjacent exit doors is demonstrated, where it is seen that in all cases it is lower than 60 ft (18’3 m).

Double-line pallet configuration upper deck layout:

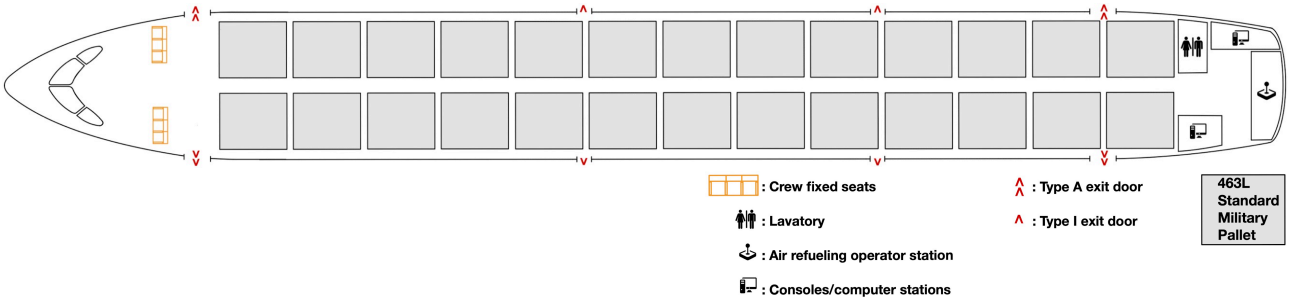

Figure 1.10: Upper deck layout in double-line pallet configuration

In the same manner than it was described at the introduction of the section, the figures show how a total number of 26 463L Standard Military Pallets are accommodated in the aircraft in a double-line configuration.

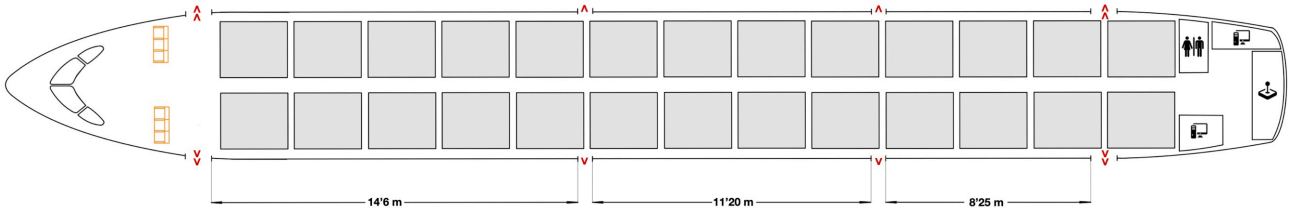

Figure 1.11: Aircraft's exit door distance between adjacent ones

Figure 1.12 illustrates the centerline configuration, where it is appreciated how 13 463L Standard Military Pallets are accommodated:

Centerline pallet configuration upper deck layout:

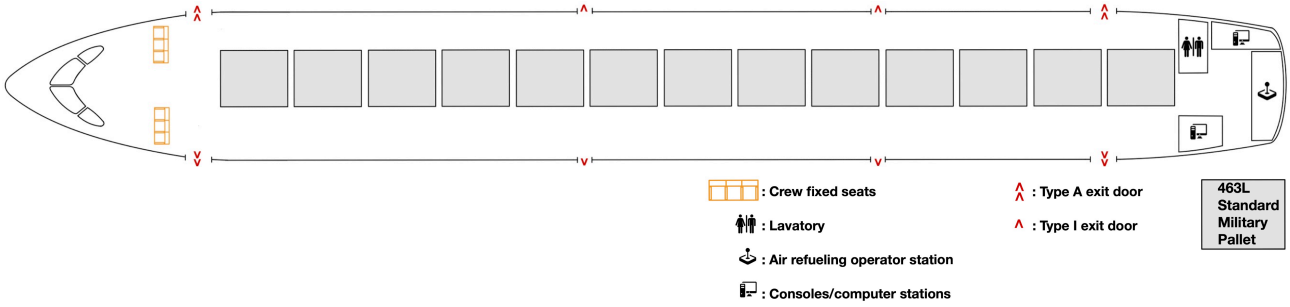

Figure 1.12: Upper deck layout in centerline pallet configuration

The next figures illustrate the seat maps of the aircraft when it is configured for passenger transport, including the certifiable and the non-certifiable extreme evacuation configurations.

Standard passenger configuration (certifiable) upper deck layout:

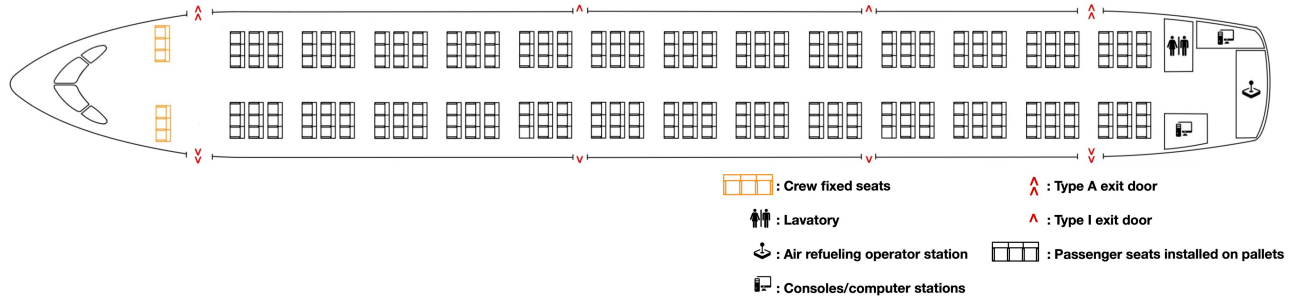

Figure 1.13: Upper deck seat map in certifiable passenger transport configuration (234 pax)

Extreme-evacuation passenger configuration (non-certifiable) upper deck layout:

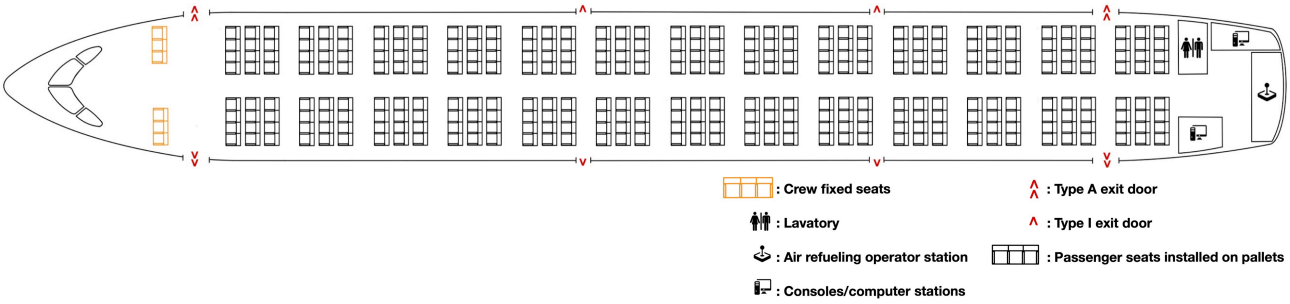

Figure 1.14: Upper deck seat map in non-certifiable passenger transport configuration (312 pax)

For the mission of aeromedical evacuation transport configuration, the upper deck layout showing the stretchers is seen in Figure 1.15. Note that there is enough space between adjacent stretchers (about 1 meter) to install the necessary basic medical equipment (vital sign monitors, electrocardiogram machines, respirators, etc).

Aeromedical evacuation transport configuration upper deck layout:

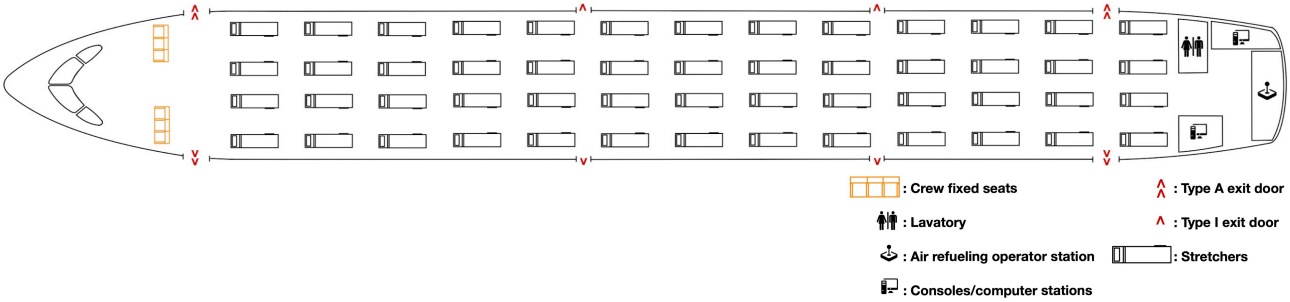

Figure 1.15: Upper deck seat map in aeromedical evacuation transport configuration (104 stretchers)

Some examples showing the versatility of the aircraft when it comes to cabin mixed configurations are shown in the next figures.

Mixed configuration example (1) upper deck layout:

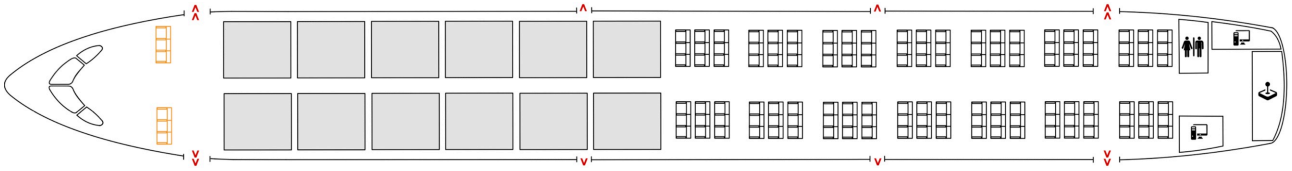

Figure 1.16: Upper deck layout in a mixed configuration example (12 cargo pallets, 126 pax)

Mixed configuration example (2) upper deck layout:

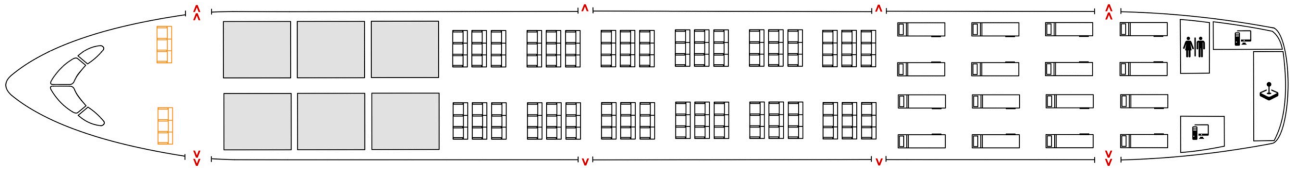

Figure 1.17: Upper deck layout in a mixed configuration example (6 cargo pallets, 108 pax, 32 stretchers)

Mixed configuration example (3) upper deck layout:

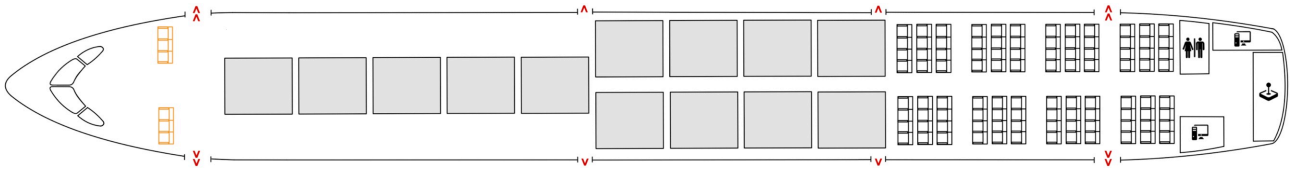

Figure 1.18: Upper deck layout in a mixed configuration example (13 cargo pallets, 96 pax)

1.3 Lower deck layout

The lower deck, as illustrated in the handling system description, is able to accommodate military pallets in a centerline configuration, LD3 standard containers and bulk cargo. It must be taken into account the division of the lower deck in two separated independent bays, due to the fact that the center wingbox, the landing gear and the hydraulic system reservoirs are accommodated in the lower deck at the center of the fuselage.

The lower deck layout when LD3 standard containers are used is seen in Figure 1.19, where a total amount of 32 containers are accommodated:

LD3 cargo transport lower deck layout:

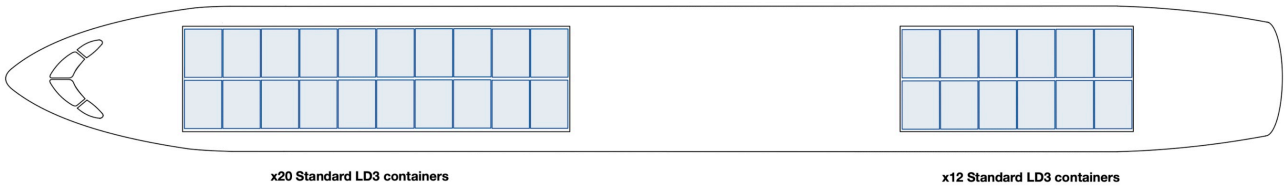

Figure 1.19: Lower deck layout for LD3 container accommodation (32 containers)

If 463L military pallets are used, a total amount of 8 pallets will be accommodated in the lower deck, as illustrated in Figure 1.20:

463L military pallets cargo transport lower deck layout:

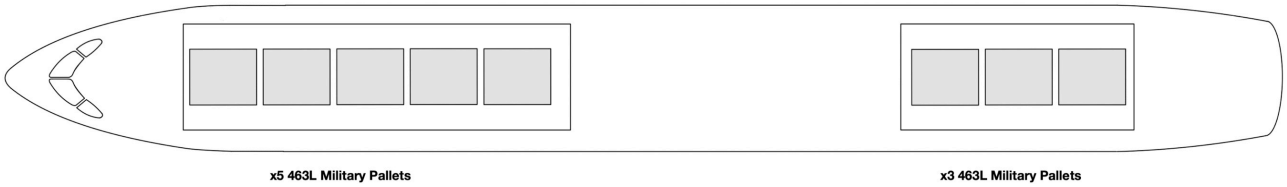

Figure 1.20: Lower deck layout for 463L military pallets accommodation (8 pallets)

Similarly to the upper deck, the lower deck of the aircraft can be configured according to the operator's needs, combining LD3 containers, military pallets and/or bulk cargo. An example is seen below in Figure 1.21:

Mixed cargo transport configuration lower deck layout:

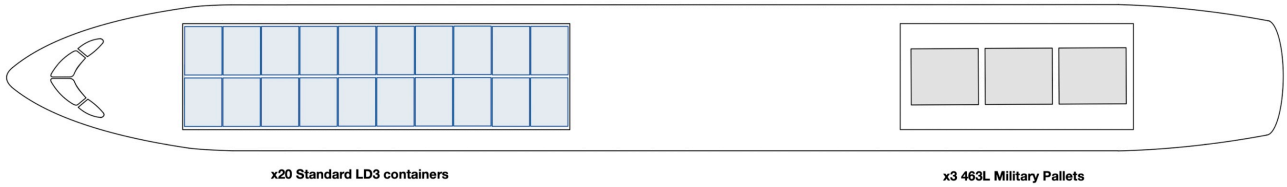

Figure 1.21: Lower deck layout for 463L military pallets accommodation (20 containers, 3 pallets)

1.4 Fuselage nose, flight deck and tail design

The fuselage of the aircraft is responsible for a significant amount of the aircraft's overall drag (20-50%). There is a variety of techniques employed in aircraft design to reduce it as much as possible: designing a shape to allow laminar flow, reducing the fuselage length and perimeter as much as possible and avoiding sharp edges which can lead to vortex separation ([22], Jan Roskam, 1986, pp. 36-39).

For the fuselage nose design, the most relevant aspects that need to be taken into account are the aerodynamic drag, the pilot's vision angles and the accommodation of the nose landing gear.

Regarding the fuselage nose aerodynamic performance, the shape must be as smooth as possible, avoiding sharp edges or strong curves to avoid flow separation and thus, an increase in drag. There is a variety of geometries used in aircraft design which comply with this requirement, but mainly the elliptical and parabolic ones are seen in real operating aircraft. In the case of subsonic aircraft and for cruise speeds $\approx$ 0'8 Mach (which is the approximate cruise speed at which LT-018 will fly at cruise), the parabolic shape provides the best aerodynamic performance ([23], Aditya Rajan Iyer, Anjali Pant, 2020, p. 3549).

Even though an almost constant parabolic shape for the fuselage nose can be kept in the horizontal cross section, it is not possible to maintain it in the vertical one, as pilot vision angles through the windshield need to comply with regulations. Despite this fact, important improvements have been achieved regarding this topic in the latest commercial aircraft by replacing traditional flat windshields with 3D curved ones, which allow smoother aerodynamic shapes and avoid sharp edges in the windshield frame itself.

Following these guidelines, the fuselage nose design is illustrated in Figure 1.22 in both an upper and side view.

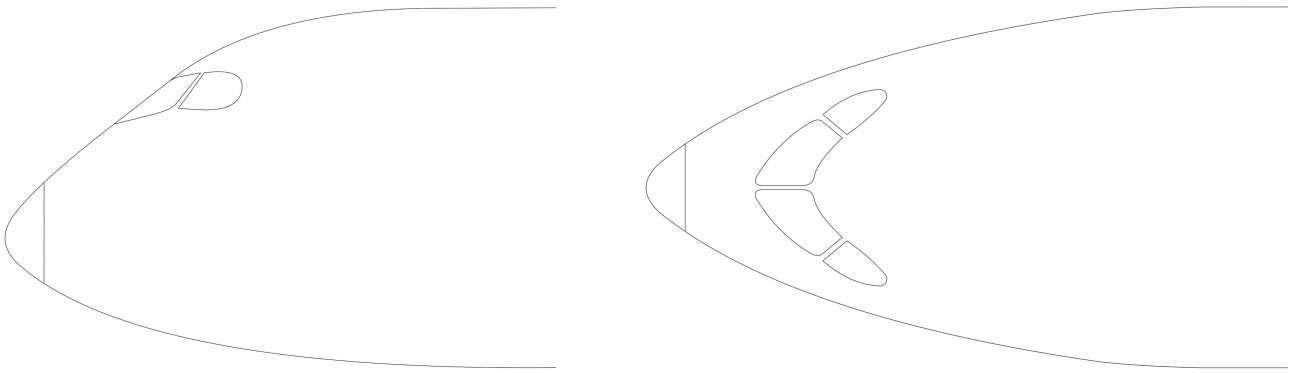

Figure 1.22: Fuselage nose shape design

The most relevant parameters which need to be taken into account when it comes to flight deck design are pilot ergonomics (regarding the control stick, the pedal and the instruments panel) and the view design considerations. The windshield is designed taking into consideration the FAA Pilot Compartment View Design Considerations, where guidelines are followed regarding angles for optimum collision avoidance. The most relevant angles and the pilot position are seen in Figure 1.23 ([24], Federal Aviation Administration, 1993). Additionally, the flight deck layout and the most relevant components of it are indicated and drawn in Figure 1.24.

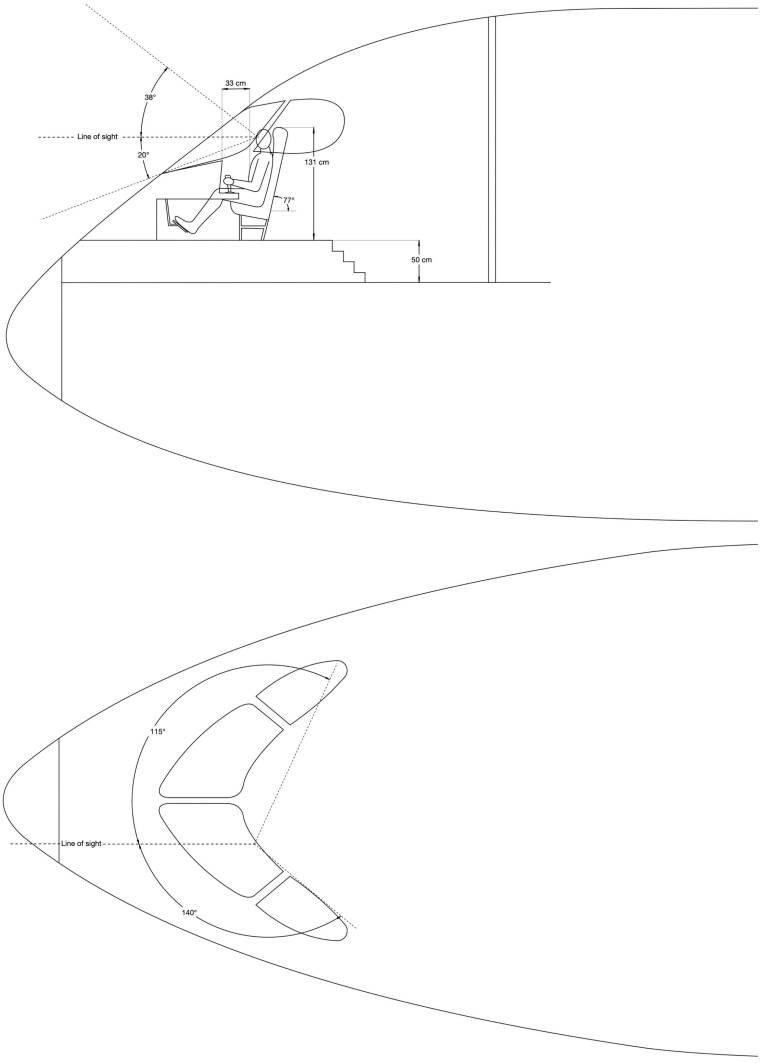

Figure 1.23 Pilot's position and relevant vision angles

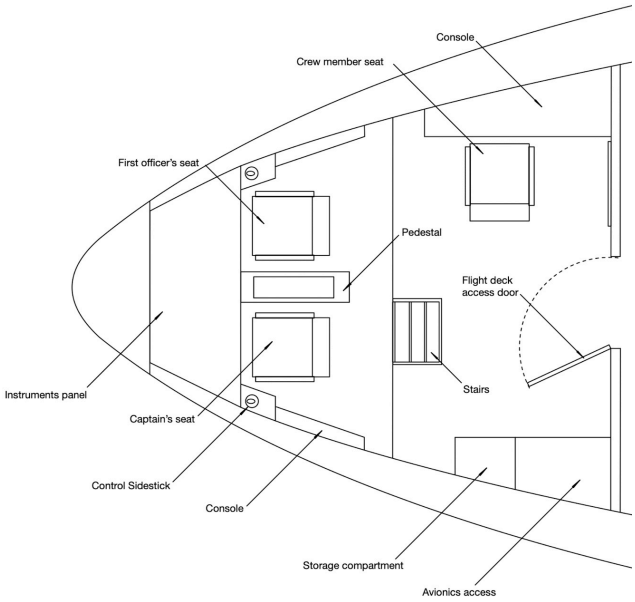

Figure 1.24 Flight deck arrangement

One of the most important aspects of the fuselage's tail design is the tailstrike (or rotation) angle. Increasing the tail's upsweep angle will increase significantly the fuselage's drag, but the tail must be designed with the necessary angle to allow takeoff and landing to occur safely without risk of tail impact against the ground. The transition from the straight fuselage to the upsweep tail must be also designed as smooth as possible to avoid sharp edges which can lead to vortex separation ([22], Jan Roskam, 1986, pp. 40-41).

For similar large widebody aircraft, tailstrike angle values oscillate between 10º - 13º ([15], Boeing, 2023) ([16], Airbus, 2021) ([17], Airbus, 2023). Note that there is an important component which needs to be installed on the aircraft's fuselage tail to perform aerial refueling and which may increase the tailstrike risk and reduce considerably the tailstrike angle: the flying boom. The ratio of the length of the fuselage's tail and the aircraft's diameter (L_{FC}/d_F) for military transports, bombers and patrol aircraft oscillates between 2'6 and 6. The middle values of the range will be selected (ensuring a feasible tailstrike angle) for the tail design, as the objective is to enhance the aircraft's efficiency as much as possible, but balance must be maintained between aerodynamic performance and weight. When the fuselage's tailcone is too short, a large amount of drag will be produced and if the tail is designed excessively large, a significant weight penalty will affect the aircraft's performance ([25], Jan Roskam, 1985, pp. 109-110).

The tail design is illustrated in Figure 1.25 in both upper and side views. Construction is made with parabolic contours. For LT-018, the ratio of the length of the fuselage's tail and the aircraft's diameter L_{FC}/d_F has a value of 3'5.

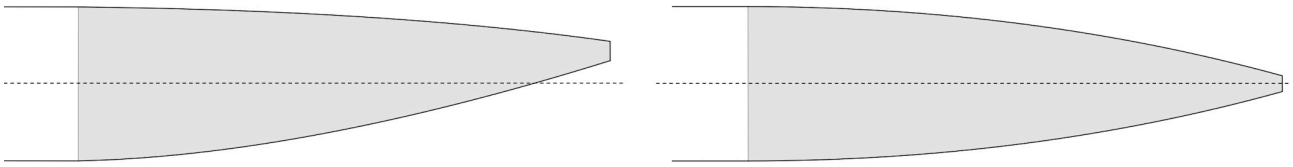

Figure 1.25: Aircraft's fuselage tail design: upper (left) and side (right) views

1.5 Fuselage assembly

At this point of the report, a 3D assembly model of the different aircraft's fuselage parts can be built using the 3D modeling software Catia V5. For the proper definition of both the nose and the tailcone, the approach consists in defining multiple circumferences and ellipses belonging to different cross-sections along the longitudinal axis based on the 2D drawings which were made and shown in the previous sections of the project.

Afterwards, using the multi-section surface tool and splines as guidelines, different surfaces are defined. The remaining step is defining the thickness to create a solid body and in the case of the nose, performing the apertures corresponding to the pilot's windshield, which are created using the tool "*pocket*" from a sketch on the YZ plane. Figures 1.26 and 1.27 show the nose and the tailcone surface design Catia models.

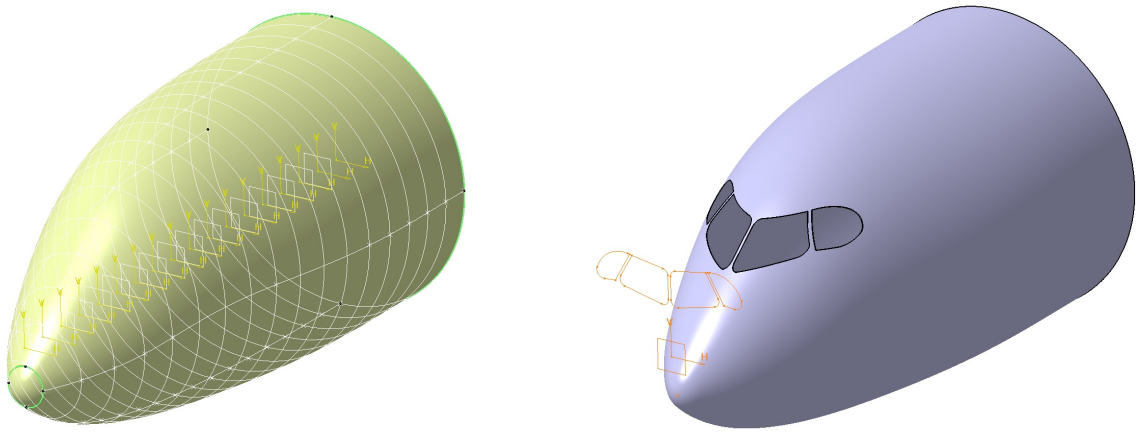

Figure 1.26: Fuselage nose 3d model design

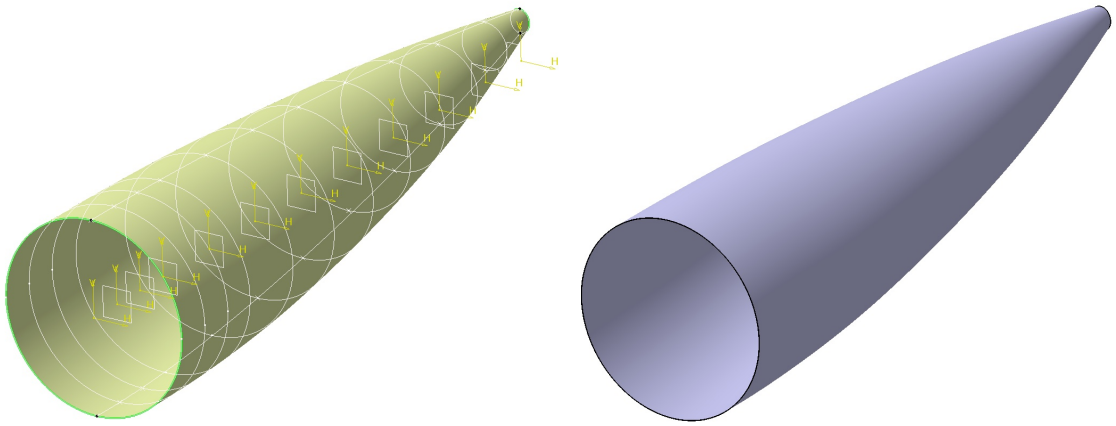

Figure 1.27: Fuselage tail 3d model design

Defining the rest of the fuselage as a hollow cylinder permits the assembly of the three major components which form it, which is illustrated in Figure 1.28.

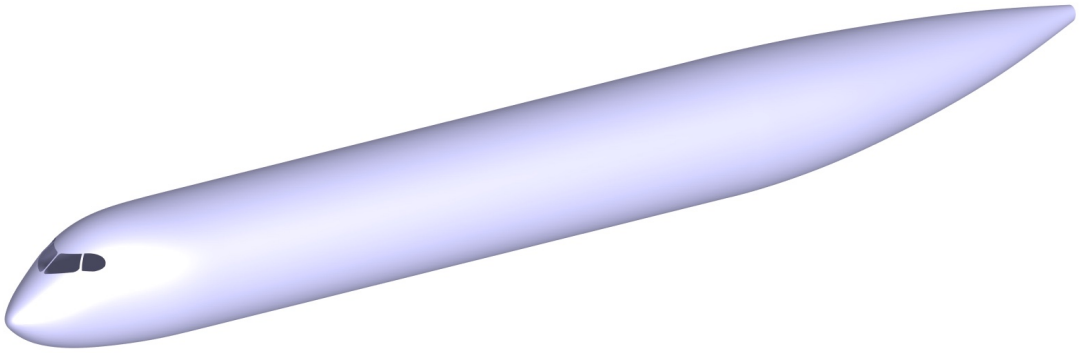

Figure 1.28: Fuselage assembly 3d model rendered

The most relevant dimensions of the fuselage are presented in Figure 1.29:

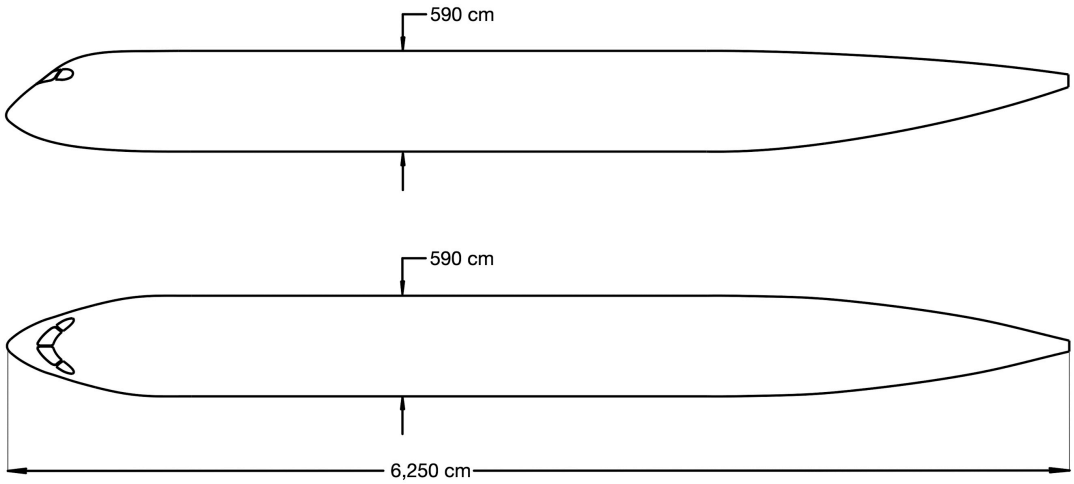

Figure 1.29: Fuselage upper and side views with dimensions

1.6 Doors and windows arrangement

- **Passenger doors:** the number, type and arrangement of passenger doors was defined previously in section 1.2. The main dimensions for Type A doors are 183 x 107 cm with corner radii not greater than 17’8 cm and for Type I, 122 x 61 cm with corner radii not greater than 20’3 cm, to ensure compliance with EASA regulations ([20], EASA, 2024).

- **Windows:** contrary to commercial airliners, military transport aircraft usually are not equipped with many windows, as they only increase structural and manufacturing complexity and for the missions carried out by this specific type of aircraft, passenger comfort is not a priority.

  Moreover, LT-018 has a higher number of doors (especially cargo ones) than commercial airliners. Those are the main reasons why a small number of windows are installed on the aircraft, to be more specific, 6 and 7 on each side respectively, to provide some daylight clarity, natural lighting and situational awareness to the crew members. For this purpose, rectangular windows with curved edges of the approximate size of those used in regional aircraft are used.

- **Cargo doors:** a total amount of three cargo doors are needed for the aircraft: one in the upper deck to load and unload pallets and two on the lower deck (to give access to each of the two different independent cargo compartments). Regarding the design of the cargo doors, the most important design aspect is to ensure that they have the necessary dimensions to allow the payload intended to be transported by the aircraft to fit and be maneuvered through them. In the same manner as the passenger doors, edges must be rounded to avoid excessive stress concentrations.

The following figures illustrate and describe the main arrangement of cargo and passenger doors and windows, indicating its most relevant dimensions:

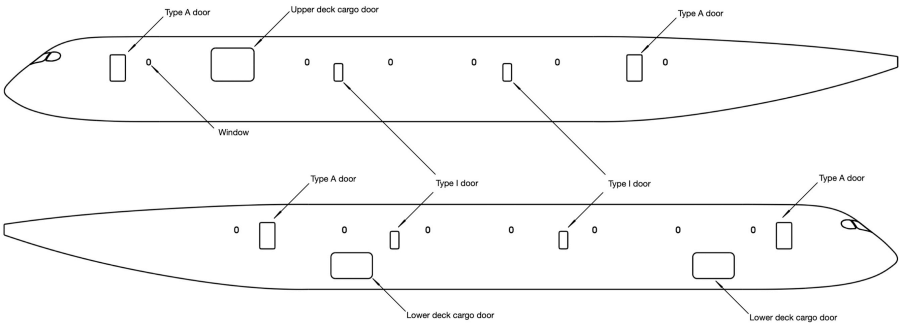

Figure 1.30: Fuselage doors and windows arrangement

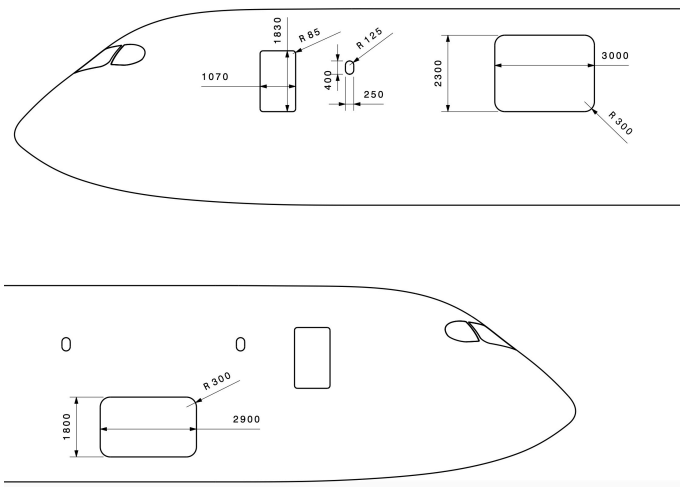

Figure 1.31: Upper deck cargo door, window, lower cargo door and Type A door dimensions (in mm)

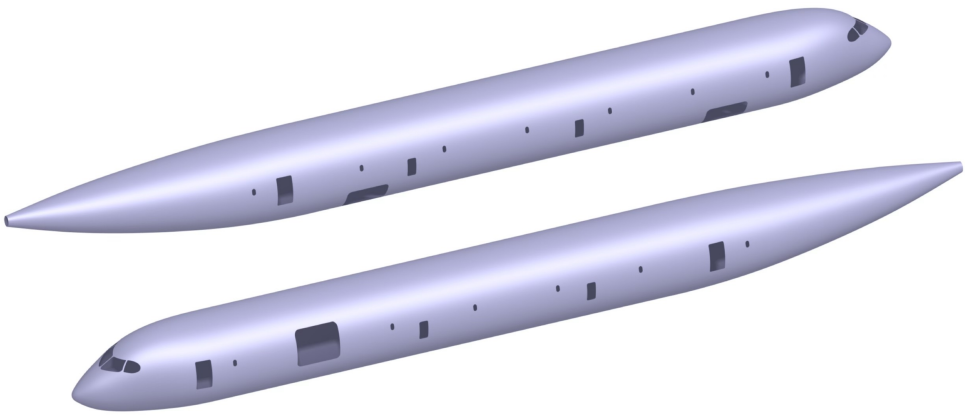

Figure 1.32: Fuselage doors, windows and cargo doors 3d model (rendered)

1.7 Fuselage structural arrangement and description

A semimonocoque structure is used for the fuselage, basing on thin sheets of material (the skin panels) stiffened by longitudinal stringers and transverse frames. Bending moments, shear forces and torsional loads induce axial stress in the stringers and skin panels and shear in the skin panels too. Fuselage frames are needed due to the fact that the skin panels may suffer buckling under relatively low values of compressive loads ([26], T.H.G. Megson, 2007, pp. 598, 638).

Note that an extensive structural calculus could be performed on the fuselage in combination with an iterative optimization process to determine the optimal number of structural components and its dimensions, but that process would extend significantly the project content (there is a variety of papers and technical reports which are solely based on this specific topic) and that is not the main intention. A preliminary layout and arrangement will be developed throughout the project on the aircraft's structure.

The first structural component to be defined are the fuselage frames. Based on operating aircraft and current state of the art semimonocoque structures, the frame pitch selected for the aircraft is 65 cm. Each frame belonging to the fuselage (except for those on the wingbox, landing gear bay, nose and tailcone sections) has a circular shape, to provide the fuselage with the cross-section shape and size described at the introduction of the project. Two different floor spars cross each frame to define the upper and lower decks' floor height. Floor tracks cross the upper floor spars transversally at 4 different points, mainly to sustain the payload. Floor struts in the upper and lower decks will connect the outer frame with floor spars. Finally, a total number of 66 stringers will pass transversally through cut-outs in the frame radially.

The different structural components are modeled and assembled in Catia V5, to illustrate all the assembly in a more realistic perspective. The following figures illustrate the fuselage structure assembly in different perspectives:

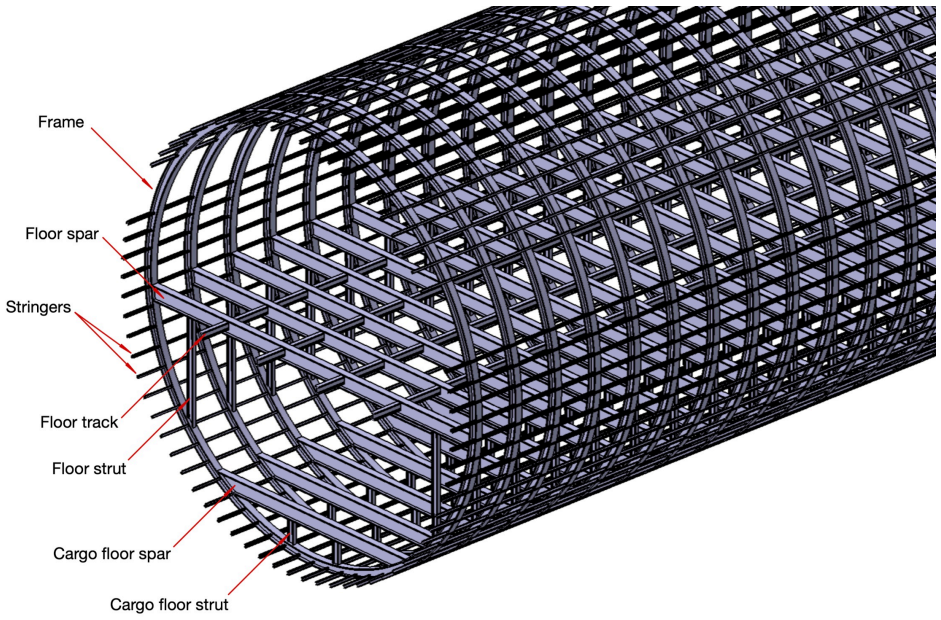

Figure 1.33: Fuselage structural members assembled

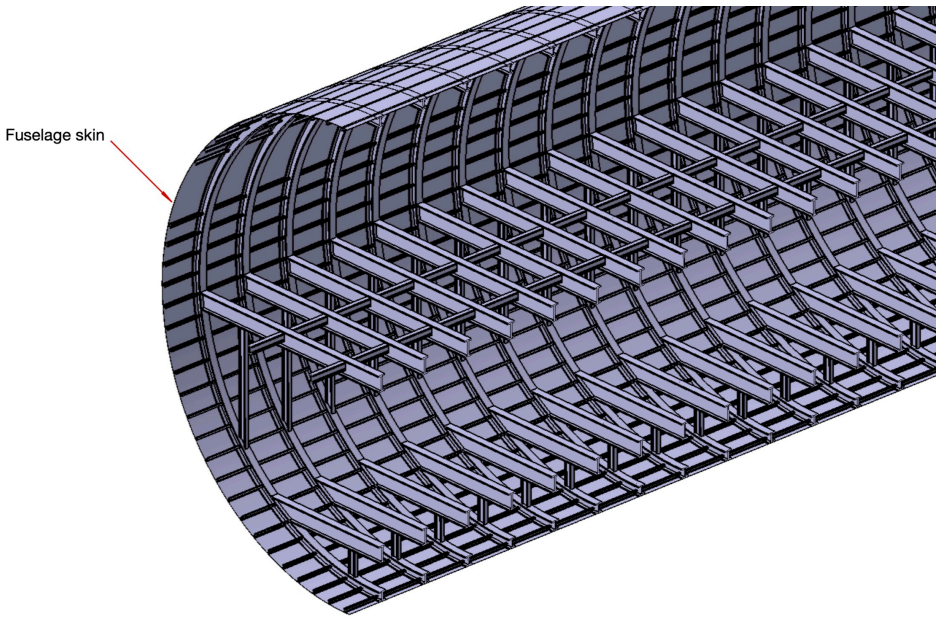

Figure 1.34: Fuselage structural members and skin assembled (cross-section)

The fuselage's structure presents modifications to allow the accommodation of apertures such as door frames. It is exemplified in Figures 1.35 and 1.36, showing some door frames on the fuselage structure and its most relevant reinforcements, in the form of lintels and intercostals.

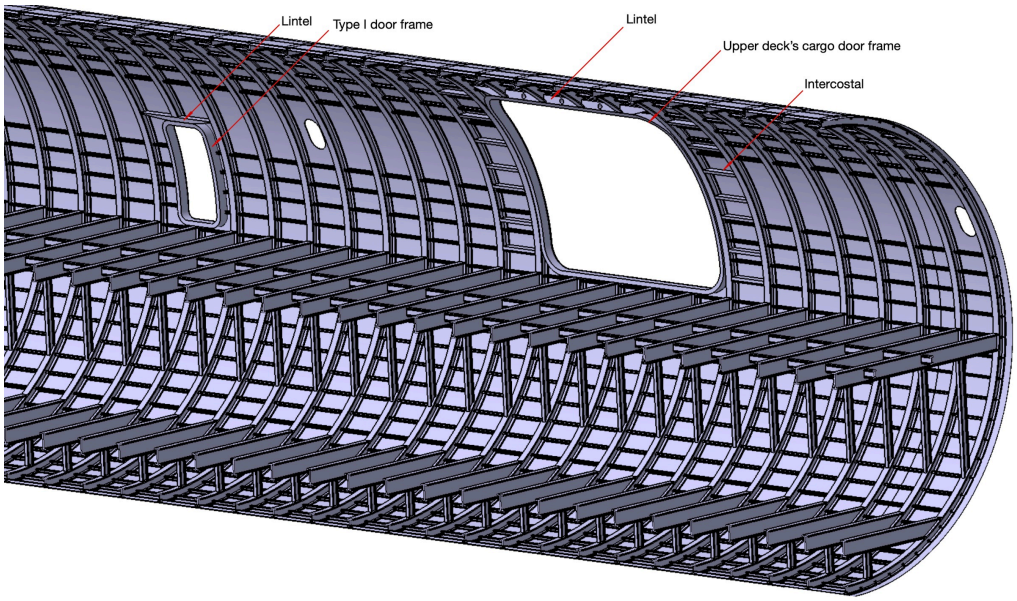

Figure 1.35: Upper cargo and Type I door's structural members

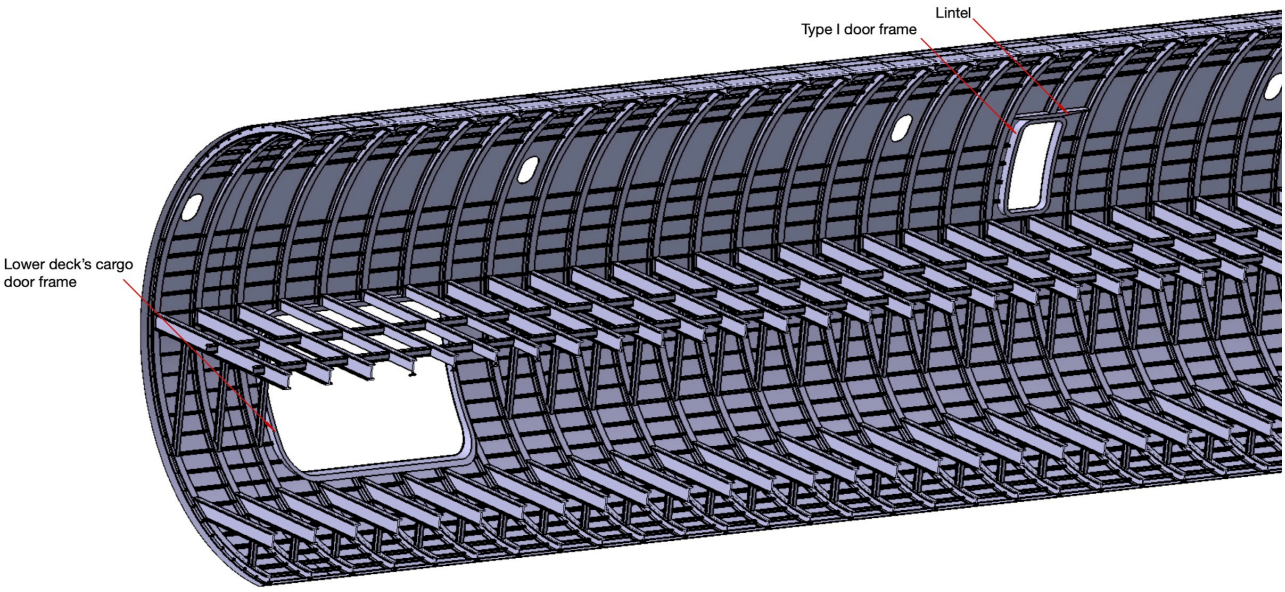

Figure 1.36: Lower cargo and Type I door's structural members

The same approach is maintained for the fuselage's nose. Structural frames will define the shape of the nose. Three remarkable components are installed in this part of the structure: one Type A door frame, the flight deck windshield frame and the forward pressure bulkhead. The assembly of the fuselage nose's structural elements is illustrated in 1.37.

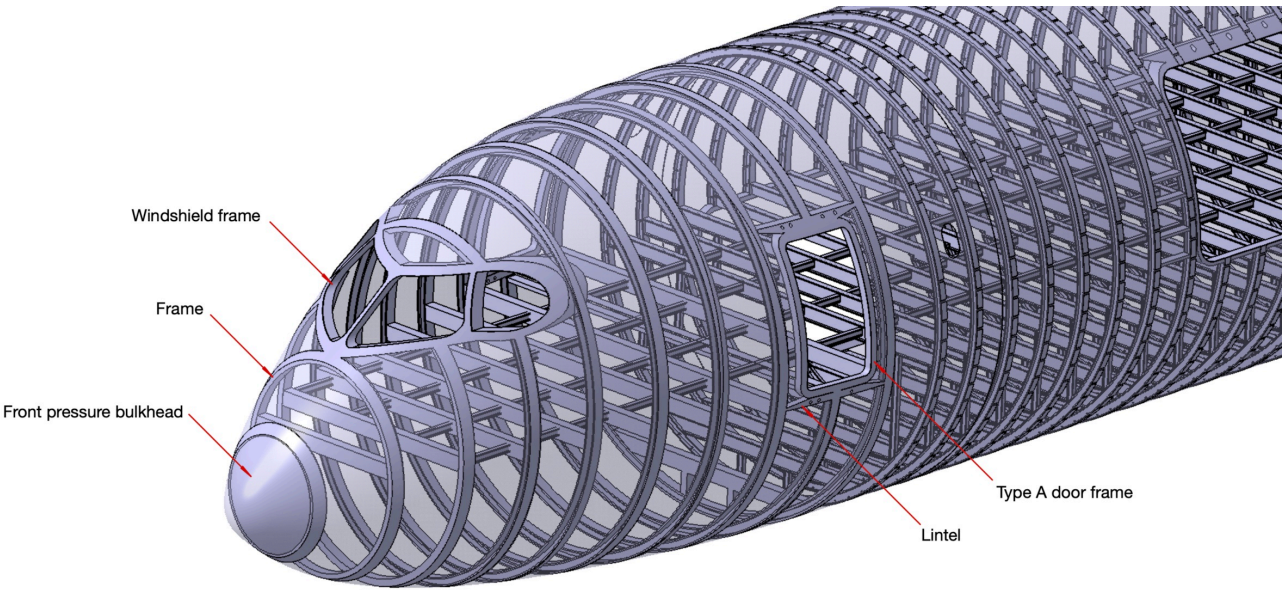

Figure 1.37: Fuselage nose structure

Chapter 2: Wing design

Throughout this chapter of the project, it is described the design process of the main wings of the aircraft covering the aerodynamic design parameters selection, the structural arrangement, the control surface definition and the fuel tanks' capacity calculations.

2.1 Wing area (S), sweep at quarter chord ($\Lambda_{c/4}$) and thickness ratio (t/c) calculation

Some of the initial relevant design parameters of the aircraft's wings are described in this section, including the area or the sweep angle.

To decide those mentioned parameters, it is followed the approach developed by Jan Roskam on its books "*Airplane Design - Part I: Preliminary Sizing of Airplanes*" and "*Airplane Design - Part II: Preliminary Configuration Design and Integration of the Propulsion System*".

LT-018 presents a cantilever wing structural approach instead of braced ones, as the trade between drag increment and wing weight is unfavorable for braced wings above airspeeds of around 200 kt, which is significantly lower than the average cruise airspeed of tanker aircraft ([25], Jan Roskam, 1985, p. 142).

With respect to the fuselage, LT-018 presents a low-wing configuration. Even though the mid wing configuration is preferable in terms of interference drag and lateral stability, the upper deck's useful volume would be significantly reduced by the center wingbox and as a result, less payload would be accommodated. Positively, low-wing configurations usually result in a lower landing gear group weight compared to high and mid-wings ([25], Jan Roskam, 1985, p. 142).

The aircraft is designed to fly in transonic flight regimes (M = 0'8-1'2), and that is the main reason why a supercritical airfoil is chosen. This type of airfoils have a relatively flat top surface, which leads to weaker terminating shocks and, as a result, create less drag. ([27], John Anderson, 2017, pp. 775-777). This effect is illustrated in Figure 2.1:

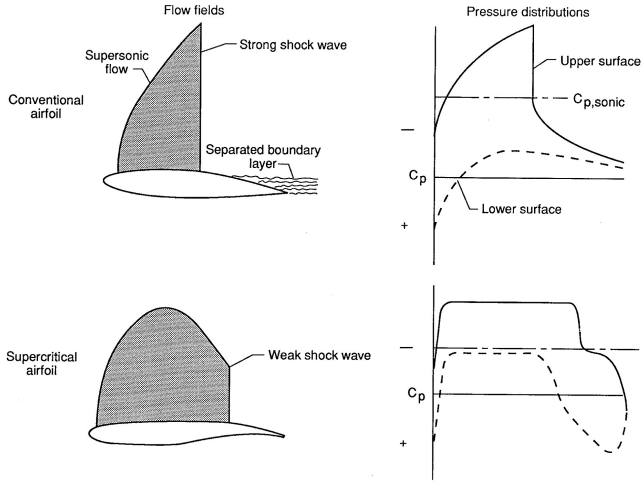

Figure 2.1: Standard NACA airfoil compared to supercritical airfoil at cruise (NASA, 1990)

At this point of the wing design phase, it is necessary to estimate the aircraft's MTOW to size the wings. Statistical data from Military Patrol, Bomb and Transport aircraft is used in accordance with aircraft which present similar fuselage length, which in this case, was designed to be 62'5 m and is probably the most relevant design variable at this point of the project to make assessments, comparisons and approximations. For example, Airbus A330 MRTT fuselage length is 57'51 m and its MTOW is approximately 220,000 kg ([29], Airbus, 2021). In the case of Boeing KC-46A, the fuselage's length is 50'5 m and its MTOW is 188,241 kg ([6], Boeing, 2023).

The average ratio between the aircraft's MTOW and the fuselage length for actual tanker aircraft results to be 3,750. Maintaining the same ratio, the MTOW that the aircraft will have can be estimated to be 230,000 kg (62'5 m · 3,750 kg/m = 234,375 kg ≈ 230,000 kg).

The wing area must be sized to ensure a safe takeoff and landing, as cruise flight does not require a large amount of C_L . That is the reason why the wings will be sized conditioned by those two stages of flight. For large wide-body commercial aircraft, takeoffs take place at airspeeds around 130-150 kt and approach speeds are usually classified in Category D according to FAA (141-166 kt) ([32], FAA, 2007).

It is assumed that if the aircraft is close to the stall condition, it will be performing either a takeoff or a landing maneuver, that is the reason why an altitude of 1,000 ft (~300 m) is chosen to determine the air density, which value is 1'18955 kg/m^3. ([31], University of Sidney, 2006).

C_{Lmax} will depend on several variables such as the airfoil, the high-lift devices and the airspeed, but typical values for Military Patrol, Bomb and Transport aircraft are located in the range of 1'6 - 2'2. Being conservative, an intermediate value (2) will be used for calculations ([30], Jan Roskam, 1985, p. 91).

Assuming the aircraft is fully loaded (MTOW = 230,000 kg) and limiting the stall speed in 130 kt (66'88 m/s), the wing loading can be calculated according to Equation 2.1, which is determinant to find the necessary wing's area:

$$L = \frac{1}{2} \cdot C_{L_{max}} \cdot S \cdot \rho_{\infty} \cdot u_{\infty}^2$$

Equation 2.1: Lift equation

If the lift force must surpass the aircraft weight for it to become airborne, the wing loading at the moment of takeoff can be determined:

$$W = \frac{1}{2} \cdot 2 \cdot S \cdot 1'18955 \cdot 66'88^2 \; ; \; W/S = 5{,}320'78 \; N/m^2$$

Isolating the wing's area and introducing the MTOW value, the wing area can be finally calculated:

$$S = \frac{W}{5{,}320'78} = \frac{230{,}000 \cdot 9'81 \; N}{5{,}320'78 \; N/m^2} = 424'05 \; m^2 \approx 420 \; m^2$$

During flight, in the upper surface of the airfoil, the local flow speed increases and there is a point where the pressure is minimum and thus, Mach number is maximum. In transonic flight regimes (M = 0'8-1'2), the critical Mach number refers to the freestream's Mach number at which sonic flow is achieved on the airfoil at that mentioned point where pressure is the lowest. Thick airfoils will have a lower critical Mach number than thinner airfoils, as the flow over them will experience a larger perturbation from the freestream. The main design issue with large aircraft is that the wing's airfoils cannot be designed excessively thin, as structural components and fuel tanks need to be accommodated inside them.

That is the main reason why positive sweep angle is needed on the wing of the aircraft, so the streamlines which flow over it encounter an airfoil with a lower thickness-to-chord ratio (t/c) compared to a straight wing design and as a result, the critical Mach number increases and the aircraft can fly at higher airspeeds without suffering the consequences of increased drag when flying above drag-divergence Mach numbers ([27], John Anderson, 2017, pp. 756-770).

Modern tankers (Airbus A330 MRTT and Boeing KC-46A) operate at a cruise airspeed around Mach 0'8 ([28], Ejército del Aire y del Espacio, 2023). The same cruise airspeed regime is kept for LT-018, to maintain standards, habits and operational procedures developed by the air forces which perform aerial refueling.

If the cruise airspeed is Mach 0'8, the quarter chord sweep angle ($\Lambda_{c/4}$) must ensure that the critical Mach number is higher than that value. The wing's thickness ratio (t/c) must be selected simultaneously with the quarter chord sweep angle. To make use of the sweep vs thickness ratio graphs provided by Jan Roskam, it is needed to estimate initially the necessary C_L during cruise.

Isolating that term from the Lift equation (Equation 2.1), it can be calculated once the wing's area has been determined. The calculation of the airspeed needs to be done according to the following equations, using International Standard Atmosphere conditions and assuming the cruise altitude to be 30,000 ft (T=218'8 K and ρ=0'379597 kg/m3), a common altitude where aerial refueling can take place ([33], NATO - OTAN, 2016).

$$c = \sqrt{\gamma \cdot R \cdot T_\infty} = \sqrt{1'4 \cdot 287 \cdot 218'8} = 296'5 \ m/s$$

Equation 2.2: Speed of sound equation

$$M = \frac{u_\infty}{c} \ ; \ u_\infty = 0'8 \cdot 296'5 = 237'2 \ m/s \approx 461 \ kt$$

Finally, the cruise C_L can be determined, assuming a 5% reduction in weight as a result of burning fuel during the climb and assuming the aircraft is flying at steady level flight, where the weight equals the lift produced by the wings:

$$L = 0'95 \cdot W = \frac{1}{2} \cdot C_L \cdot S \cdot \rho_\infty \cdot u_\infty^2$$

$$C_L = \frac{2 \cdot 0'95 \cdot 230{,}000 \cdot 9'81}{420 \cdot 0'379597 \cdot 237'2^2} = 0'458$$

At this point, where C_L is known, making use of the table presented by Jan Roskam in Figure 2.2, $\Lambda_{c/4}$ and t/c can be defined:

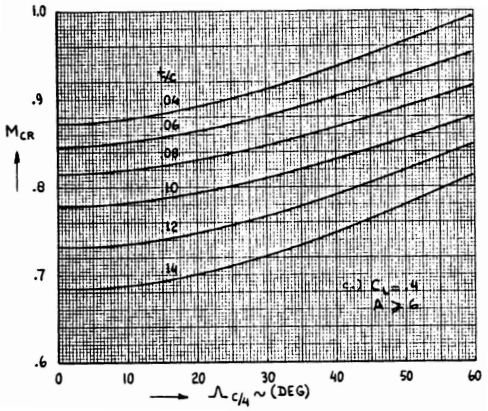

Figure 2.2: Effect of t/c and $\Lambda_{c/4}$ on Critical Mach number for C_L =0'4 ([25], Jan Roskam, 1985, p. 151)

Leaving an airspeed safety margin of M=0'025, the resultant M_{CR} would be located at an airspeed of M=0'825. Drawing a straight line on the graph at that specific M_{CR} value, the highest possible value of t/c that can be chosen is 0'1 for $\Lambda_{c/4}$ = 35º.

2.2 Airfoil selection

As it was mentioned previously, the aircraft's wings need to be made out of supercritical airfoils whose maximum t/c value must not surpass 0'1. For this selection, the catalogue of NASA Supercritical Airfoils is used. The airfoil which best meets the aircraft's requirements is SC(2)-0610, which was designed for 0'6 Lift Coefficient and has a t/c maximum of 0'1. It is illustrated below in Figure 2.3:

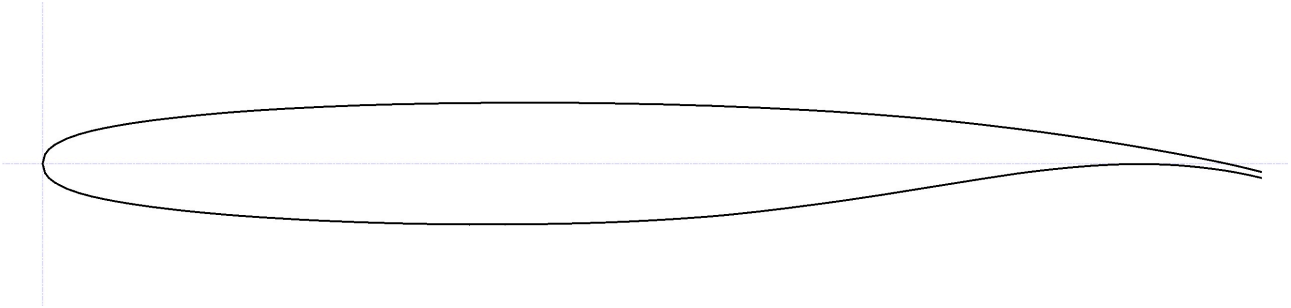

Figure 2.3: NASA SC(2)-0610 Airfoil

SC(2)-0610 design parameters:

- Maximum thickness: 10%
- Maximum thickness location: 38% of the chord
- Maximum camber: 1'8%
- Maximum camber location: 82% of the chord

2.3 Wing planform design

The wing is designed at this point of the project taking into consideration the design parameters accorded during the previous sections. The most relevant known parameters to consider when designing the wing planform are the area (420 m^2) and the sweep at quarter chord (35º).

The lift distribution which provides minimum induced drag in the absence of aerodynamic or geometrical twist will be provided by an elliptical wing planform, which produces a homogeneous downwash. On the contrary, a rectangular wing planform will provide very inefficient lift distributions, which are far from being optimum. Taper ratio (λ) is used in wings to resemble the elliptical lift distribution without needing to design an elliptical wing planform, which are hard to manufacture and impractical to operate ([27], John Anderson, 2017, p. 449).

Another important design variable to consider in the planform design is the aspect ratio (AR), which has a strong impact on the wing's induced drag coefficient (C_{Di}). To be more specific, C_{Di} is inversely proportional to the AR. Even though large Aspect Ratio wings will provide the lowest values of induced drag, it must be kept a balance between the structural members needed to install long slender wings and the benefit that they will provide in terms of efficiency ([28], John Anderson, 2017, p. 452). The trend in modern high performance commercial aircraft is to increase the aspect ratio with each new generation of airliners up to a limit. Modern airliners do not usually exceed an AR of 9'5-10, mainly because the additional structural design effort starts to be impractical and operations inside airports become difficult and restrictive.

For wings with aspects ratios ranging from 4 to 10, the taper ratio which provides less induced drag is located in the range of 0'2-0'4 ([27], John Anderson, 2017, p. 452).

A maximum wingspan close to 60-65 meters is limited, so the aircraft can operate in all the air force bases and airports where current operating large-scale tankers do. Sticking to these mentioned constraints, the final wing's planform design is shown in Figure 2.4, including its main dimensions and design parameters.

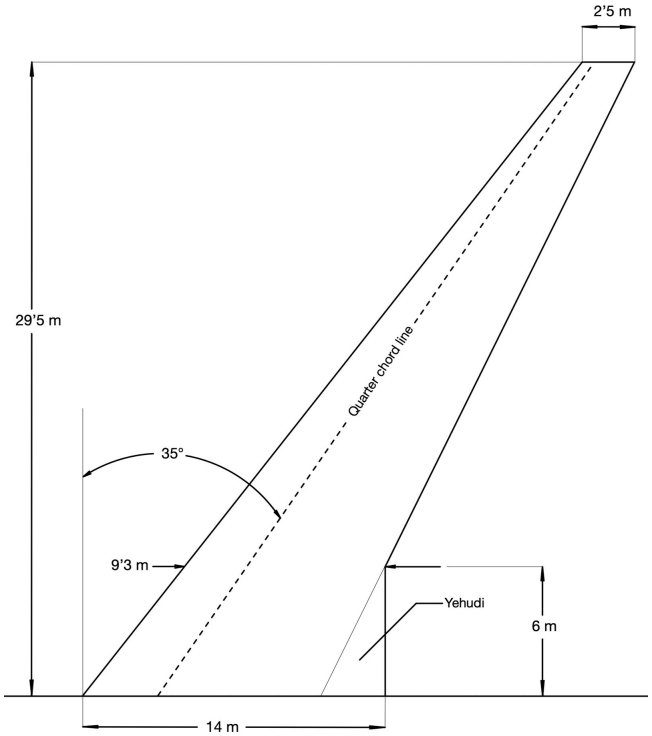

Wing design parameters	
Semi-wing span (m)	29'5
Semi-wing area (m^2)	207'66
Aspect Ratio (total)	10'14
Taper ratio λ	0'18
Quarter chord sweep $\Lambda_{c/4}$	35º
Wing root chord (m)	14
Wing tip chord (m)	2'5

Figure 2.4: Wing planform design and parameters

The wing presents all the design variables which were decided and explained in the previous sections. The last design aspect to consider in this section is the dihedral angle (Γ). In this case (low wing configuration), a positive dihedral angle is defined. In large aircraft, probably the most critical factor when selecting the wing's dihedral is ground clearance required by regulations (with nacelles / propellers) during flare altitude for a 5º bank angle ([25], Jan Roskam, 1985, p. 154). A dihedral angle of Γ = 3º is selected basing on the aircraft's dimensions and on the powerplant and nacelle's expected size.

2.4 Wing aerodynamic performance study & optimization

This section of the project focuses on the aerodynamic analysis and optimization process of the aircraft's main wing, which is done without modifying its planform shape.

Aeolus ASP software is used for this purpose. In a nutshell, this software is able to define a fixed-wing, study its aerodynamic behavior and it has an option to modify several design parameters to optimize specific flight conditions. For this purpose, the software will modify the wing's twist values along the wingspan using advanced optimization algorithms to optimize the wing for different objectives (in this case, to reduce fuel burn and increase the range). The wing is modeled in the software, as it is illustrated in Figure 2.5.

Afterwards, the aircraft's weight (MTOW - 5% of the weight which corresponds for fuel burnt assumed for climb) and the cruise flight conditions are defined to perform the aerodynamic analysis. The most relevant parameters (altitude and airspeed) are defined, and it is seen how the software calculates the Mach number which, as expected, results to be M=0'8 (seen in Figure 2.6).

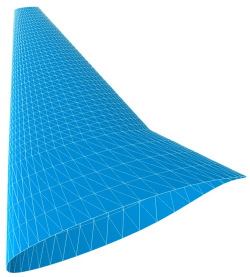

Figure 2.5: Wing modeled in Aeolus ASP

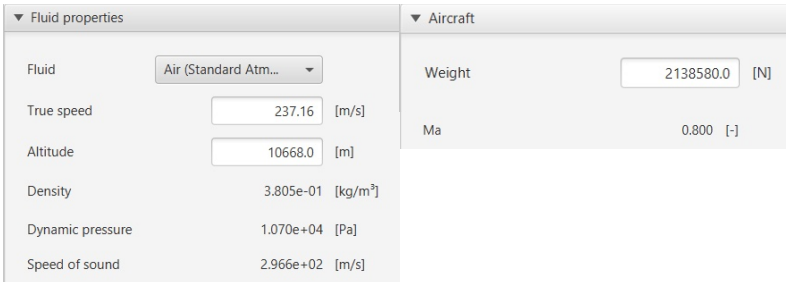

Figure 2.6: Flight conditions definition

The analysis tool is ran on the wing. The most relevant results and conclusions obtained from the analysis are listed below:

- The wing presents the required C_L for cruise flight (which was 0’458) at an angle of attack of α=3’25º (C_L-α graph is illustrated in Figure 2.7).
- For this angle of attack, C_{Di} has a value of 0’007875 (C_{Di}-α graph is illustrated in Figure 2.8).
- The lift distribution along the wingspan resembles closely the elliptical distribution. In Figure 2.9, it is appreciated the difference.
- The local induced drag coefficient starts to increase noticeably beyond 22’5 m of semi-wingspan, as a result of wing tip vortices (seen in Figure 2.10).
- The aerodynamic efficiency (C_L/C_D) at cruise flight has a value of 24’4 (note that only the wings are being considered by the software).

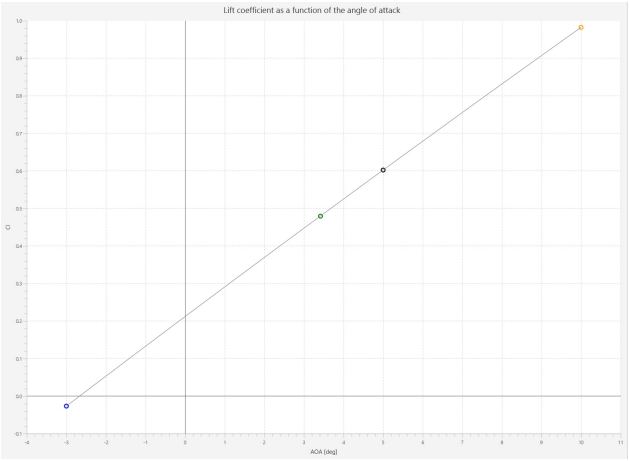

Figure 2.7: C_L-α graph

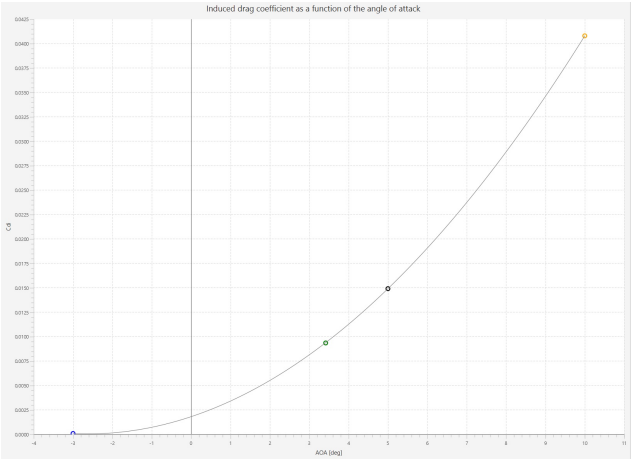

Figure 2.8: C_{Di}-α graph

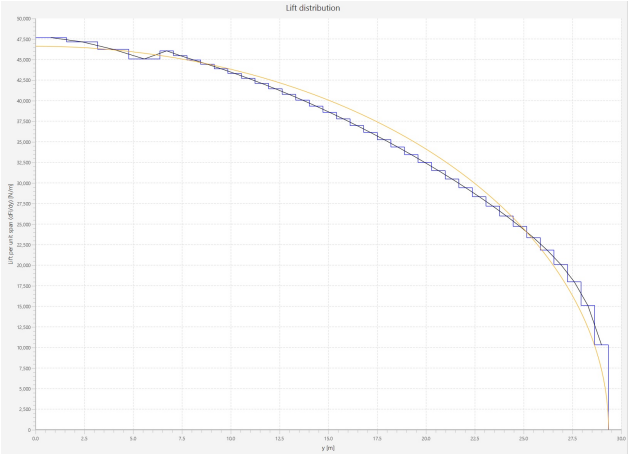

Figure 2.9: Lift distribution along the wingspan (orange line accounts for elliptical reference)

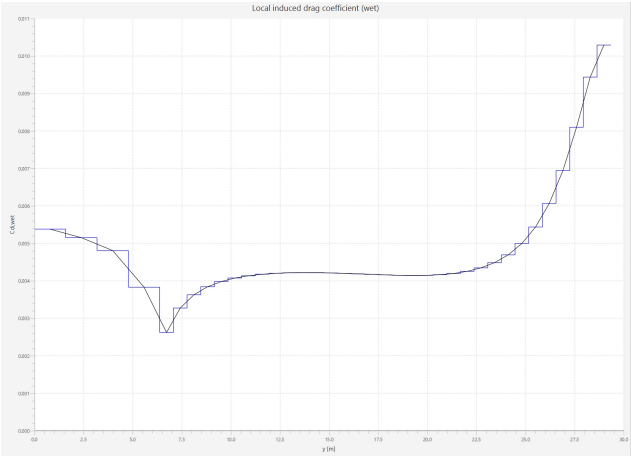

Figure 2.10: Induced drag distribution along the wingspan

Once the analysis has been performed, the next step is to define the necessary conditions to study the possibility of enhancing the aerodynamic performance making use of the integrated optimization tool. In the objective definition, it is selected the maximization of the Lift/Drag ratio.

The design variables which are selected to be optimized; in this case, are the twist angles of several different airfoils which were selected to define the wing along the wingspan on the software (the root chord, the end of the Yehudi and the tip chord).

After several iterations (50 approximately), the software provides the necessary twist angles at different points along the wingspan to increase the aerodynamic efficiency. Note that there is not a high margin of aerodynamic efficiency improvement, as the C_L must not decrease and the wingspan and chord length's should not be modified. The twist angles provided by the software to increase the aerodynamic efficiency during cruise are listed below:

- Root chord twist angle: -0'92º
- End of Yehudi chord twist angle: 0'9º
- Wing tip twist angle: -0'7º

The overall wing's aerodynamic efficiency (C_L/C_D) is increased slightly from 24'4 to 24'5.

2.5 High-lift devices and control surfaces

Regarding the high-lift devices, a combination of flaps and slats is used on the aircraft.

For the flap design and type selection, a reasonable balance must be kept between the high-lift requirements, the drag considerations and the complexity and weight of the system chosen. On one hand, the type of flaps which provide the highest maximum C_L (Fowler flaps) present a complex functioning and maintenance, as well as high costs and weight.

On the other hand, simpler mechanisms such as plain flaps usually do not meet the necessary requirements in large aircraft. To keep a balance for this project, slotted flaps are selected, following the trend in modern aircraft of reducing maintenance costs and complexity when it comes to high-lift devices.

2 groups of flaps are located at the trailing edge of the wing (inboard and outboard flaps), adding a total number of 5 flaps per semi-wing which deployment takes place streamwise.

The same approach is kept with the leading edge high-lift devices, choosing slats for being a balanced option between performance and complexity. 3 separated arrays of slats are located at the leading edge of the wing, adding a total number of 8 per semi-wing.

Spoilers are deployed by means of a linear hydraulic actuator, located in the same position than the flap deployment mechanisms. 2 separated arrays of spoilers are located at the wing, adding a total number of 5 spoilers per semi-wing.

Lastly, a high speed aileron is placed at each wingtip to control the aircraft's rolling moment.

Sizing of the high-lift devices is determined basing on layouts installed on similar aircraft (mainly Boeing 777 or Airbus A330) and following Jan Roskam's "Class I Method for sizing high lift devices", where useful graphs are presented regarding the $\Delta C_{Lmax}/C_L$ for a wide variety of real high-lift devices types. The following Figures illustrates the wings' high lift devices arrangement, as well as the functioning and deployment mechanisms of them.

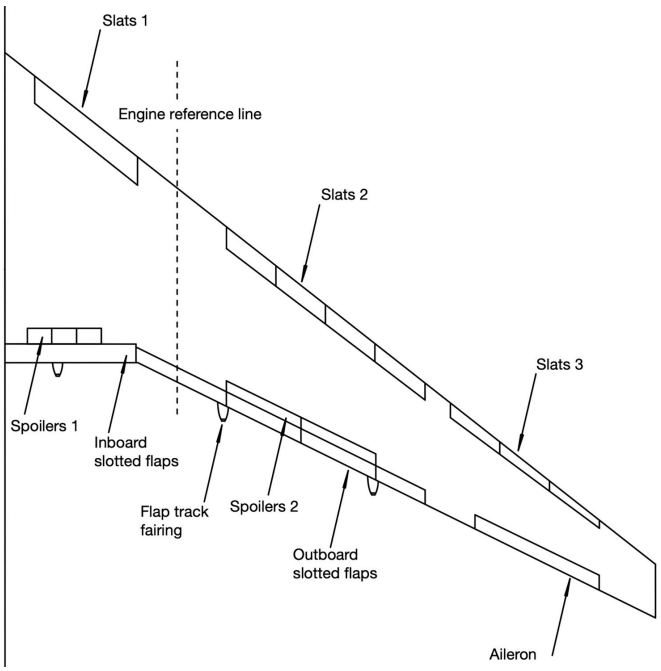

Figure 2.11: High-lift devices arrangement

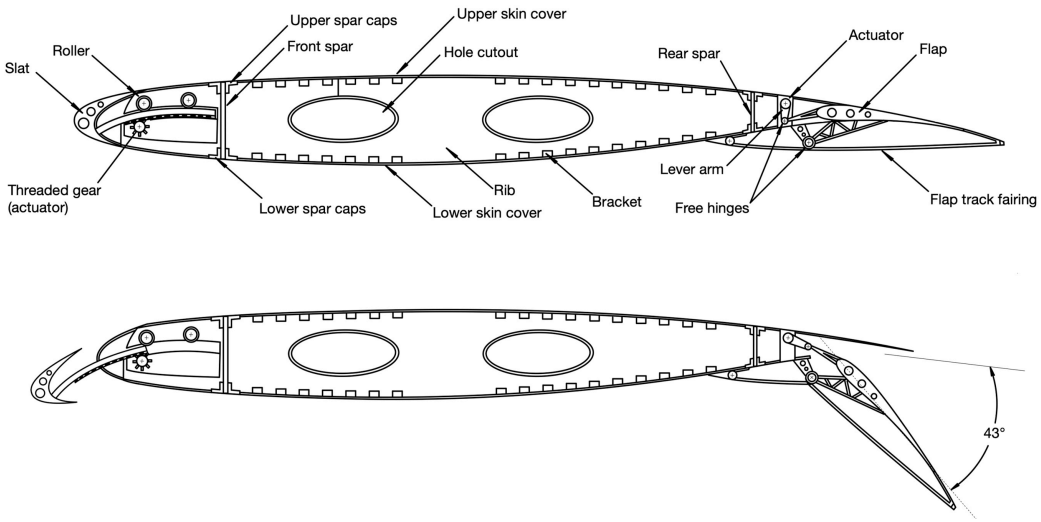

Figure 2.12: Flap and Slat deployment system

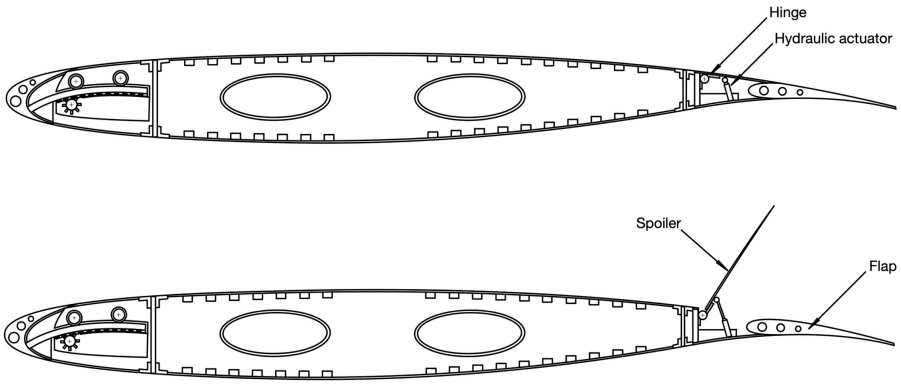

Figure 2.13: Spoiler deployment system

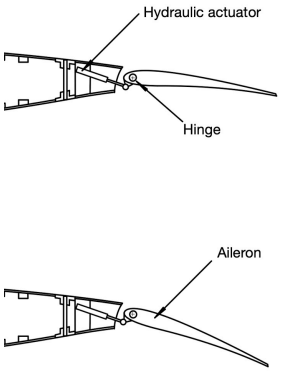

Figure 2.14: Aileron control system

2.6 Wing's structural arrangement

The wings' structure is composed by different members and components. The skin and the ribs will resist the aerodynamic pressure loads on the wing. In addition, the ribs will increase the longitudinal stiffeners' buckling stress, maintain the airfoil's shape along the wingspan and their size will be variable along it (as the wing is tapered). In the same manner than in the fuselage, stringers are attached to the skin and the ribs, as the skin will buckle too under low compressive loads. The wing spars will resist shear, torsional loads and will exert a stabilizing influence on the skin ([26], T.H.G. Megson, 2007, pp. 379-380).

2 spars are located at the front and the rear parts of the wing's torque box. The front spar is located at 15% of the chord all along the wingspan and the rear spar at 77% of the chord length. The decision is taken considering the location of the high-lift devices and trying to maximize the fuel volume.

The total number of ribs per semi-wing is 27, which stabilize the torque box skins and serve as an attachment point for high-lift devices and control surfaces. A rib pitch of 120 cm is defined, distance which also ensures that the proper maintenance, revision and repairs can take place through the 22 tank access doors which are installed (per semi-wing).

The center wingbox is reinforced by transversal beams. It is also worth mentioning that the landing gear support beam in the Yehudi is attached to the 4^{th} and 8^{th} ribs. Ribs are placed perpendicular to the rear spar to reduce the manufacturing complexity and bending deformations on them, compared to ribs placed parallel to the flight path. Several leading and flap supporting structures (extensions of the ribs) are placed along the span to reinforce them and to define the airfoil shape. Figure 2.15 illustrates the main structural arrangement:

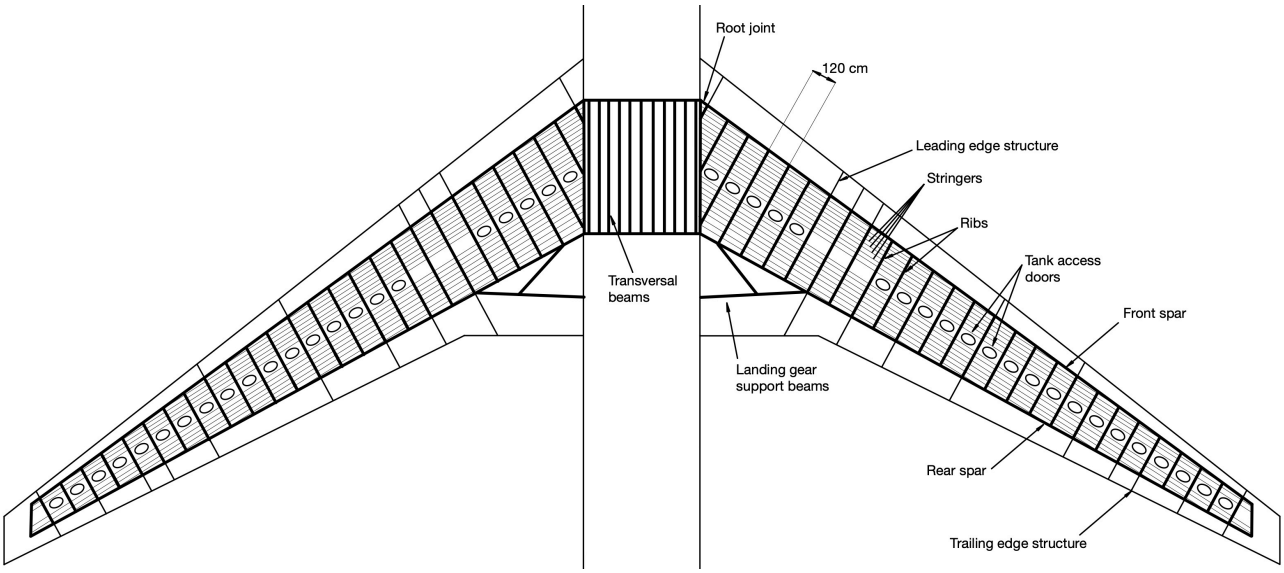

Figure 2.15: Wing structural arrangement

2.7 Wing assembly

In the same manner than the fuselage, the complete wing is designed and assembled using the 3D modeling software Catia V5. Initially, the airfoil's coordinates are imported into the software and they are scaled, rotated and moved to a position where the wing's sweep and dihedral angles are properly defined. Using the multi-section surface tool with straight lines as guides, the wing's surface is defined as seen below in Figure 2.16.

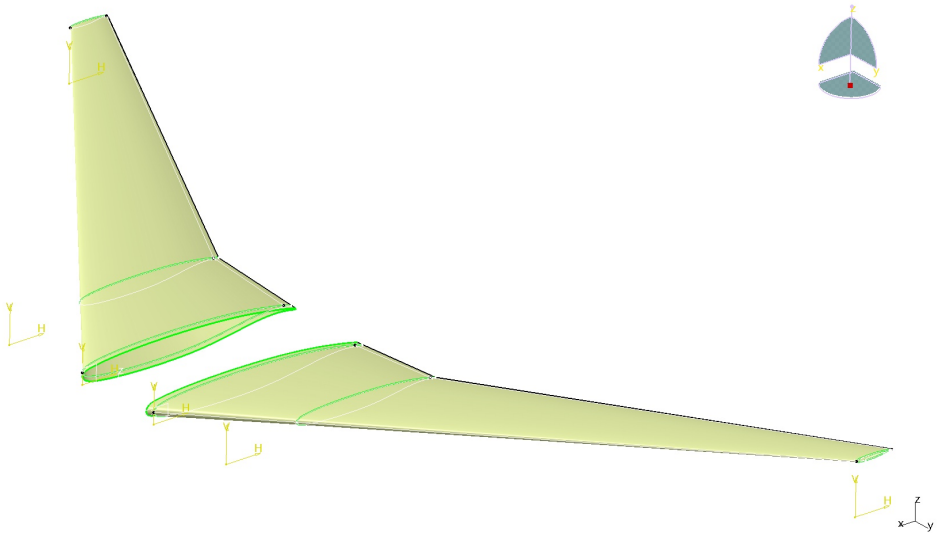

Figure 2.16: Wing surface modeled in Catia V5

The structural members are modeled too. Initially, the spars are modeled, followed by the ribs, setting as the solid's boundaries the wing's surface which was created in the previous step. Leading and trailing edge (flap) structures are defined too.

The last step is defining the the stringers over and below the wing's torque box. Multiple planes, lines as guides, sketches, surface-based tools and symmetry elements are used for this purpose. The final result is illustrated in Figure 2.17:

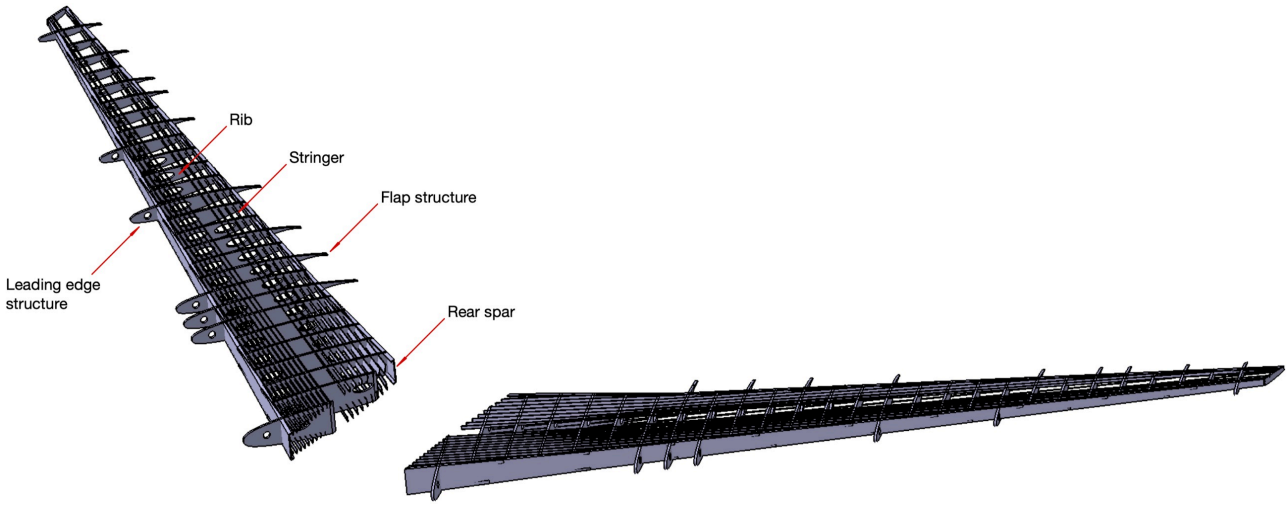

Figure 2.17: Wing spars, ribs and stringers

2.8 Center wingbox: wing-to-fuselage assembly

The center wingbox joins the left and right wing's structural elements and is located in the lower deck of the fuselage. Its main function is to maintain the wing's structural integrity and transmit the aerodynamic loads to the whole airframe.

As it was illustrated in Figure 2.15, it also presents transversal beams (similar to the wing's ribs) which cross it entirely and provide the necessary stiffness. Hole cutouts are needed to communicate the wing's systems (hydraulic, fuel pipes, electric) with the rest of the aircraft. The center wingbox and its most relevant dimensions are seen in Figure 2.18.

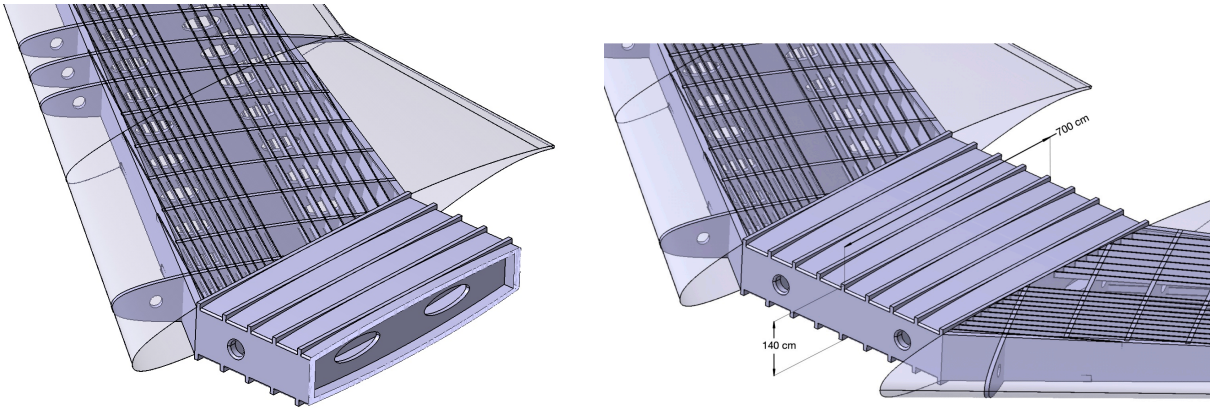

Figure 2.18: Wing's center wingbox with dimensions

A significant portion of the aircraft's mass will account for the fuel, the main landing gear, the engines and the wing structure. That is the reason why the position of the wings with respect to the fuselage affects significantly the position of the center of gravity. At this point of the design phase, the wings must be placed in a position where they do not move excessively rearwards the center of gravity and they do not interfere with the cargo doors.

Basing on this criteria, the center wingbox is placed at a distance of 2,000 cm from the aircraft's nose, which is approximately the center of the fuselage.

The fuselage and wing assembly is illustrated in a better perspective in Figure 2.19:

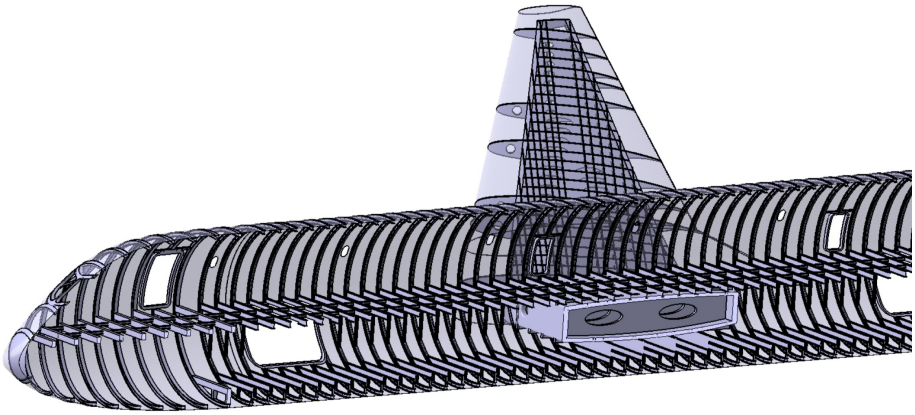

Figure 2.19: Fuselage and wingbox assembly

The whole assembly, including the center wingbox, the main wing's structure and the skin is illustrated in Figure 2.20:

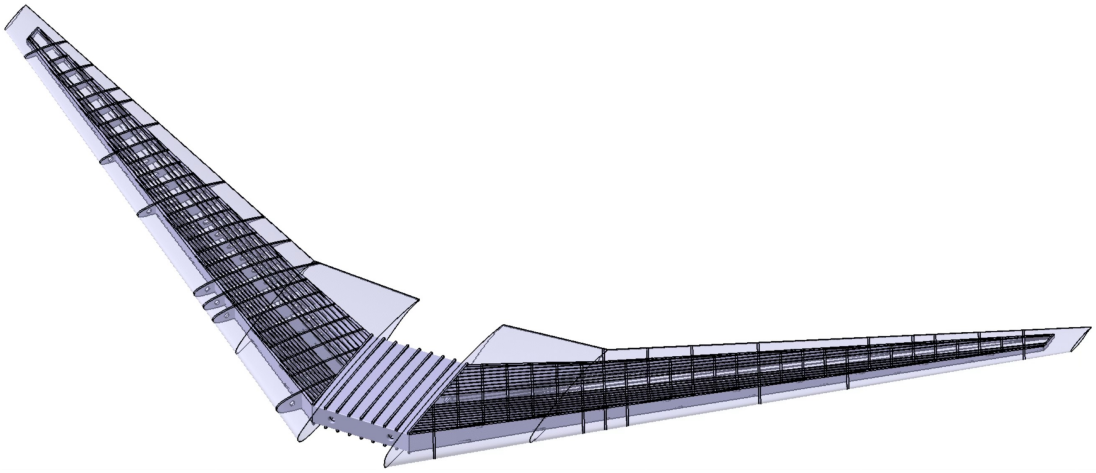

Figure 2.20: Wing assembly (3D model)

2.9 Fuel capacity

The fuel volume of the aircraft is calculated. Making use of the 3D models which have been built, volumes can be calculated using one of Catia V5 tools called "*Measure Inertia"*, which calculates volumes, areas, masses, inertias, etc of solid bodies. Fuel is carried in the wing's torque box, which is sealed to serve as a fuel tank. Some of the ribs along the wingspan will serve as tank ends. The fuel tanks' arrangement and capacities are defined in the following paragraphs:

Center fuel tank: located in the center wingbox.
• Fuel capacity of 25'76 m^3 (25,760 L) (17'07 % of the total capacity)

Inner wing's fuel tank: located at the inner part of the wing (limited by ribs 1 and 12).
• Fuel capacity (per semi-wing) of 47'03 m^3 (47,030 L) (31'17 % of the total capacity).

Outer wing's fuel tank: located at the outer part of the wing (limited by ribs 12 and 21).
• Fuel capacity (per semi-wing) of 13'24 m^3 (13,240 L) (8'77% of the total capacity).

Surge tank: located almost at the wingtip (limited by ribs 21 and 26)
• Fuel capacity (per semi-wing) of 2'28 m^3 (2,280 L) (1'51 % of the total capacity).

The complete aircraft's fuel capacity can be calculated adding the capacity of each independent tank according to Equation 2.3:

$$FC = FC_{center\ tank} + 2 \cdot FC_{inner\ tank} + 2 \cdot FC_{outer\ tank} + 2 \cdot FC_{surge\ tank} =$$
$$= 25{,}760 + 2 \cdot 47{,}030 + 2 \cdot 13{,}240 + 2 \cdot 2{,}280 = 150{,}860\ L$$

Equation 2.3: Fuel volume calculation

In terms of mass, knowing that jet fuel density is approximately 0'8 kg/m^3 ([34], ICAO, 2024), the maximum fuel mass which can be accommodated in the aircraft's fuel tanks can be determined to be 120,688 kg (120'69 tonnes).

The fuel tank's arrangement is illustrated in Figures 2.21 and 2.22:

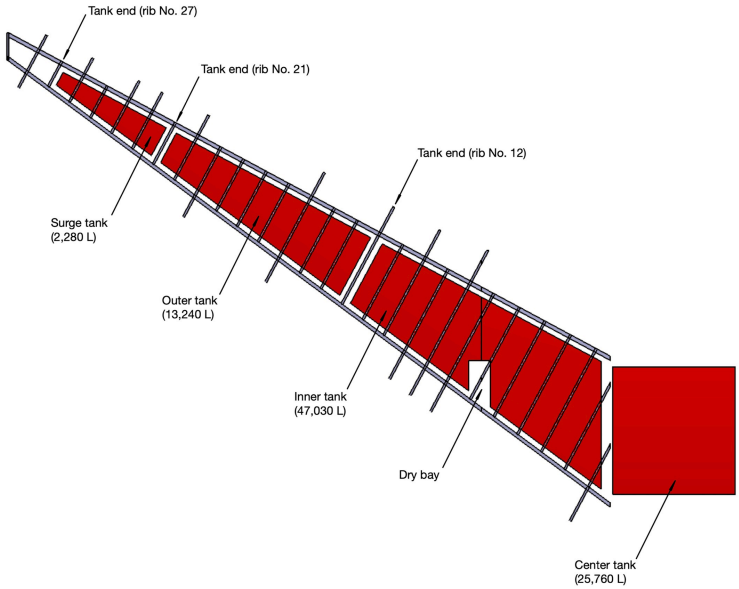

Figure 2.21: Wing's fuel tanks (fuel represented in red color)

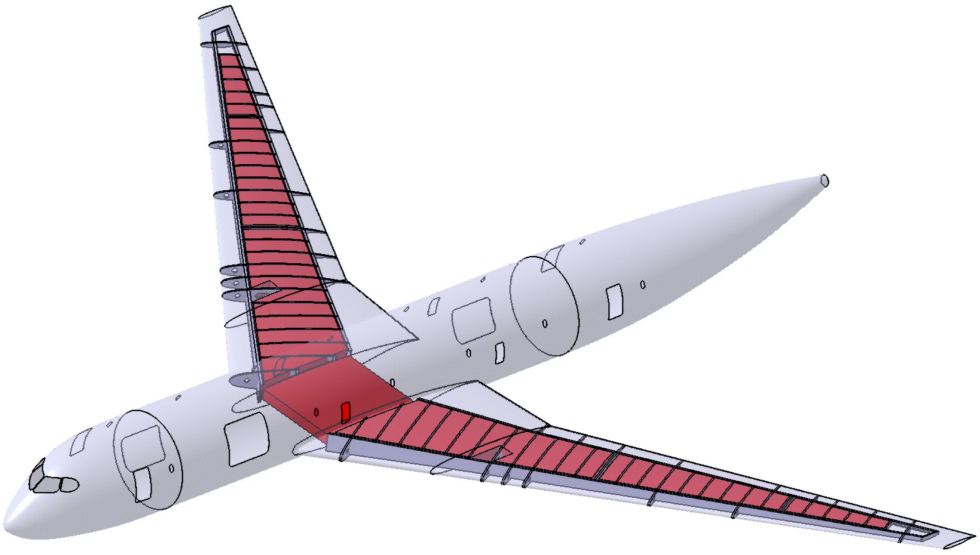

Figure 2.22: Fuel capacity (for perspective, fuel represented in red color)

2.10 Wing root fairing

Fairings are needed to define a smooth transition between the wing and the fuselage on the attachment point, as the main purpose of them is to decrease interference drag. A single piece is installed in the lower part of the fuselage at the center wingbox location.

The aircraft's wing root fairing is designed basing on variable-size ellipses, which will provide a surface which resembles closely the parabolic shape. Using the surface tools of Catia V5, the wing's fairings are defined as it is seen in Figures 2.23 and 2.24.

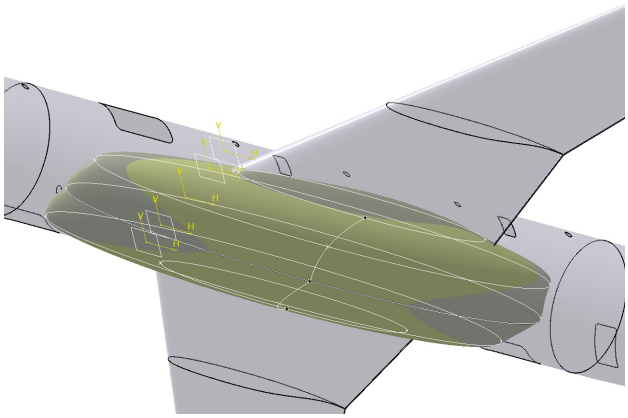

Figure 2.23: Wing's root fairing shape design using Catia V5

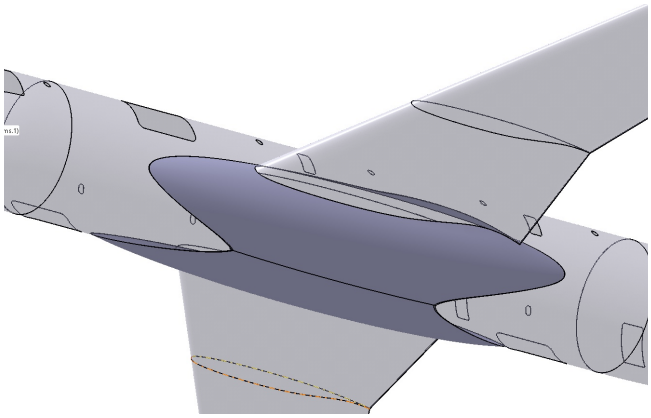

Figure 2.24: Wing's root fairing 3D model (solid)

In the same manner, flap track fairings are defined too (in addition to all the control surfaces), as it is seen in Figure 2.25:

Figure 2.25: Flap track fairings' 3D models

2.11 Wingtip devices

In the results of the aerodynamic analysis of the wing performed with Aeolus ASP, it was determined how the local induced drag coefficient starts to increase beyond a certain point of the wingspan, as a consequence of wingtip vortices (Figure 2.10 illustrates the induced drag distribution along the wingspan). Wingtip vortices are created as a consequence of the lift force.

Due to the pressure imbalance on the wing, the flow is forced from the high-pressure region of the wing (intrados) to the low-pressure region (extrados), causing a trailing vortex at the wingtip which induces a small downward velocity component and drags the surrounding air with it ([27], John Anderson, 2017, pp. 427-429).

One of the most effective manners to reduce induced drag is increasing the aspect ratio of the wings (as C_{Di} is inversely proportional to AR) but as it was mentioned previously, some balance must be maintained between the wing's weight, the structural reinforcement, ground operations and maneuvering and the aerodynamic efficiency.

Wingtip devices are used to decrease the lift-induced drag of the wing, mainly reducing the vortices' velocity. Several geometries have been purposed and used in the aviation industry over the years trying to improve the aerodynamic performance of aircraft. The optimal wingtip device's design parameters (angle, curvature, shape and size) are still not clear, but studies and aerodynamic simulations using Computational Fluid Dynamics software suggest that "feather" type winglets (those which resemble the ones installed on Boeing 737 MAX or Airbus A380, also called split-tip winglets) present one of the highest aerodynamic efficiency increases (up to 4-5 %) ([35], Nikola N. Gavrilović, Boško P. Rašuo, George S. Dulikravich, Vladimir B. Parezanović, 2014).

The winglet design of the aircraft is based on this specific type of winglets (resembling the ones which equips the A320ceo, seen in Figure 2.26). This specific type of wingtip device fulfills several interesting requirements for the aircraft which is being designed on this project: it will reduce the strength of wingtip vortices while maintaining a low weight and not increasing the overall wingspan.

Figure 2.26: Airbus A320 winglets (Sebastian Sowa, 2024)

Wingtip devices are defined using Catia V5 too. Figure 2.27 illustrates the complete design of the wingtips. In Figure 2.28, the winglets are seen in a side view, to provide a better perspective of them compared with the whole wing.

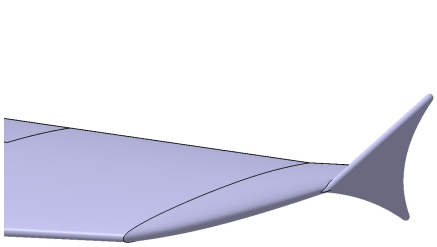

Figure 2.27: Wingtip device design (winglets)

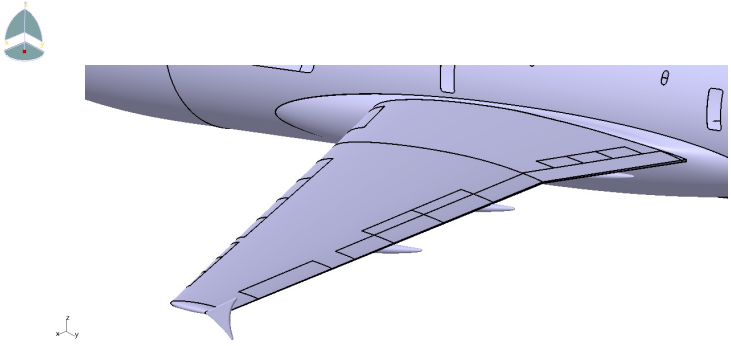

Figure 2.28: Wingtip device design (winglets), side view

2.12 Span efficiency factor calculation

The Oswald factor (e) is the span efficiency factor for a finite wing (being 1 the maximum achievable for planar wings, which corresponds to the elliptical lift distribution). The Oswald efficiency factor will also affect significantly the wing's induced drag coefficient (C_{Di}) and thus, the overall aerodynamic efficiency or finesse (L/D).

An approximation of the Oswald factor can be calculated basing on the wing's Aspect Ratio using Daniel Raymer's empirical expression, which is based on data obtained from actual aircraft. The equation is written below in Equation 2.4:

$$e \approx 1'78 \cdot (1 - 0'045 \cdot AR^{0'68}) - 0'64 = 1'78 \cdot (1 - 0'045 \cdot 10'14^{0'68}) - 0'64 = 0'753$$

Equation 2.4: Oswald factor empirical expression ([36], Daniel P. Raymer, 2006)

Chapter 3: Empennage design

This chapter describes the aircraft's empennage design process, where the horizontal and vertical stabilizers are defined, as well as the main empennage's structural arrangement and any other relevant element which is located in this section of the aircraft (such as the pitch trim system or the rear trim fuel tanks).

3.1 Weight, Center of Gravity and Aerodynamic Center calculation

The main purpose of the horizontal stabilizer and its control surfaces (the elevators) is to control the pitching moment of the aircraft. Either to climb, perform a descent maneuver or to maintain a level flight, the horizontal stabilizer is directly involved in those maneuvers.

For an appropriate design of the horizontal stabilizer, it is necessary to perform an estimation of the location of the aircraft's center of gravity. The weight estimation of the aircraft's components needs to be computed in order to obtain the location of the center of gravity. For this purpose, Jan Roskam's "*Class I Method for estimating airplane component weights*" will be used ([37], Jan Roskam, 1985, pp. 3-11, 152-175).

Making use of the group weight data presented in the book of jet transporters and similar military jet transports and applying the necessary corrections using a weighted average (as some components are intended to be manufactured in composite materials, such as the fuselage and the wings structural members), the weight estimations are calculated.

Note that the aircraft's MTOW was estimated previously to be 230,000 kg. Jan Roskam's method performs the calculations basing on the aircraft's flight design gross weight (GW), which will be assumed to be 95 % of the MTOW (218,500 kg, assuming a 5% of the total mass is fuel burnt to perform the takeoff and climb maneuvers).

Group weight estimation data:

Component	Component's weight / GW	Weight estimation
Wing group	0'0913	19,949'05 kg
Landing Gear group	0'039	8,521'5 kg
Empennage group	0'0197	4,304'45 kg
Power plant group	0'076	16,606 kg
Fuselage	0'0757	16,540'45 kg
Fixed equipment	0'175	38,237'5 kg
Nacelles	0'013	2,840'5 kg
Crew weight	0'00366	800 kg
		Σ = 107,799'45 kg

For calculations, it will be exemplified a scenario with a proper distribution of the payload in the aircraft, where 70,000 kg of fuel are accommodated in the fuel tanks and 40,000 kg of payload are being transported.

Initially, the center of gravity is calculated for the aircraft's operating weight (where no payload is loaded; but only the fuel estimated for the flight, the crew and the operating items).

The group components and its respective weights are drawn in the diagram presented in Figure 3.1. Each letter (A-K) in the Figure accounts for different masses and group components. The name of each respective component is listed too:

- ***A***: Nose landing gear: 1,704'3 kg
- ***B***: Fixed equipment (assumed to be equally distributed): 38,237'5 kg
- ***C***: Fuselage group + Crew: 17,340'5 kg
- ***D***: Nacelles + powerplant group: 19,446'05 kg
- ***E***: Wing group: 19,949'05 kg
- ***F***: Center fuel tank: 20,608 kg
- ***G***: Inner fuel tanks: 30,000 kg
- ***H***: Outer fuel tank: 18,000 kg
- ***I***: Surge tank: 1,392 kg
- ***J***: Main landing gear: 6,817'2 kg
- ***K***: Empennage group: 4,304'45 kg

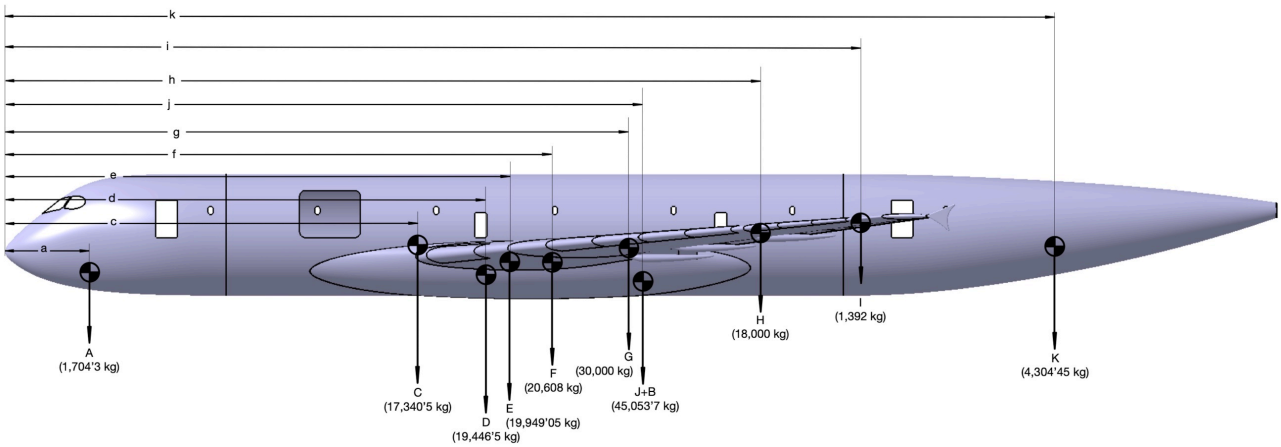

Figure 3.1: Group components' weights and locations

The lower case letters account for the distances measured from the front of the fuselage to each component. Their respective values are listed below:

- ***a***: 4'15 m
- ***c***: 20'28 m
- ***d***: 23'6 m
- ***e***: 24'77 m
- ***f***: 26'84 m
- ***g***: 30'59 m
- ***j***: 31'25 m
- ***h***: 37'06 m
- ***i***: 42'05 m
- ***k***: 51'53 m

The location of the center of gravity can be calculated adding the value of the moments produced by all the forces, which correspond to the weights of the aircraft's components. Setting an equation where the resultant force accounts for the sum of all the different weights, the location of the CG can be computed, taking as the pivot point the front of the fuselage:

$$R \cdot x_{CG} = A \cdot a + C \cdot c + D \cdot d + E \cdot e + F \cdot f + G \cdot g + (J + B) \cdot j + H \cdot h + I \cdot i + K \cdot k$$

$$R = \sum m = 1{,}704'3 + 17{,}340'5 + 19{,}446'5 + 19{,}949'05 + 20{,}608 + 30{,}000 + 45{,}053'7 + 18{,}000 + \\ + 1{,}392 + 4{,}304'45 = 177{,}798'5 \ kg$$

$$177{,}798'5 \cdot x_{CG} = 1{,}704'3 \cdot 4'15 + 17{,}340'5 \cdot 20'28 + 19{,}446'5 \cdot 23'6 + 19{,}949'05 \cdot 24'77 + \\ + 20{,}608 \cdot 26'68 + 40{,}000 \cdot 30'59 + 45{,}053'7 \cdot 31'25 + 8{,}000 \cdot 37'06 + 1{,}392 \cdot 42'05 + \\ 4{,}304'45 \cdot 51'53 = 5{,}069{,}778'947 \ kgf \cdot m$$

$$x_{CG} = \frac{5{,}069{,}778'947}{177{,}737'5} = 28'52 \ m$$

Equation 3.1: Center of gravity location (aircraft's operating weight)

For this scenario, the fuel is distributed in the following manner:

- Center tank: 100% of its capacity (20,608 kg of fuel)
- Inner tanks: 39'86% of its capacity (30,000 kg of fuel)
- Outer tanks: 84'97% of its capacity (18,000 kg of fuel)
- Surge tanks: 38'16% of its capacity (1,392 kg of fuel)

It is worth remarking that the distribution of the fuel volume along the wingspan is useful to control the location of the center of gravity. The purposed scenario considers a distribution where the majority of the mass is concentrated in the center and inner tanks and where the outer and surge tanks are used mainly for wing's bending alleviation.

Regarding the useful payload, the scenario used for calculations considers a total mass of 40,000 kg, as mentioned before, being half of it located in the upper deck and the remaining half in the lower deck of the fuselage. The upper deck payload is considered to be troops, uniformly distributed along the aircraft's interior (on the usable payload-loading zone). Figure 3.2 illustrates the payload's locations on the aircraft.

Lower case letters in the diagram, in the same manner, account for the distances measured from the front of fuselage to each payload component. Their respective values are listed below:

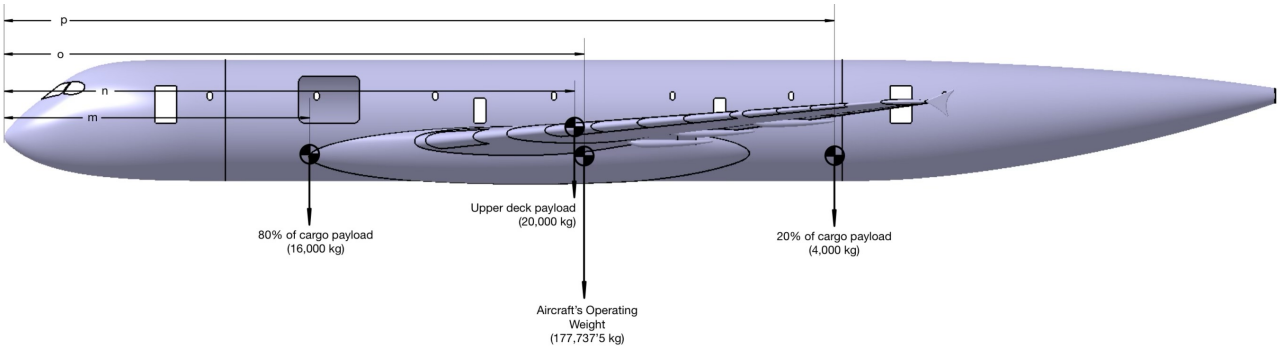

Figure 3.2: Usable payload components' weights and locations

The aircraft's center of gravity can be calculated, repeating the same process which was employed previously:

$$R \cdot x_{CG} = 16{,}000 \cdot m + 20{,}000 \cdot n + \cdot 177{,}737'5 \cdot o + 4{,}000 \cdot p$$

$$R = \sum m = 16{,}000 + 20{,}0000 + 177{,}737'5 + 4{,}000 = 217{,}737'5 \ kg$$

$$217{,}737'5 \cdot x_{CG} = 16{,}000 \cdot 14'9 + 20{,}000 \cdot 28 + 177{,}737'5 \cdot 28'5 + 4{,}000 \cdot 40'8 = 6{,}027{,}118'75 \ kgf \cdot m$$

$$x_{CG} = \frac{6{,}027{,}118'75}{217{,}737'5} = 27'68 \ m$$

Equation 3.2: Center of gravity location (flight design gross weight)

The center of gravity of the aircraft for the exemplified transport mission scenario would be located at a distance of 27,68 m from the front of the fuselage.

To verify the aircraft's longitudinal static stability, the position of the main wing's aerodynamic center is calculated in Figure 3.3:

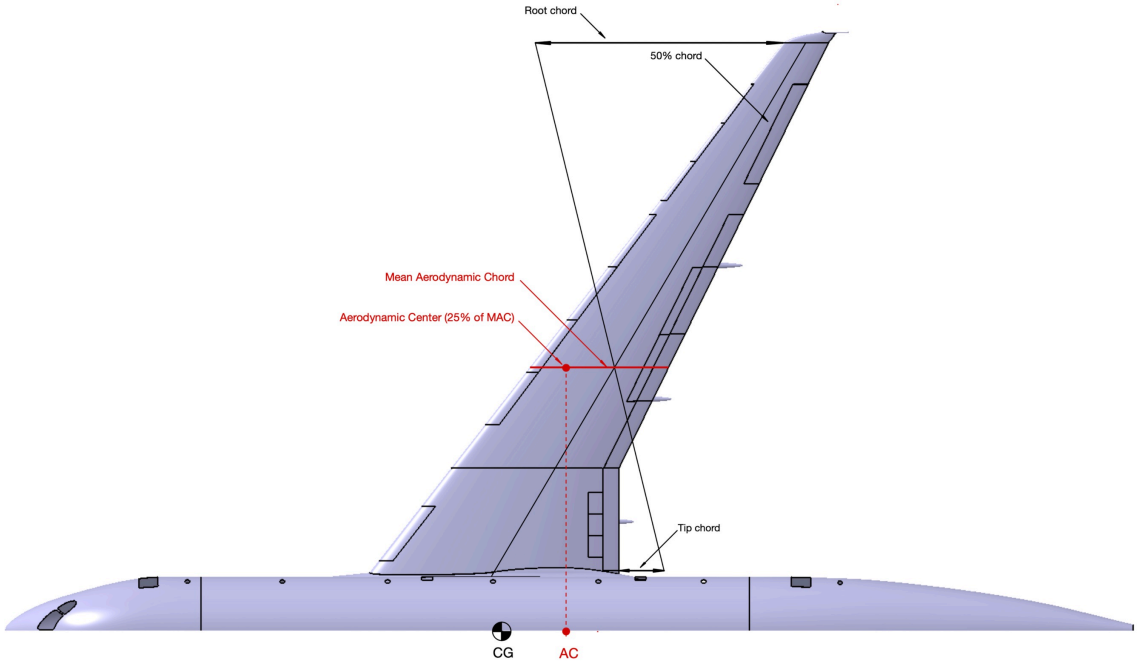

Figure 3.3: Aerodynamic center calculation

The aerodynamic center of the aircraft (AC) is located at a distance of 31’05 m from the from the front of the fuselage and the mean aerodynamic chord’s length has a value of 7’66 m. It is demonstrated then, for the purposed mission scenario, that the wing-tail combination will be unconditionally stable as the center of gravity is forward of the aerodynamic center of the main wing ([38], Warren F. Phillips, 2004, p. 356).

The aerodynamic center is defined as the point around which the pitching moment is constant and does not depend on the angle of attack (for a given airspeed), being highly convenient for stability calculations and force-and-moment diagrams ([27], John Anderson, 2017, pp. 331, 361).

3.2 Horizontal stabilizer design

The aircraft’s horizontal stabilizer, as mentioned previously, is responsible for controlling the aircraft’s pitching moment and is crucial to perform maneuvers such as climbing, descending or trimming the aircraft to maintain level flight. A conventional (tails aft) empennage layout is selected for the tanker aircraft, which is the most convenient as it presents the highest trimmed L/D value ([22], Jan Roskam, 1986, p. 251), as LT-018 will spend the majority of the flight time trimmed in cruise flight.

To minimize the wetted area, the product of the lift produced by the horizontal stabilizer and the moment arm must be maximized trying to increase as much as possible the moment arm. To calculate the horizontal (and vertical) stabilizer’s necessary area, “*Class I Method for empennage sizing and disposition*” will be applied, ([25], Jan Roskam, 1985, pp. 187-215). The necessary horizontal stabilizer’s area can be calculated using the V-method (tail volume coefficients), seen in Equation 3.3:

$$S_h = \frac{\bar{V}_h \cdot S \cdot \bar{c}}{x_h}$$

Equation 3.3: Horizontal stabilizer area definition using tail volume coefficients

$\bar{V}_h$ can be chosen basing on data for jet driven military patrol, bomb and transport airplanes which present similar configurations. In this case, the aircraft's data on the list which most resembles the tanker being designed is McDonell Douglas KC-10, which $\bar{V}_h$ is 0'89.

The wing area (S) was defined to be 420 m^2 and the mean aerodynamic chord's length ($\bar{c}$) was determined to be 7'66 m in section 3.1 of this same chapter. Using the location of the center of gravity which was calculated for the transport mission purposed in the previous section, the horizontal tail lever arm's length (x_h) is illustrated in Figure 3.4, basing on the expected future location of the horizontal stabilizer.

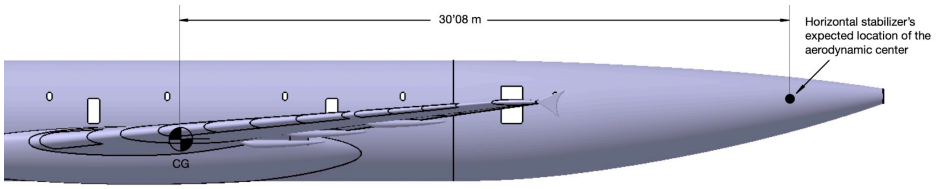

Figure 3.4: Horizontal tail lever arm's length (x_h)

Substituting in Equation 3.3, the resultant horizontal stabilizer's area is calculated:

$$S_h = \frac{\bar{V}_h \cdot S \cdot \bar{c}}{x_h} = \frac{0'89 \cdot 420 \cdot 7'66}{30'08} = 95'19\ m^2$$

The necessary horizontal stabilizer's lift force to trim the aircraft for steady level flight needs to be determined to select an appropriate airfoil. Making use of the software Aeolus ASP again, the location of the center of pressure of the main wing can be calculated for cruise flight conditions:

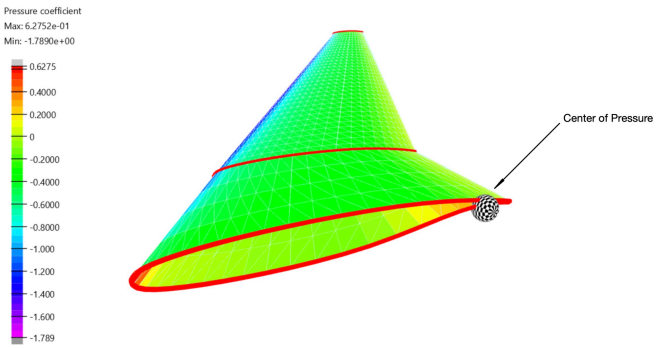

Figure 3.5: Center of pressure location at cruise flight

The software determines the location of the center of pressure for level flight at cruise conditions at a distance of 12'8 m from the leading edge of the wing. The lift force is then represented at the mean aerodynamic center adding the wing's pitching moment (M_{ac}), illustrated in Figure 3.6. The distance between the center of pressure and the aerodynamic center (d) has a value of 2'5 m.

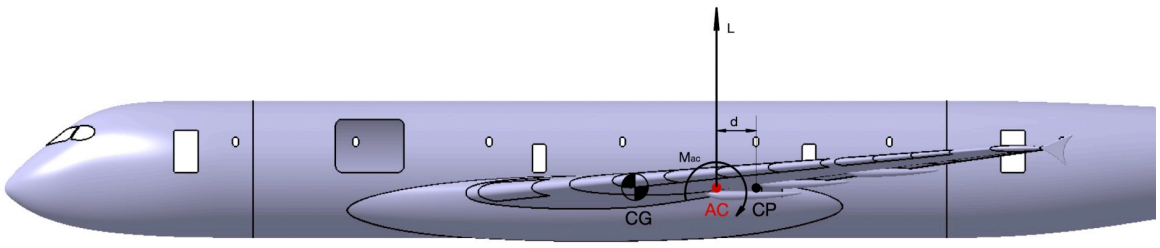

Figure 3.6: Lift force and moment diagram about the aerodynamic center

The value of M_{ac} can be calculated according to Equation 3.4:

$$M_{ac} = L \cdot d = 218{,}500 \cdot 2'5 = 546{,}250\ kgf \cdot m = 5{,}358{,}712'5\ N \cdot m$$

Equation 3.4: Pitching moment about the aerodynamic center

The wing and tail combination can be studied to determine the necessary amount of lift which needs to be produced by the horizontal stabilizer. Note that the pitching moment about the horizontal stabilizer's aerodynamic center is not considered, as its value can be neglected compared to that of the main wings' pitching moment about the aerodynamic center.

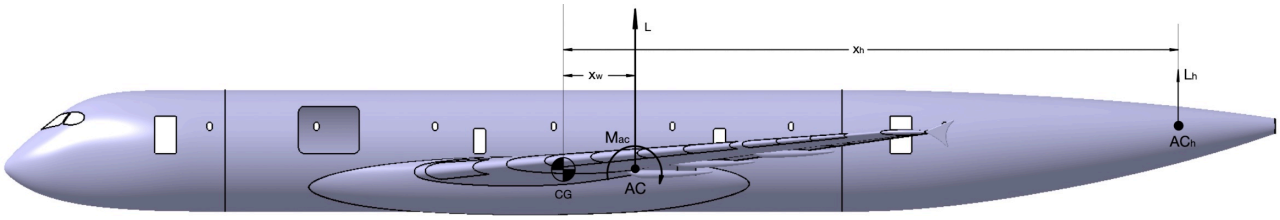

Figure 3.7: Wing and tail combination forces diagram

$$\sum M = 0;\ L \cdot x_w + M_{ac} + L_h \cdot x_h = 0;\ 218{,}500 \cdot 9'81 \cdot 3'37 + 5{,}358{,}712'5 + L_h \cdot 30'08 = 0$$

$$7{,}223{,}544'45 + 5{,}358{,}712'5 + L_h \cdot 30'08 = 0;\ L_h = \frac{-7{,}223{,}544'45 - 5{,}358{,}712'5}{30'08} =$$

$$= -418{,}293'12\ N$$

Equation 3.5: Horizontal stabilizer's lift force calculation

A total lift force of 418,293'12 N downwards (42,639'46 kgf) is needed to trim the aircraft in cruise at steady level flight. The necessary horizontal stabilizer's lift coefficient (C_{Lh}) can be calculated applying the lift equation for the same cruise conditions:

$$L_h = \frac{1}{2} \cdot C_{L_h} \cdot S_h \cdot \rho_\infty \cdot u_\infty^2;\ C_{L_h} = \frac{2 \cdot L_h}{S_h \cdot \rho_\infty \cdot u_\infty^2} = \frac{2 \cdot 418{,}293'12}{95'19 \cdot 0'379597 \cdot 237'2^2} = 0'41$$

Equation 3.6: Horizontal stabilizer's lift coefficient calculation

To select an appropriate airfoil, considerations on the critical Mach number need to be taken into account too, as it is higher in the horizontal stabilizer compared to the main wings. The thickness ratio (t/c) selected is 0'1, the same that the wings' airfoil present. Regarding the quarter chord sweep angle ($\Lambda_{c/4}$), its value for the horizontal stabilizer is selected to be 37° (basing on the graph presented previously in Figure 2.2), where an increment of ΔM=0'05 in the critical Mach number is considered, sufficient to define it ([25], Jan Roskam, 1985). Note that the airfoil is inverted to produce an upwash and thus, create a resultant lift force downwards.

A slightly cambered airfoil which presents a maximum thickness ratio of 0'1 is chosen. In this case, NACA 1410, illustrated in Figure 3.8:

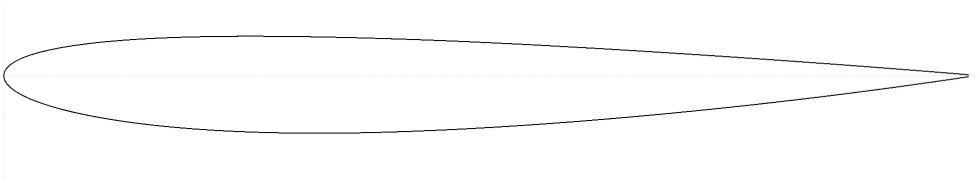

Figure 3.8: NACA 1410 airfoil

The most relevant parameters of NACA 1410 are listed below:
- Maximum thickness: 10%
- Maximum camber: 1%
- Maximum camber location: 40% of the chord

The elevator chord is sized to be 0'3 of the airfoil's chord length, which is the average value present in military patrol, bomb and transport airplanes ([25], Jan Roskam, 1985, p. 201). The dihedral angle is kept the same than the main wing's one. Considering the mentioned design constraints, the planform of the horizontal stabilizer is illustrated in Figure 3.9. The location of the mean aerodynamic center of the horizontal stabilizer is calculated in Figure 3.10, which will be used to locate it properly on its desired location in the 3D model of the aircraft's assembly.

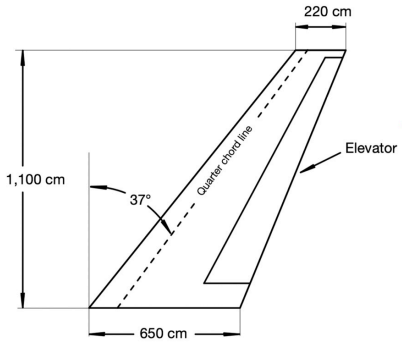

Figure 3.9: Horizontal Stabilizer planform design

Horizontal stabilizer design parameters	
Semi-wing span (m)	11
Semi-wing area (m^2)	47'85
Aspect Ratio (total)	5'06
Taper ratio λ	0'34
Quarter chord sweep $\Lambda_{c/4}$	37°
Root chord (m)	6'5
Tip chord (m)	2'2

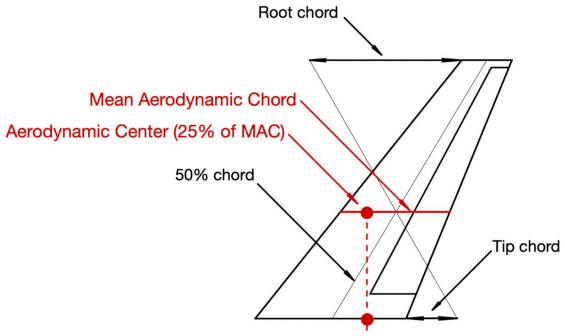

Figure 3.10: Horizontal stabilizer's Aerodynamic Center location calculation

The aerodynamic center of the horizontal stabilizer is located at a distance of 4'82 m from the leading edge of the root chord.

3.3 Vertical stabilizer design

The vertical stabilizer's function is to control the aircraft's yawing moment. The most critical design variable of the vertical stabilizer is the engine-out condition, meaning that if one of the engines becomes inoperative, the vertical stabilizer and the rudder must be able to counteract the yawing moment produced by the operative engine. When using the V-method to calculate the volume coefficient of the vertical stabilizer, care must be taken that the lateral disposition of the engines is not too dissimilar than the reference which is going to be used ([25], Jan Roskam, 1985, p. 190).

Even though the engines of the aircraft have not been decided and/or studied at this point of the design, their approximate position is known and was shown previously in the project when the main wings' high-lift devices and the control surface arrangement was designed (see Figure 2.11).

Moreover, similar wide-body aircraft can be used as a reference for the vertical stabilizer design process. The aircraft's engines will be located at a distance of 10 m approximately from the symmetry plane of the fuselage. From the data of tail volume coefficients presented by Jan Roskam, the jet transporter which engines' position resemble the most to LT-018 is Boeing 767 (having a lateral distance from the engines to center of gravity of approximately 8 m) ([39], Boeing, 2021, p. 2-2). Its respective vertical tail volume coefficient ($\bar{V}_v$) is 0'067.

Considering the other aircraft's data and applying the necessary corrections, a tail volume coefficient of 0'083 would be suitable for the aircraft which is being designed. The vertical stabilizer's area is calculated according to Equation 3.7:

$$S_v = \frac{\bar{V}_h \cdot S \cdot b}{x_v}$$

Equation 3.7: Vertical stabilizer area definition using tail volume coefficients

The wingspan (b) has a value of 64'9 m (considering the fuselage too). The value of the vertical tail lever arm's length (x_v) is illustrated in Figure 3.11, which is positioned using as a reference similar actual wide-body aircraft:

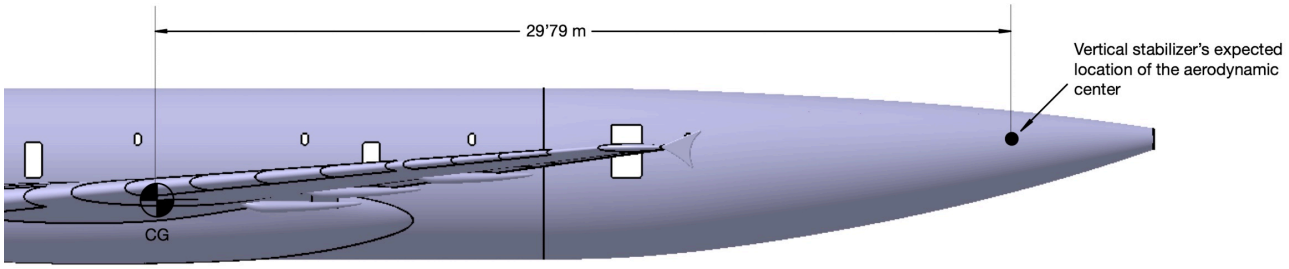

Figure 3.11: Vertical tail lever arm's length (x_v)

Substituting all data in Equation 3.7, the value of the vertical stabilizer's area is calculated:

$$S_v = \frac{\bar{V}_h \cdot S \cdot b}{x_v} = \frac{0'083 \cdot 414 \cdot 64'9}{29'79} = 74'86\ m^2$$

The quarter chord sweep angle ($\Lambda_{c/4}$) is increased to 48º, not only for an aesthetic reason, but also because it will provide an aerodynamic effectiveness closest to the optimum one ([22], Jan Roskam, 1986, p. 260). The thickness ratio (t/c) is kept identical to the horizontal stabilizer and the wing's one (0'1). For the vertical stabilizer, a symmetrical airfoil is selected: NACA 0010, illustrated in Figure 3.12.

Figure 3.12: NACA 0010 airfoil

The average rudder chord is sized to be 0'39 of the airfoil's chord length, slightly higher than the average values shown in Jan Roskam's data of jet transports (0'35), as the location of LT-018 engines is further from the fuselage's plane of symmetry than in any of them.

The planform of the vertical stabilizer, as well as its design parameters are illustrated in Figure 3.13. The location of the mean aerodynamic center of the vertical stabilizer is calculated in Figure 3.14, which will be used to locate it properly on its desired point in the aircraft's assembly too.

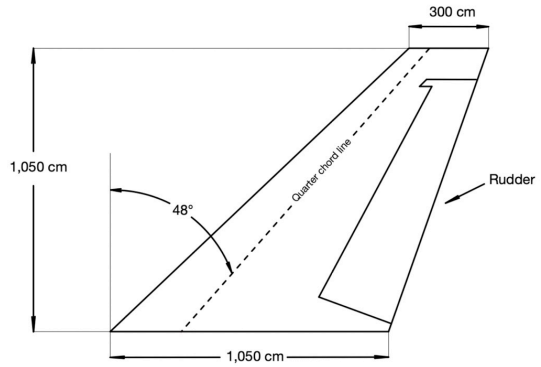

Figure 3.13: Vertical Stabilizer planform design

Vertical stabilizer design parameters	
Span (m)	10'5
Area (m^2)	70'88
Aspect Ratio	6'22
Taper ratio λ	0'285
Quarter chord sweep $\Lambda_{c/4}$	48º
Root chord (m)	10'5
Tip chord (m)	3

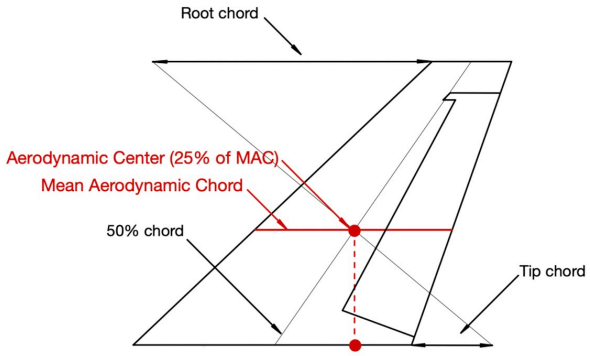

Figure 3.14: Vertical stabilizer's Aerodynamic Center location calculation

The aerodynamic center of the horizontal stabilizer is located at a distance of 8'22 m from the leading edge of the root chord.

3.4 Tail assembly

3D models of the vertical and horizontal stabilizers are created too in Catia V5, to be included in the aircraft's assembly. Following a similar process than that which was used for the wings' definition, the airfoils (NACA 0010 & NACA 1410) are imported in the software, scaled and translated to be located on its correct positions to define the sweep and dihedral angles.

The aircraft's horizontal and vertical stabilizers' surfaces are defined then, as it is illustrated in Figure 3.15:

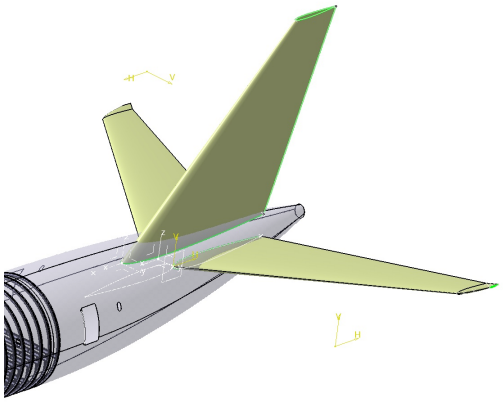

Figure 3.15: Vertical & horizontal stabilizers' surface definition in Catia V5

The vertical stabilizer's attachment point to the fuselage is modified to create a smoother transition (the dorsal fin, circled in red in Figure 3.16), mainly to reduce interference drag. Surfaces are then transformed to solid bodies and the control surfaces are defined. The main result is shown in Figure 3.17.

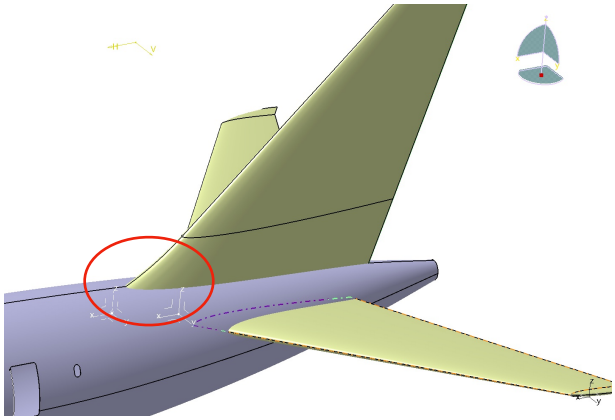

Figure 3.16: Dorsal fin surface definition

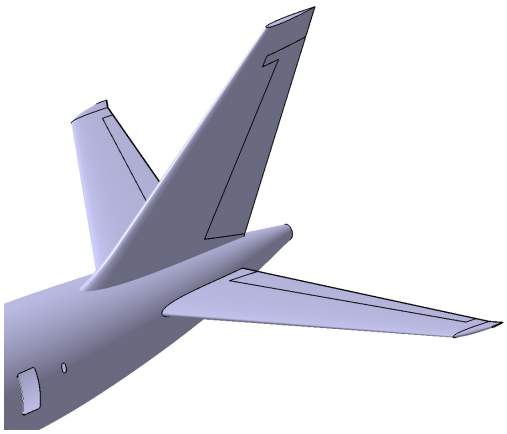

Figure 3.17: Empennage 3D model in Catia V5

3.5 Structural arrangement

Several members form the whole empennage's structural arrangement. Regarding the fuselage, the same arrangement of frames, floor struts and spars will extend along the pressurized cabin, ending in the rear pressure bulkhead. Beyond the rear pressure bulkhead and up to the end of the fuselage (unpressurized zone and where no payload is accommodated), frames will define the tailcone's shape and will allow the assembly of the vertical stabilizer, the horizontal stabilizer's wingbox and the fuselage.

The horizontal stabilizer's structure is similar to the one of the wing. Two spars and are defined, which combined with the upper and lower skin form the torque box. 18 ribs per semi-wing are placed perpendicular to the rear spar with a rib pitch of 61 cm, similar to the average horizontal stabilizer's rib pitch used in jet transport aircraft ([22], Jan Roskam, 1986, p. 277). Figure 3.18 shows the main structural arrangement of the horizontal stabilizer.

In the case of the vertical stabilizer, a front and rear spar combined with the lateral skins will form the torque box too. The spars are mechanically attached to the upper side of the tailcone's frames. 21 ribs with a rib pitch similar to the one defined in the horizontal stabilizer (61 cm) and secondary ribs placed perpendicular to the tailcone's fuselage frames define the shape of the vertical stabilizer and the dorsal fin. Figure 3.19 illustrates the main structural arrangement of the vertical stabilizer.

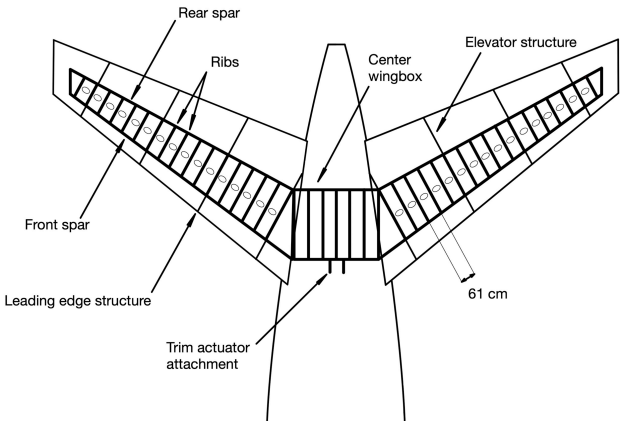

Figure 3.18: Horizontal stabilizer structural arrangement

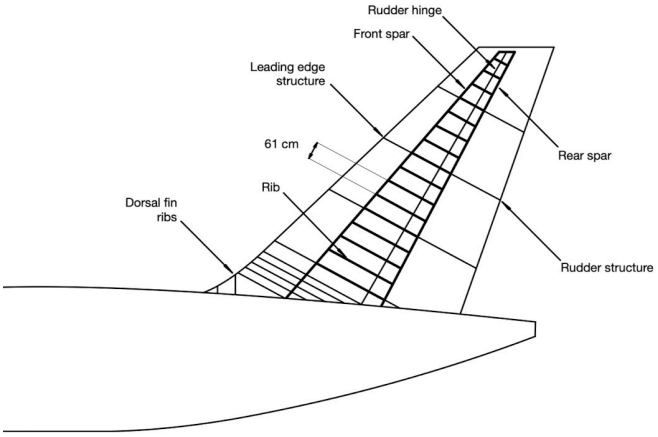

Figure 3.19: Vertical stabilizer structural arrangement

Regarding the position of the spars of both the vertical and horizontal stabilizers, the front one is located at the quarter chord line (25% of the chord length) and the rear one next to its respective control surfaces (rudder and elevators). 3D models of the structure are built as well. The following figures illustrate and describe the main components of the aircraft's empennage structure:

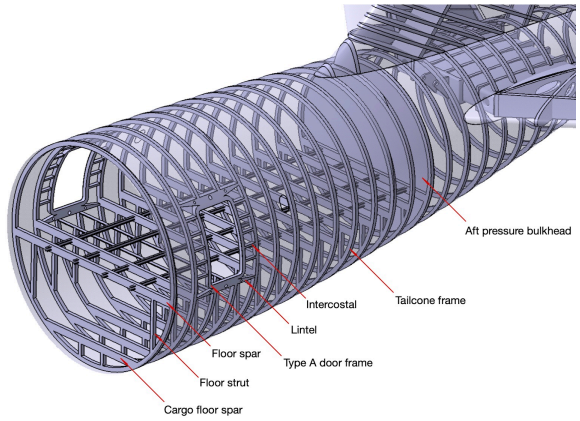

Figure 3.20: Empennage tailcone structural members

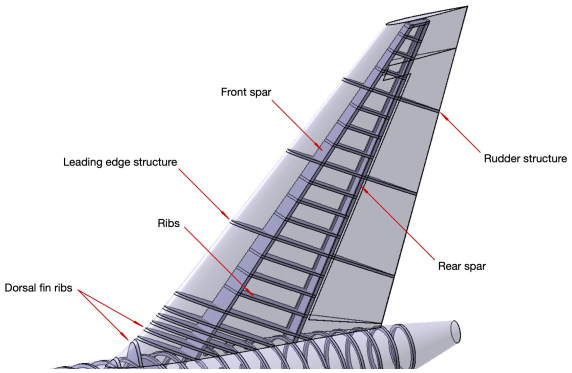

Figure 3.21: Vertical stabilizer structural assembly

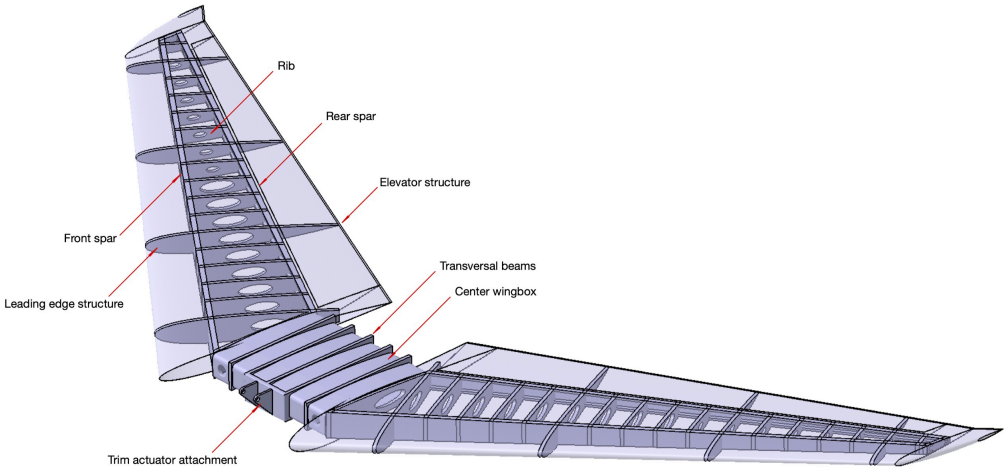

Figure 3.22: Horizontal stabilizer structural assembly

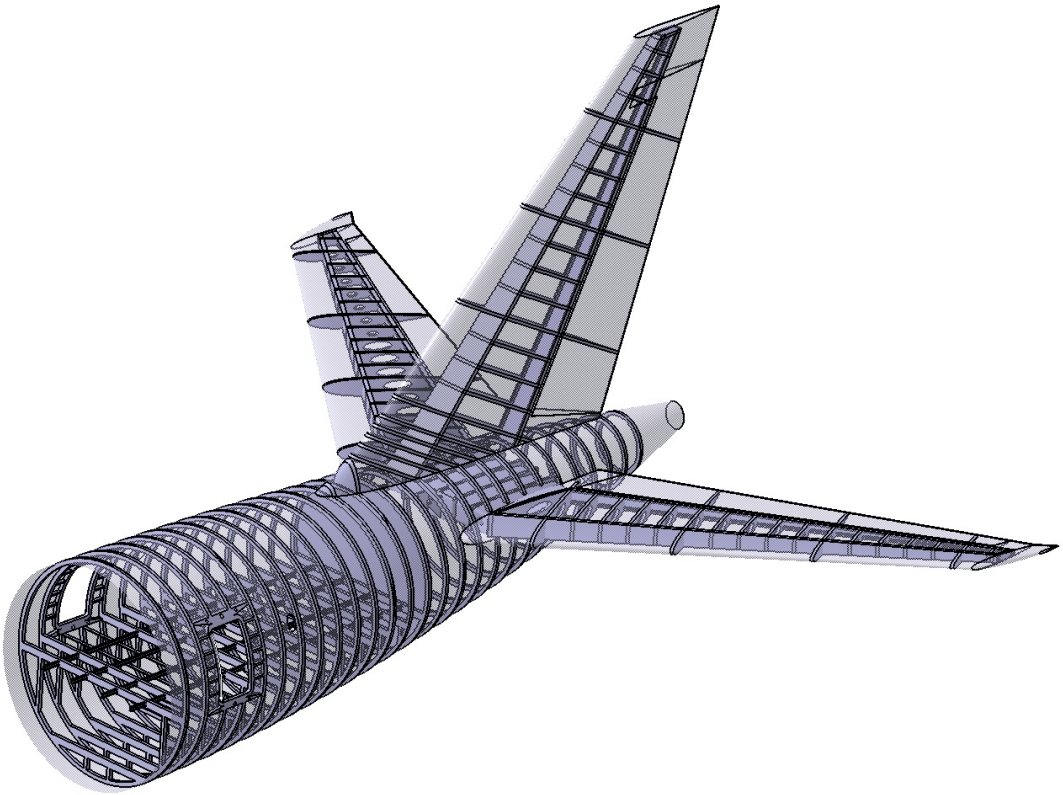

Figure 3.23: Complete empennage structural assembly

3.6 Longitudinal stability: trim condition

During cruise flight and especially during aerial refueling operations, the aircraft must remain as steady as possible. When the aircraft's controls are set in a manner that the resultant forces and moments about the center of gravity are zero, the aircraft is said to be in trim (static equilibrium) ([38], Warren F. Phillips, 2004, p. 339). As it was studied in section 3.2, it is the main function of the horizontal stabilizer to be able to maintain a level flight. To achieve this purpose, a downwards lift force is generated, as it was calculated previously.

But there are different phases during the flight in which the aircraft's mass and center of gravity location vary and move. For example, for LT-018, the fuel stored in the aircraft's wing tanks "pulls" the center of gravity aft and it will tend to move forward as the fuel burns. Payload movement inside the upper deck of the aircraft or fuel transfer during aerial refueling will also vary the position of the center of gravity. For that reason, the amount of lift force that the horizontal stabilizer must exert is not fixed and varies throughout all the stages of flight.

There are three main design solutions to counteract this issue and maintain the aircraft trimmed at any moment of the flight. The first one consists in varying the elevator's deflection angle to modify the camber of the horizontal stabilizer's airfoil, producing the desired amount of lift necessary to trim the aircraft. This design solution is usually used in small light aircraft.

The second approach, widely used in large aircraft, consists in varying the angle of attack of the whole horizontal stabilizer by means of an actuator, as the ΔC_{Lh} needed is too large to be attained just by elevator deflections. Moreover, this approach removes structural stress from the elevator's actuator pivot point and generally reduces drag as well.

The third approach is sometimes used in large aircraft (Boeing 747, Airbus A330 or even Concorde, for example), as the necessary lift force to trim the aircraft is usually quite high. To avoid the increase of the horizontal stabilizer's angle of attack to produce more lift (which as a result will produce a higher amount of induced drag), fuel is transferred during flight to rear trim tanks, located usually at the tailcone or inside the horizontal stabilizer's wingbox. As a consequence, the center of gravity of the aircraft will be pulled aft, reducing the distance between the aerodynamic center and the center of gravity, what will lead to a reduction in the pitching moment and thus, a reduction in the necessary downwards lift force that the horizontal stabilizer needs to exert ([40], Lewis Boyd, 2008, pp. 1-5).

LT-018 equips two different independent but correlated methods to achieve the trim condition: a pitch trim system consisting in an actuator to modify the whole horizontal stabilizer's angle of attack and a rear trim fuel tank to transfer fuel as the flight progresses, making use of its large tail members. Both systems are intended to trim the aircraft in the most efficient possible manner (always trying to reduce the horizontal stabilizer's lift force as much as possible).

Maintaining the same payload transport case which was raised previously for the center of gravity calculations, it was determined that the necessary horizontal stabilizer's lift force to trim the aircraft in cruise for the aircraft's flight design gross weight is 418,293'12 N (without taking into consideration the displacement of fuel volume to the rear trim tank).

To calculate the lift reduction that the rear trim tank will produce, it is necessary to define previously the rear trim tanks. Following the same approach than for the main wing fuel tanks, the fuel volume is calculated in Catia using the "*Measure Inertia*" tool.

Rear main trim tanks: located in the center wingbox and in the left and right semi-wings (limited by ribs 15 and 11 respectively).
- Fuel capacity of 11'72 m^3 (11,720 L), which corresponds to 9,376 kg of jet fuel.

Rear trim surge tank: located at the outer part of the left semi-wing (limited by ribs 11 and 15).
- Fuel capacity of 0'33 m^3 (330 L), which corresponds to 211'2 kg of jet fuel.

Figure 3.24 illustrates the horizontal stabilizer and the fuel inside the torque box (represented in red color):

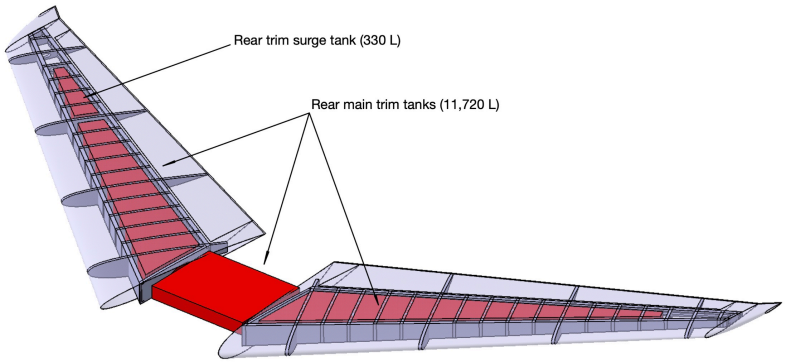

Figure 3.24: Rear trim fuel tanks (fuel represented in red color)

Calculations on the center of gravity position and the necessary lift force are computed again, assuming that fuel from the wing's center fuel tank is transferred to fill completely the trim tanks (9,587'2 kg of fuel). The resultant new force diagram and the CG position variation calculation is developed in the following paragraphs.

Figure 3.25 illustrates the force diagram once the rear trim tanks have been filled. 45% of the center fuel tank's mass ("F") is transferred to the rear trim tanks, which is represented with the letter "L" in the force diagram, at a distance "*l*" (57'68 m). The rest of the values and distances are kept identical to the diagram built previously in Figure 3.1.

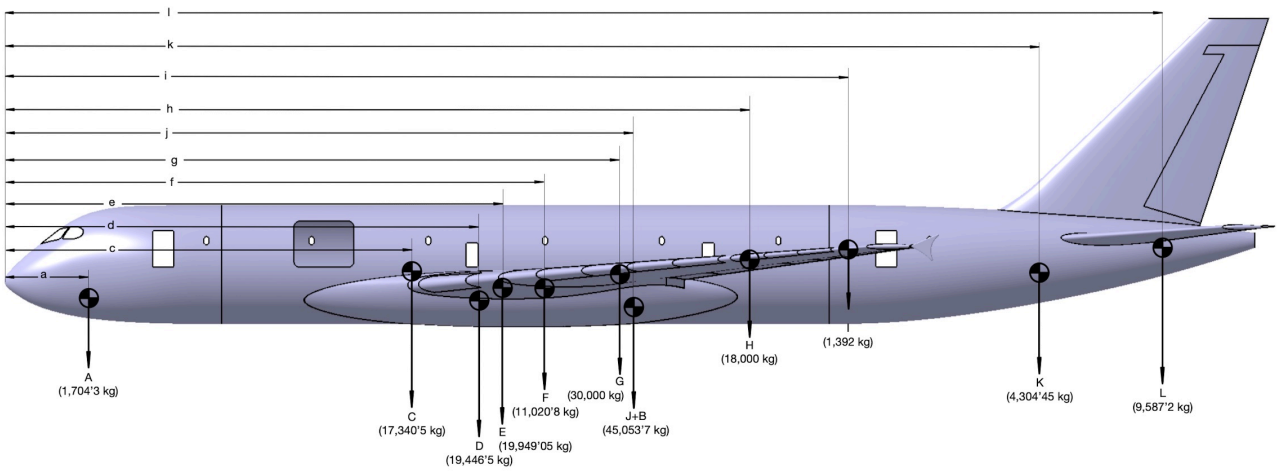

Figure 3.25: Group components' weights and locations (adding the rear trim tanks)

$$R \cdot x_{CG} = A \cdot a + C \cdot c + D \cdot d + E \cdot e + F \cdot f + G \cdot g + (J + B) \cdot j + H \cdot h + I \cdot i + K \cdot k + L \cdot l$$

$$R = \sum m = 1{,}704'3 + 17{,}340'5 + 19{,}446'5 + 19{,}949'05 + 11{,}020'8 + 30{,}000 + 45{,}053'7 + 18{,}000 + \\ + 1{,}392 + 4{,}304'45 + 9{,}587'2 = 177{,}798'5 \ kg$$

$$177{,}798'5 \cdot x_{CG} = 1{,}704'3 \cdot 4'15 + 17{,}340'5 \cdot 20'28 + 19{,}446'5 \cdot 23'6 + 19{,}949'05 \cdot 24'77 + \\ + 11{,}020'8 \cdot 26'68 + 40{,}000 \cdot 30'59 + 45{,}053'7 \cdot 31'25 + 8{,}000 \cdot 37'06 + 1{,}392 \cdot 42'05 + \\ 4{,}304'45 \cdot 51'53 + 9{,}587'2 \cdot 57'68 = 5{,}367{,}188'227 \ kgf \cdot m$$

$$x_{CG} = \frac{5{,}069{,}778'947}{177{,}737'5} = 30'18\ m$$

Equation 3.8: Center of gravity location (aircraft's operating weight, rear trim tanks filled)

If the payload distribution is not modified, the location of the center of gravity is calculated in the same manner, taking into consideration the previous position of the CG for the aircraft's operating weight which was calculated:

$$R = \sum m = 16{,}000 + 20{,}0000 + 177{,}737'5 + 4{,}000 = 217{,}737'5\ kg$$

$$217{,}737'5 \cdot x_{CG} = 16{,}000 \cdot 14'9 + 20{,}000 \cdot 28 + 177{,}737'5 \cdot 30'18 + 4{,}000 \cdot 40'8 = 6{,}325{,}717'75\ kgf \cdot m$$

$$x_{CG} = \frac{6{,}325{,}717'75}{217{,}737'5} = 29'05\ m$$

Equation 3.9: Center of gravity position variation (flight design gross weight, rear trim tanks filled)

The stability condition for the wing-tail combination is not altered, as the center of gravity is still in front of the aerodynamic center. Finally, the reduction on the lift force exerted by the horizontal stabilizer can be calculated. Note that the pitching moment about the aerodynamic center (M_{ac}) is constant and does not vary. On the contrary, the main wing lever arm's length (x_w) is reduced from 3'37 m to 2 m.

$$\sum M = 0;\ L \cdot x_w + M_{ac} + L_h \cdot x_h = 0;\ 218{,}500 \cdot 9'81 \cdot 2 + 5{,}358{,}712'5 + L_h \cdot 30'08 = 0$$
$$4{,}286{,}970 + 5{,}358{,}712'5 + L_h \cdot 30'08 = 0;\ L_h = \frac{-4{,}286{,}970 - 5{,}358{,}712'5}{30'08} =$$
$$= -320{,}667'64\ N$$

Equation 3.10: Horizontal stabilizer's lift force calculation (rear trim tanks filled)

$$L_h = \frac{1}{2} \cdot C_{L_h} \cdot S_h \cdot \rho_\infty \cdot u_\infty^2;\ C_{L_h} = \frac{2 \cdot L_h}{S_h \cdot \rho_\infty \cdot u_\infty^2} = \frac{2 \cdot 320{,}667'64}{95'19 \cdot 0'379597 \cdot 237'2^2} = 0'31$$

Equation 3.11: Horizontal stabilizer's lift coefficient calculation (rear trim tanks filled)

The necessary lift coefficient to trim the aircraft in cruise conditions is reduced by 24'39% (0'41 vs 0'31). This will result in a significant reduction in induced drag produced by the horizontal stabilizer during cruise, as it increases with the square of C_L. The induced drag coefficient (C_{Di}) is defined as:

$$C_{D_i} = \frac{C_L^2}{\pi \cdot AR \cdot e}$$

Equation 3.12: Induced drag coefficient equation

Approximating the value of the Oswald efficiency factor using Daniel Raymer's equation again (seen previously in section 2.12), the reduction in induced drag can be calculated for the horizontal stabilizer:

$$e \approx 1'78 \cdot (1 - 0'045 \cdot AR^{0'68}) - 0'64 = 1'78 \cdot (1 - 0'045 \cdot 5'06^{0'68}) - 0'64 = 0'898$$

Equation 3.13: Oswald factor empirical expression ([36], Daniel P. Raymer, 2006)

$$C_{D_i} = \frac{C_L^2}{\pi \cdot AR \cdot e} = = \frac{0'41^2}{\pi \cdot 5'06 \cdot 0'898} = 0'0117758$$

Equation 3.14: Induced drag coefficient equation (rear trim tanks empty)

$$C_{D_i} = \frac{C_L^2}{\pi \cdot AR \cdot e} = = \frac{0'31^2}{\pi \cdot 5'06 \cdot 0'898} = 0'0067320$$

Equation 3.15: Induced drag coefficient equation (rear trim tanks filled)

The amount of induced drag produced by the horizontal stabilizer is reduced by 42'83 % making use of the rear trim tanks at cruise conditions for the aircraft's flight design gross weight and the payload transport mission scenario purposed.

The necessary angle of attack in the horizontal stabilizer for the aircraft to be trimmed in cruise flight can be calculated using Aeolus ASP software again. Considering that the rear trim tanks are being used, the lift coefficient needed is C_{Lh} = 0'31. The horizontal stabilizer is modeled in the software in the same manner than the wing, to perform an aerodynamic analysis setting the cruise conditions. Maintaining the same cruise conditions than those which were set for the main wing analysis, the analysis is performed.

For this specific section, the only result of interest is the C_L-α graph, to find the necessary horizontal stabilizer's angle of attack to trim the aircraft. The graph plotted by the software is illustrated in Figure 3.27:

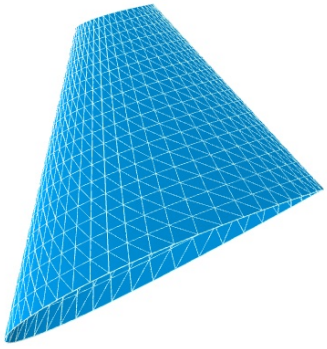

Figure 3.26: Horizontal stabilizer modeled in the software

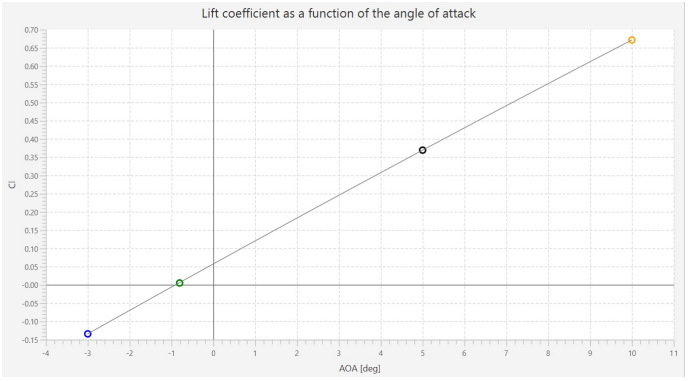

Figure 3.27: C_L-α graph for the horizontal stabilizer

The necessary lift coefficient to trim the aircraft in cruise flight conditions (0'31) is achieved at an angle of attack of α=-4° (relative to the freestream). The pitch trim system acts by means of an electric trim actuator located in the tailcone of the aircraft, which spins a jackscrew to control the angle of attack of the whole horizontal stabilizer.

Figure 3.28 illustrates the aircraft's pitch trim system actuator:

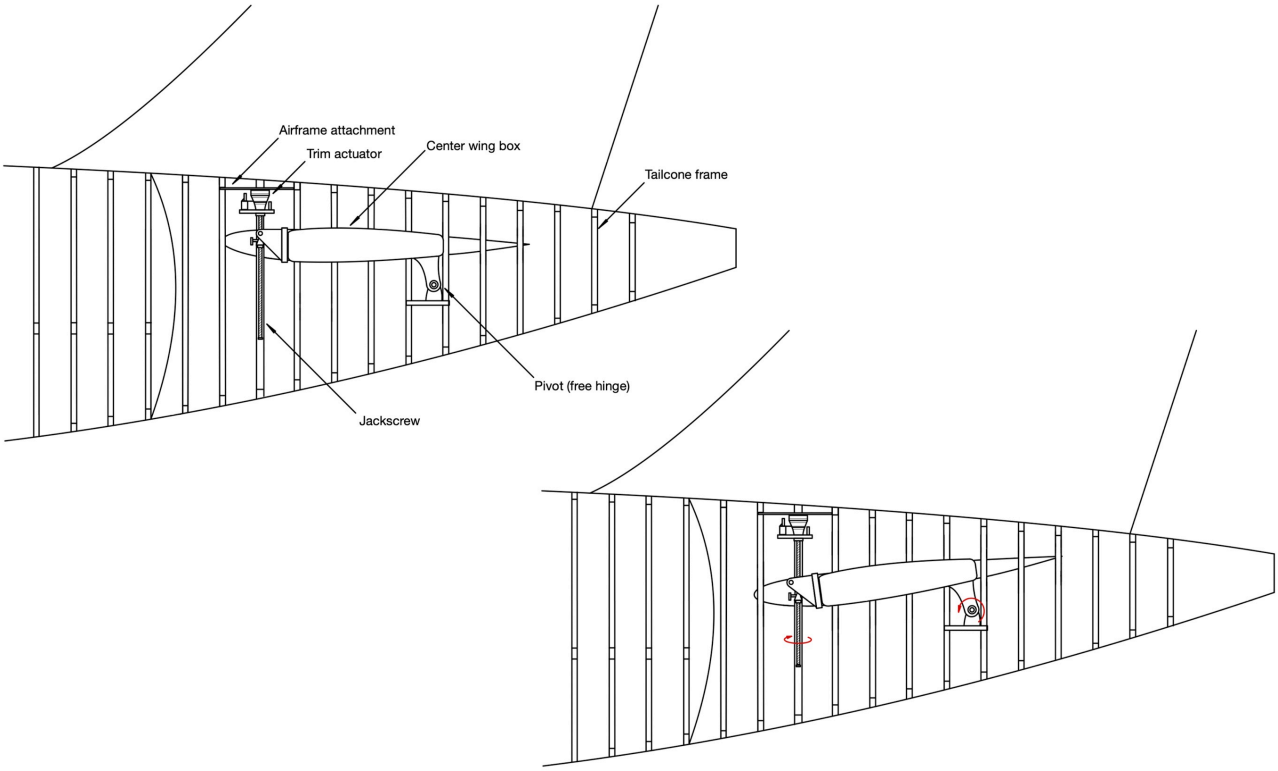

Figure 3.28: Pitch trim system actuator mechanism

Chapter 4: Aerial Refueling Systems

This chapter describes the aerial refueling systems' design and layout. Its overall design process, devices, locations and dimensions are developed and explained in detail.

As it occurs with currently operating tanker aircraft, different systems are installed to perform aerial refueling. Some of them are used independently but configurations can be made where several of them operate simultaneously.

4.1 Aerial refueling wing pods

Wing pods are one of the various systems which tanker aircraft use to perform aerial refueling. Thy are usually removable and placed under the wings of the tanker aircraft. Three major components make it possible for this system to function properly: the fuel boost pump, the hose and the drogue.

Wing pods are connected to the tanker's wing fuel tanks, from where they obtain the necessary fuel to be delivered to receiver aircraft. Inside the wing pod structure, a fuel boost pump is the main responsible of pumping fuel through the hose. The fuel pump can operate making use of the aircraft's power, but it is usually self-powered by means of a ram air turbine located at the front of it, facing the freestream (ram air turbines [RAT] are devices which equip propellers and are able to extract power from the airstream when they rotate, to feed electric or hydraulic systems) ([41], Collins Aerospace, 2024).

The hose is usually maintained rolled in the hose drum inside the wing pod during maneuvers like takeoff or landing. When aerial refueling is going to take place, the hose is unrolled and completely deployed, ending in a drogue assembly to perform aerial refueling by means of the probe and drogue system. The following figure illustrates the most relevant components of a real aerial refueling wind pod:

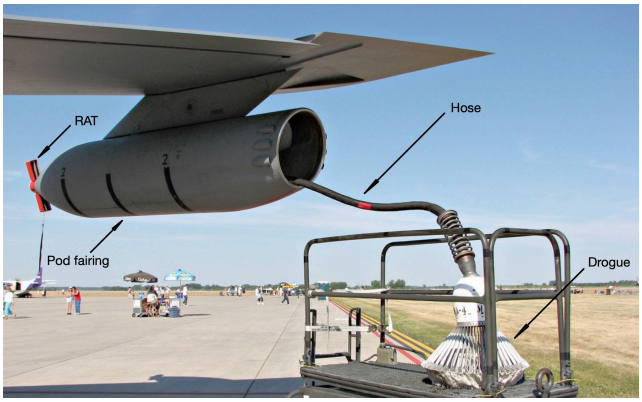

Figure 4.1: Aerial refueling wing pod
(Raunak Kunde, 2022)

The most relevant design parameters to consider for the wing pods are their shape and size. An efficient aerodynamic shape is important, in this case, to perturb the airflow as little as possible and create as little induced drag as possible. Additionally, they must be designed to be narrow to minimize their wetted area and thus, achieve the minimum possible parasitic drag.

A parabolic shape is chosen for the front part of the wing pod. The rear part of it presents a cavity where the drogue is embedded when the hose is rolled. For the pylon design, where the aerial refueling pod is connected to the airframe and where fuel is transferred, a thin symmetric airfoil with a maximum thickness ratio (t/c) of 0'1 is chosen. In this case, NACA 0010, which was used previously in the vertical stabilizer of the aircraft.

Figures 4.2 and 4.3 show the wing pods surface design in Catia V5. All the major components which were mentioned are defined too, including the drogue, the hose and the ram air turbine propeller. The wing pods are connected to the wing between the outboard slotted flaps and the aileron, exactly to rib No. 22. Figure 4.4 shows the wing pod assembly under the wing of the aircraft.

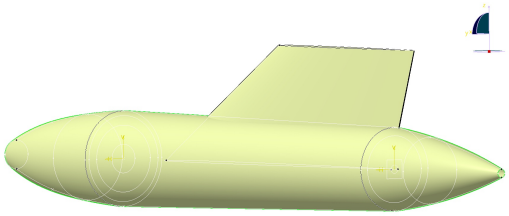

Figure 4.2: Aerial refueling wing pods surface design in Catia V5

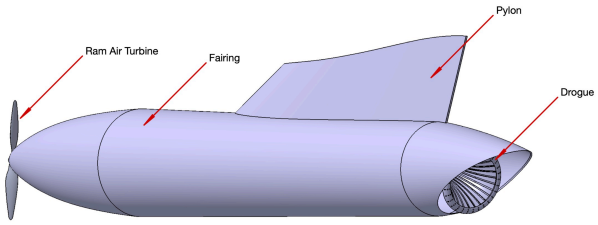

Figure 4.3: Aerial refueling wing pods final design

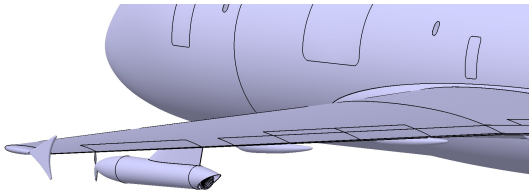

Figure 4.4: Aerial refueling wind pod mounted on the wing

Inside the aerial refueling wing pods, there are several interconnected components which carry out the fuel transfer to the receiver aircraft, listed and explained below:

- **Fuel pump**: directly connected to the ram air turbine, its main function is to pump the fuel from the supply (in this case, the wing tanks) to the hose of the wing pod.
- **Refueling control system**: hosts the main sensor in charge of monitoring the pressure and thus, the amount of fuel which is being transferred.
- **Fuel control valve**: through electrical signals, this valve's main function is to regulate the fuel pressure.
- **Vane pump**: specific type of self-priming positive displacement pump which provides constant flow when pressure varies ([43], Northridge pumps, 2019).
- **Tensator motor unit**: electric motor connected to a belt responsible for spinning the hose drum and as a consequence, rolling and releasing the hose.

Systems are illustrated below in Figure 4.5, where a cross-section drawing of the wing pod is shown:

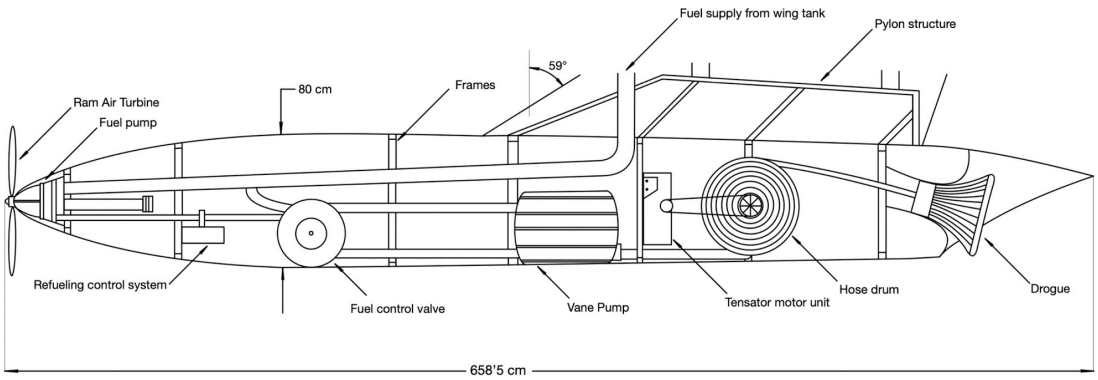

Figure 4.5: Aerial refueling wind pod cross section with dimensions

4.2 Flying boom

The second air refueling method which the aircraft equips is the flying boom. As it was mentioned in the introduction of the project, the flying boom is usually located at the empennage of the fuselage and it consists in a fuel pipe which is fitted with small wings at the end to control it from the tanker, either manually by an aircrew member operator or autonomously via software. This allows the fuel transfer nozzle to be properly directed and guided into the receiver aircraft's port to perform in-flight aerial refueling.

The main advantage of the flying boom compared to the probe and drogue system is the amount of fuel that can be pumped, being significantly higher in comparison. To be more specific, the flying boom can transfer fuel at a rate of approximately 2,700 kg/min, whereas the probe and drogue system has a maximum transfer rate of 900 kg/min approximately. But it is worth remarking that not every aircraft which is able to perform aerial refueling can accept the boom's maximum rate, especially fighter aircraft, which maximum fuel-receiving rate is close to the maximum probe and drogue system transfer rate. Contrary to that, bombers and large aircraft (such as Rockwell B-1 Lancer or Lockheed C-5 Galaxy) usually benefit from the elevated fuel transfer rate which the boom is able to deliver. ([42], Christopher Bolkcom, 2006, p. 2).

The main components which form the flying boom are the fixed boom, the retractable boom, the wings and the fuel transfer nozzle. When aerial refueling operations take place, the flying boom is deployed and the retractable boom extends, so the length of it increases noticeably to provide a safer environment, maintain a reasonable distance between both aircraft and function as a damper. To allow the flying boom to move freely and to rotate about the three axis, the pivot point where the flying boom connects to the fuselage consists on a gimbaled attachment. Additionally, to deploy and stow the flying boom, an electric motor with a belt installed inside the tailcone spins a drum to roll and unroll the cable which is connected to the structure of the flying boom.

Figure 4.6 shows the flying boom attachment fairing design, where the mentioned gimbal is located and the fixed boom connects to the fuselage. It is shown too, the support for the flying boom when it is stowed and the cable is shortened to the minimum:

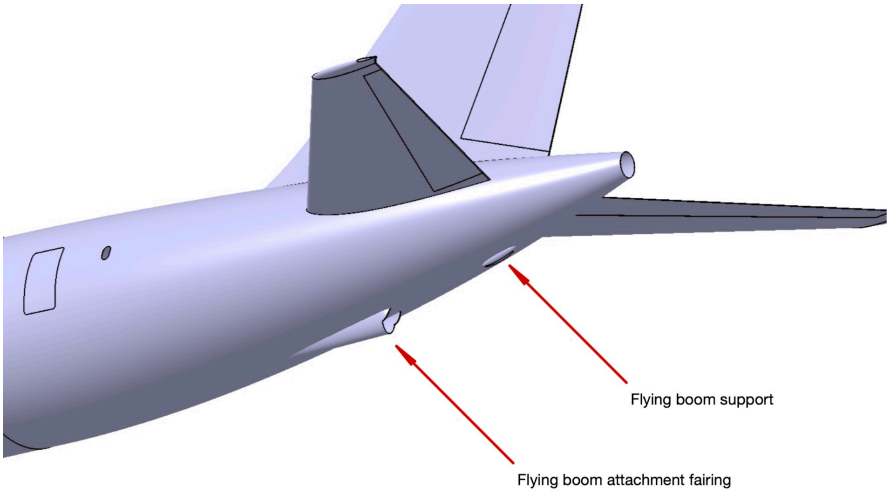

Figure 4.6: Flying boom attachment point design

To design the fixed boom, an elliptical cross-section shape is chosen, which will provide better aerodynamic performance (less drag) than an ordinary cylindrical pipe. The length of the fixed boom is defined to be 9'2 m, which is chosen basing on dimensions of existing tanker aircraft adapted to the one which is being designed in this project ([44], Air Force Reserve Command, 2024).

Regarding the retractable boom, the same elliptical shape (smaller in size) is chosen, so it can fit inside the fixed boom when it is stowed. At its end, it is located the fuel transfer nozzle, which will connect to the port on the receiver aircraft to transfer fuel. The nozzle presents a valve which does not allow fuel to flow out of the flying boom unless it is properly attached and fastened. Figure 4.7 shows the fuel transfer nozzle installed in Airbus A330 MRTT.

Figure 4.7: Fuel transfer nozzle in a real operating tanker aircraft (Yonhap News Agency, 2019)

Figures 4.8 and 4.9 show the flying boom and the two different positions of the retractable boom (extended and retracted):

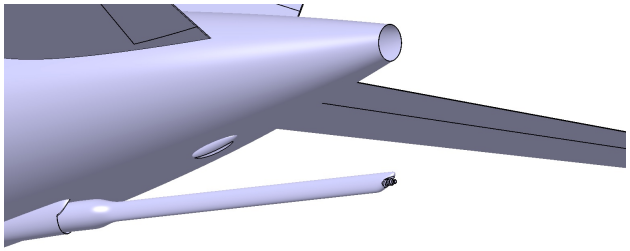

Figure 4.8: Retractable boom (retracted position)

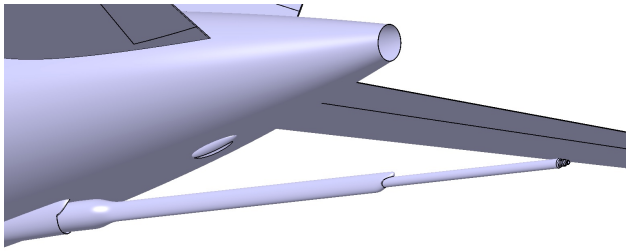

Figure 4.9: Retractable boom (extended)

Even though different approaches are used to control the flying boom, the most common configurations are V-shaped wings (also called ruddervators) or H-shaped rudder-and-elevator assemblies. LT-018 flying boom equips a V-shaped wing assembly, which is more convenient for this specific purpose as it will reduce both the weight and the wetted area (and thus, the amount of drag). Even though an H-shaped assembly could potentially provide slightly higher controllability and mechanism simplicity, the increase in weight and area that it would suppose is not necessary, as the purpose of the wings installed on the flying boom is simply to perform small precise maneuvers and corrections.

Wings will rotate to vary their angle of attack depending on their position and on the stage of flight to remain neutral ($\alpha=0^{o}$) always, either when the flying boom is deployed or stowed. To perform pitch and rolling maneuvers, electric-powered actuators will control the small $\Delta\alpha$ to control the flying boom's position. The airfoil chosen for the flying boom wings is NACA 0010, the same symmetric airfoil chosen for the wing pods' pylons. As it was mentioned previously, these will only perform small deflections to carry out the necessary corrections and guidance maneuvers, so a large area is not needed.

A high dihedral angle is mandatory as the wing assembly will consist in a V-type one, but attention needs to be paid so that the wings do not damage the fuselage when the whole flying boom assembly is stowed. Considering this design constraints, the wings are defined and can be seen in Figure 4.10.

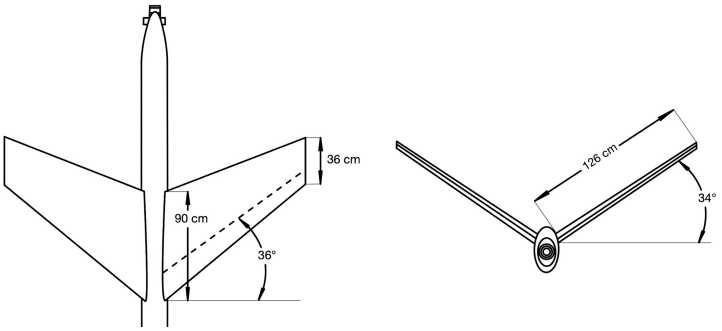

Figure 4.10: Flying boom wings dimensions (upper and back view)

Figures 4.11 and 4.12 show the whole flying boom assembly in both positions with a better perspective, where the wings are also assembled:

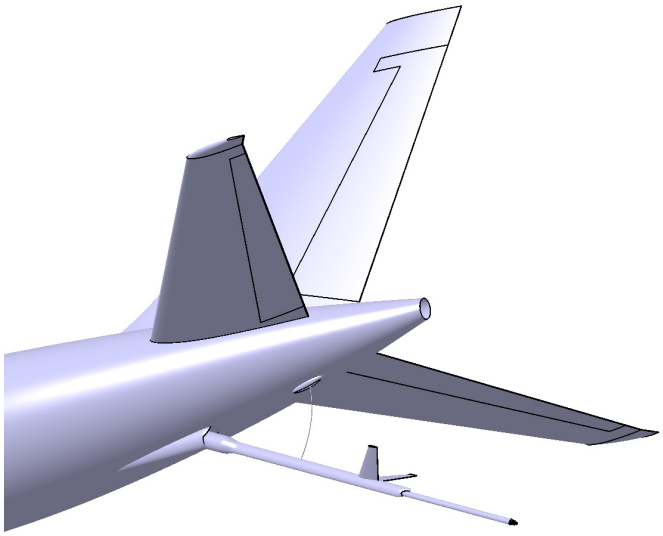

Figure 4.11: Flying boom (completely deployed, 3D model)

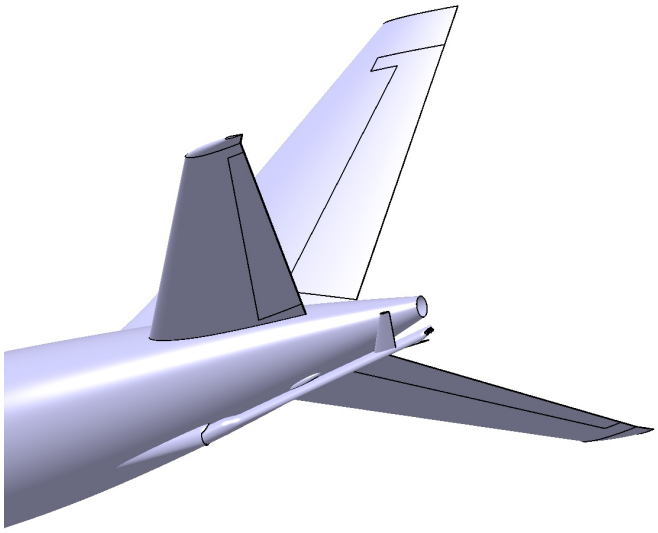

Figure 4.12: Flying boom (stowed position, 3D model)

Figures 4.13 and 4.14 illustrate the flying boom's stowed and deployed positions, indicating the most relevant dimensions and angles.

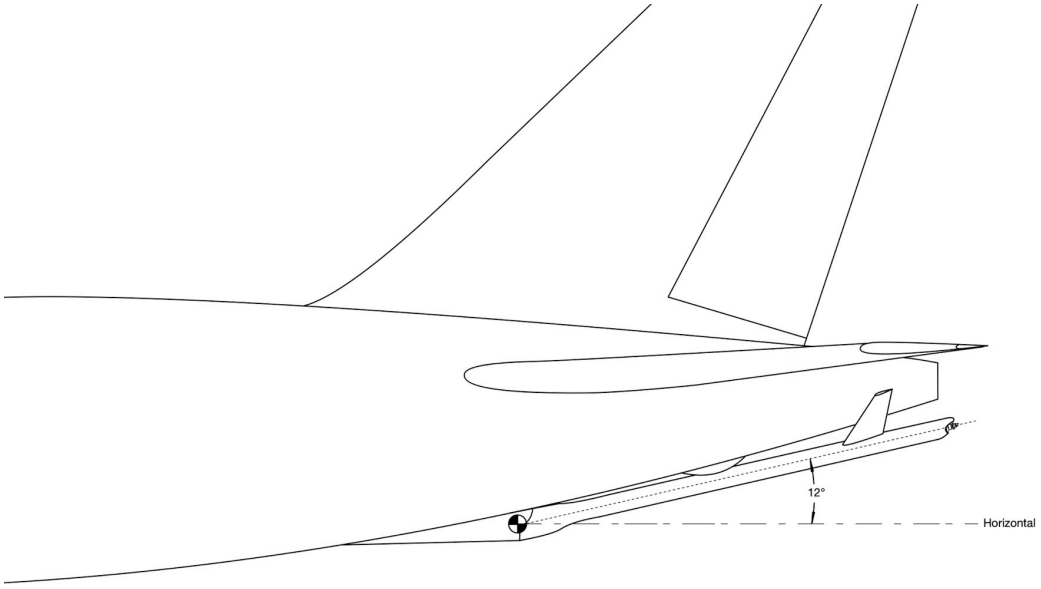

Figure 4.13: Flying boom (stowed position)

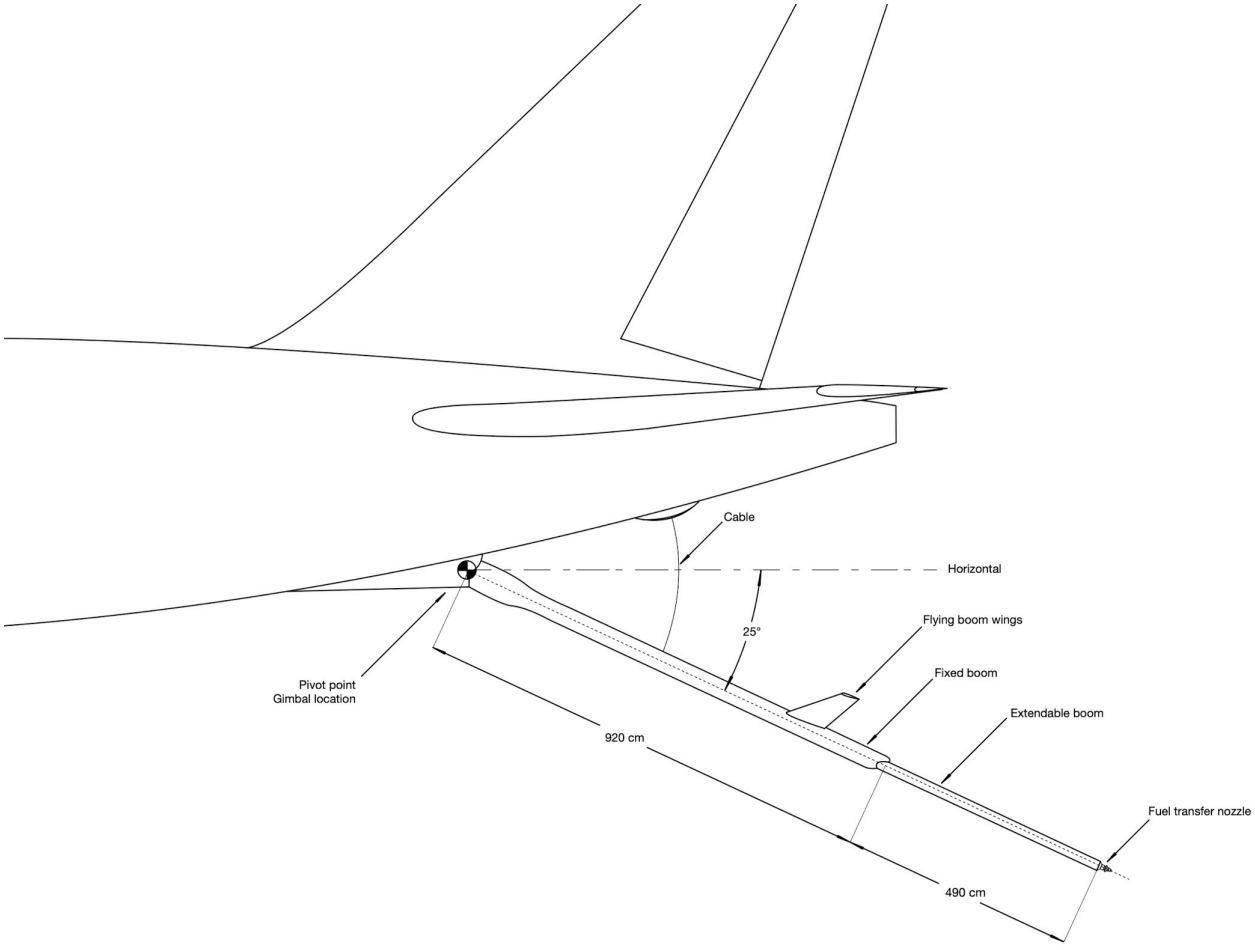

Figure 4.14: Flying boom (completely deployed)

4.3 Centerline drogue

One of the main requirements of the LT-018 is both versatility and convenience. To avoid making use of external adapters to use the flying boom with the probe-and-drogue system (Boom-Drogue Adaptor [BDA] kits), which were mentioned in the introduction, a centerline drogue is installed in the tanker.

The system's functioning approach is similar to that installed in the wing pods, but the hose and drogue are embedded inside the flying boom's attachment fairing in the lower part of the fuselage, next to it.

In the same manner than the wing pods, the hose remains retracted during the majority of the flight phases and unrolls completely when aerial refueling is going to take place.

As an additional remark, the centerline drogue and the flying boom are compatible but cannot operate simultaneously, as it exists the risk that the hose interferes with the flying boom and it remains stuck, creating a high probability of damaging the fuselage and transforming the landing maneuver into a dangerous operation. Moreover, two aircraft would not be able to refuel simultaneously from the flying boom and the centerline drogue while keeping a reasonable safe distance. For that reason, the flying boom and the centerline drogue can make use of the same fuel transfer systems, and there is no need to install 2 independent ones. Figure 4.15 shows the centerline drogue stowed and deployed.

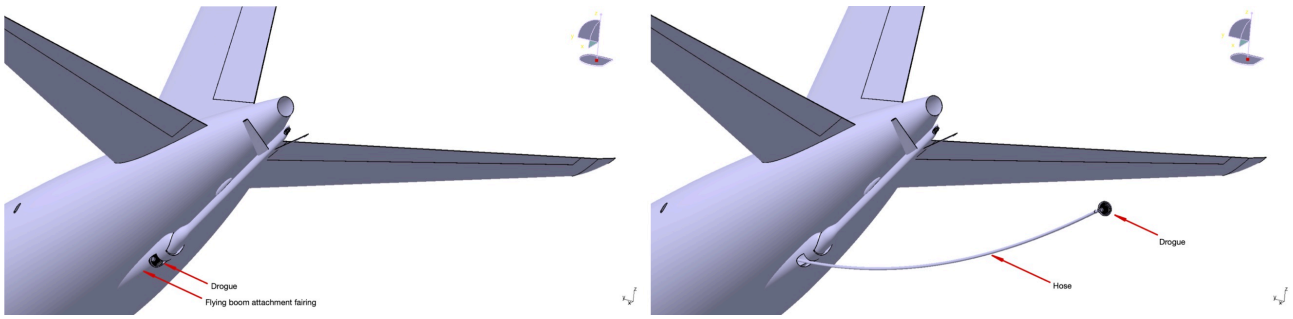

Figure 4.15: Centerline drogue (stowed [left] and deployed [right])

Both systems in charge of deploying and stowing the centerline drogue and the flying boom are located after the aft pressure bulkhead. They are shown in Figure 4.16.

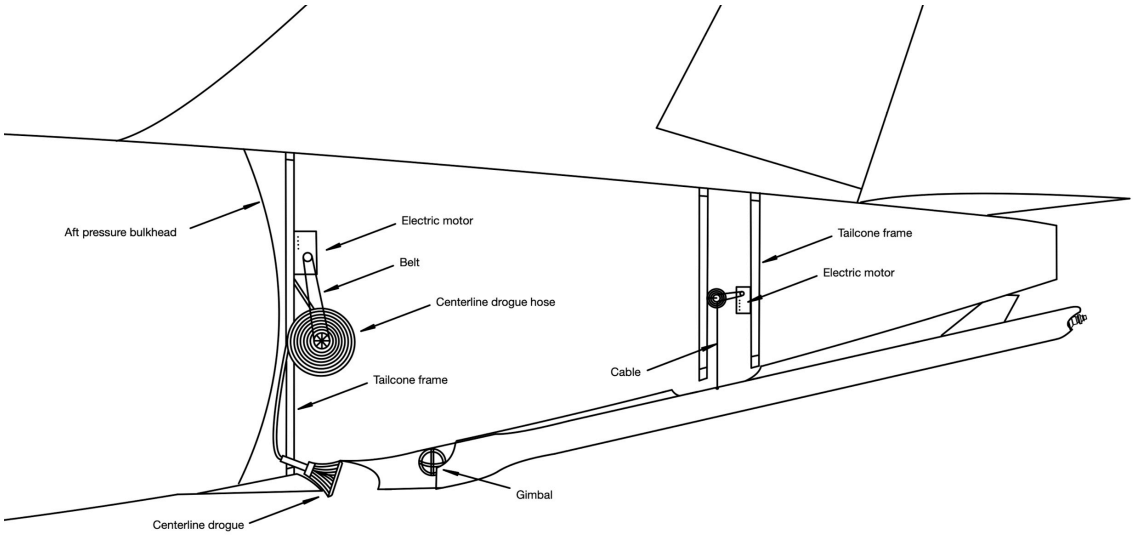

Figure 4.16: Flying boom and centerline drogue deployment systems

4.4 In-flight aerial refueling vision and control systems

As it would be expected, coupling maneuvers to carry out aerial refueling are complex and tedious. In the past, it was mandatory to perform exhaustive and intense training by special aircrew members (boom operators) to carry out aerial refueling, as it was completely done manually controlling the flying boom in the tanker aircraft at the boom's operator station. Usually, that station was located at the same location than the boom, as the only manner to see the maneuver was through windows at the lower part of the aircraft's fuselage. The following figures show the boom operator's station installed in Boeing KC-135.

Figure 4.17: Boeing KC-135 Boom operator station (inside)
(Rapid City Journal, 2019)

Figure 4.18: Boeing KC-135 Boom operator station (outside)
(NARA & DVIDS Public Domain Archive, 1987)

There are several major drawbacks with this approach. Initially, structural reinforcement weight must be added to perform an aperture on the fuselage to install a window. Additionally, when atmospheric and weather conditions are not ideal (fog, rain, water condensation, etc), visibility through the boom operator's station window could be severely reduced and thus, increase the complexity and risk of the aerial refueling maneuver. Moreover, the operator needs to be positioned in a semi-crouched position to look constantly downwards and hold the joystick, which can produce fatigue and tiredness after a short period of time.

For that reason, thanks to technological advancements and computers, modern tankers are equipped with in-flight refueling video systems which monitor all the process through a set of cameras located the different locations of the aircraft.

The boom operator station is then positioned in any other location of the tanker, which allows to perform a safer aerial refueling maneuver with even more comfort, as the station is located in a more ergonomic position. Figure 4.19 shows the boom operator's station in Boeing KC-46 A Pegasus:

Figure 4.19: Boeing KC-46 A Pegasus boom operator's station
(United States Air Force, 2015)

LT-018 equips a set of cameras to provide situation awareness and to perform the necessary flying boom's maneuvers to perform aerial refueling. Thanks to this systems, aerial refueling can be carried out autonomously via software, as it happens in actual tankers (for example, in Airbus A330 MRTT, as it was mentioned in the introduction).

The name and function of the designed systems which the aircraft equips to carry out successful aerial refueling maneuvers is explained below:

- **BoomCam**: set of cameras located next to the aircraft's flying boom which provide an upper view of the receiver aircraft during the approach and coupling maneuver. This set of cameras equips ultra-high definition and night-vision cameras, both with an optic zoom installed on them and a laser rangefinder to measure the distance between the tanker and the receiver aircraft.
- **PathAlignCams**: set of two cameras located at the sides of the fuselage's tailcone which look at the fuel transfer nozzle sideways for a more precise control of the flying boom's rolling maneuvers and to ensure a proper alignment and a smooth coupling to the receiver aircraft.
- **PanoramCams**: set of two ultra-wide angle cameras located at the middle of the fuselage approximately, behind the wing root's fairing, which provide a wide-angle panoramic view of the complete tanker's refueling area (wing pods, centerline drogue and flying boom). This images are projected in the boom operator's station in a long LCD screen, to provide a better understanding of the surrounding situation and positioning of both the tanker and the receiver aircraft.
- **Vanguard Sensor Array**: multiple sensors are installed on the aircraft to perform autonomous aerial refueling in a safe manner, including proximity sensors, inertial measurement units and laser range finders.
- **StratoGuard Aerial Refueling Network**: the main system in charge of performing autonomous aerial refueling, which integrates both the boom control system and the data link system (which obtains measurements and real-time image recognition from the cameras and the sensors). This system's duty is to extend, retract and align the flying boom with the receiver aircraft's port sending inputs to all the actuators basing on real-time measurements.

The location of the main cameras which form the in-flight video and control system is indicated in Figure 4.20:

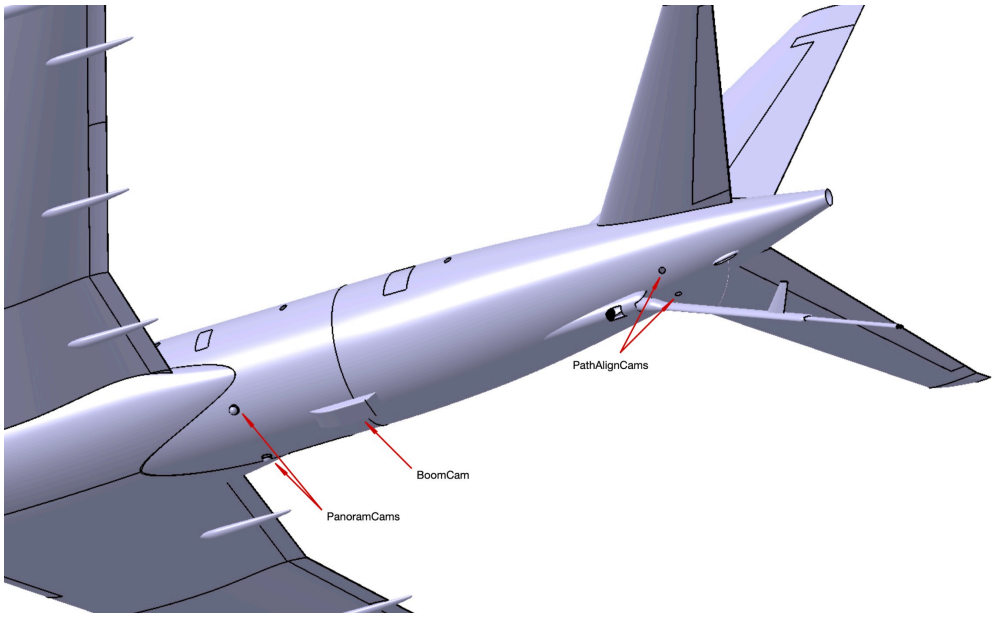

Figure 4.20: Vision system for aerial refueling (location of the main cameras)

4.5 Boom operators station

The boom operator station is located next to the aft pressure bulkhead, as it was shown in the different diagrams showing the aircraft configurations (Figures 1.10 to 1.18).

From that location, boom operators will monitor and control all the in-flight refueling vision and control systems, including all the cameras, sensors and flying boom maneuvers (in the case that human intervention is required for any reason). The station is formed mainly by high resolution LCD (Liquid Crystal Displays), a control stick similar to the one which pilots use to maneuver the aircraft and several consoles to control additional refueling operations (fuel transfer, extend the retractable boom, change the cameras vision systems, etc).

Regarding the screens, a wide panoramic LCD is located at the upper part of the station, showing a wide angular view of the aircraft's exterior provided by PanoramCams. A secondary large LCD in the middle of the station provides the BoomCam real-time image, where additional information is also shown regarding both the tanker and the receiver aircraft (airspeed, distance, bank angle, pitch attitude, etc).

The location of the boom operators station and its main components are shown in Figures 4.21 and 4.22.

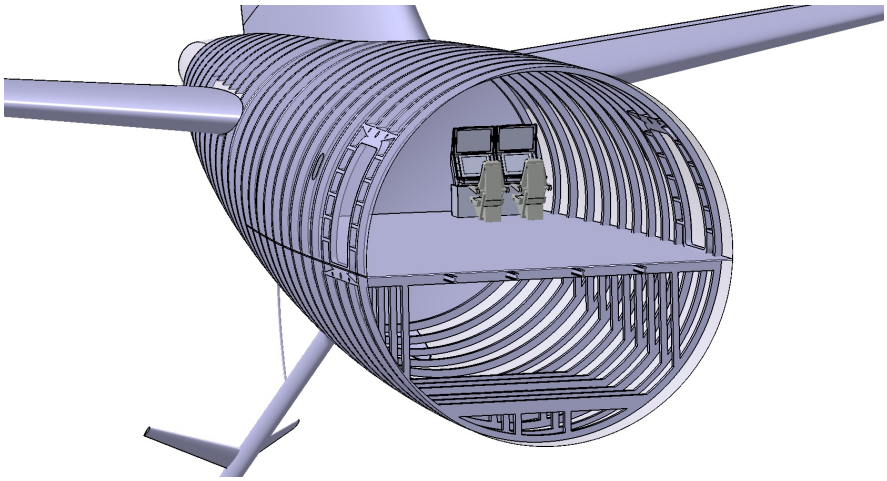

Figure 4.21: Boom operators control station location

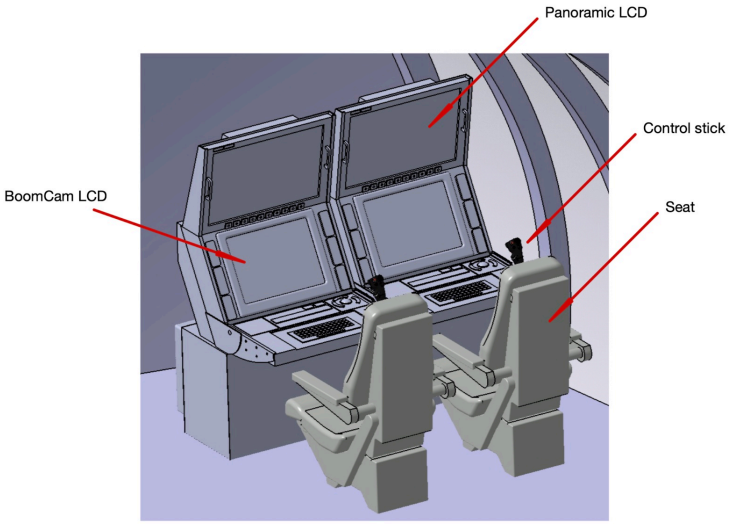

Figure 4.22: Boom operators control station components

Chapter 5: CFD Simulation and Powerplant selection

This chapter of the project covers the computational fluid dynamics aerodynamic analysis and the powerplant selection process. Additional calculations and designs related to this specific design topic such as the range calculations, the engine pylon design or the Auxiliary Power Unit are described and explained too.

5.1 CFD Simulation

To make future engine and flight mechanics calculations, is necessary to know the value of the drag force that the aircraft creates. To achieve this purpose, CFD (Computational Fluid Dynamics) is used, to be more specific, the software Ansys Fluent.

CFD simulations have been widely used in engineering in the latest years as they are a powerful instrument to prognosticate and study fluid dynamics in a wide variety of applications. Ansys Fluent is a CFD software which is able to simulate fluids' flow, heat transfer and fluid-structure interaction problems, employing the finite volume method to solve the equations which govern fluid dynamics and thermal conduction scenarios. In a nutshell, Ansys Fluent discretizes the simulation into a network of control volumes and the different variables are computed at the centroids of them. Afterwards, iterative techniques solve the governing equations and obtain a converged solution ([45], MR-CFD Co, 2024).

1. Geometry and wind tunnel definition

The 3D model which is being built throughout the project is going to be used to perform the CFD simulation in Ansys Fluent. Before starting to set the simulation, it is necessary to rescale the complete model and reduce its size considerably.

The decision to scale down the model is mainly due to computational constraints linked to CFD simulations on large-scale models. Given the high complexity, details and large size of the full-scale model, the required computational resources to achieve accurate simulations and even to manage the geometry file become quite demanding. Scaling down the aircraft's model will enable a more efficient use of computational resources and the risk related to system crashing during the analysis will be significantly reduced.

Additionally, fine details (such as the fuel transfer nozzle, the drogues, the windows, etc) which result in complex intersecting surfaces are omitted to reduce potential issues with surface discretization and meshing. The scale selected is 1:62'5, meaning that the scaled model is 62'5 times smaller than the original one. The scaled 3D model which is going to be used for CFD simulations is shown in Figure 5.1:

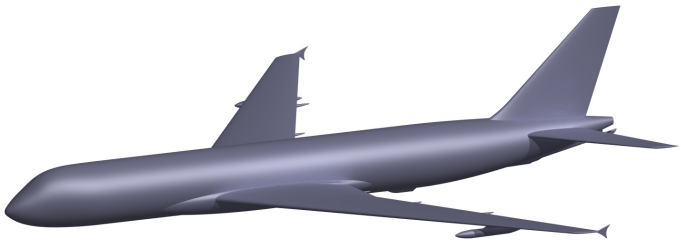

Figure 5.1: 3D model for CFD (scaled to 1:62'5)

The whole assembly is then exported as an "igs" format, generated by Catia V5, which is one of the geometry file formats which the software accepts to perform CFD simulations. The geometry file is then imported into Ansys Fluent DesignModeler, which is one of the geometry creation and modification tools included in the software. The model imported in Ansys Fluent is shown in Figure 5.2:

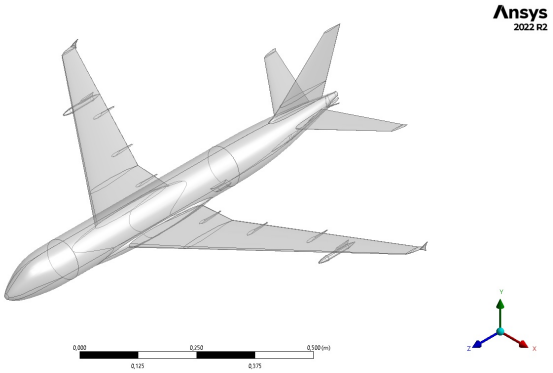

Figure 5.2: Scaled aircraft model imported in Ansys Fluent DesginModeler

The next step is to define the aircraft's angle of attack, which is defined with a body transformation rotating the aircraft model about the X axis. Initially, the expected angle of attack during cruise is defined (3'25º). Afterwards, this angle is parametrized to be changed later to perform several CFD simulation cases at different angles of attack:

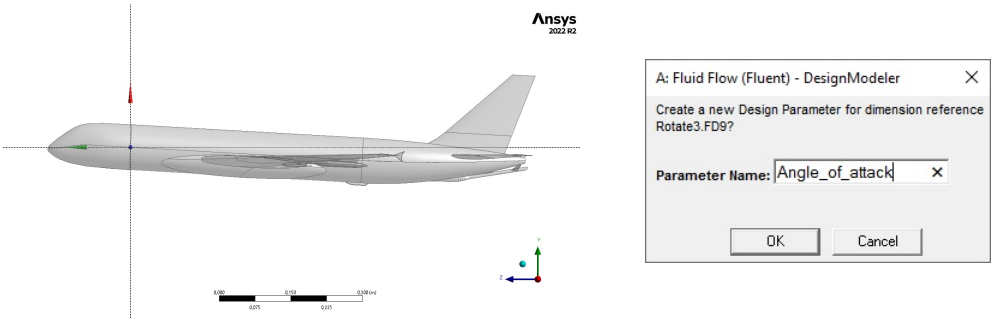

Figure 5.3: Angle of attack definition and variable parametrization

The wind tunnel size (the fluid domain) is defined then. To obtain accurate results in external flow simulations, at least 5 chord lengths in all directions must be defined to avoid the walls effect, having preferably a larger length in the downstream direction, ([46], Ansys Innovative Space, 2018). Knowing that the fuselage length in the scaled model is 1 m long, the distance to the wind tunnel walls in all directions is defined to be 5 m, except for the one in the downstream direction, which length is set to 10 m. Using the tool "Enclosure", the wind tunnel is defined. Figure 5.4 shows in perspective the wind tunnel size compared to the aircraft model:

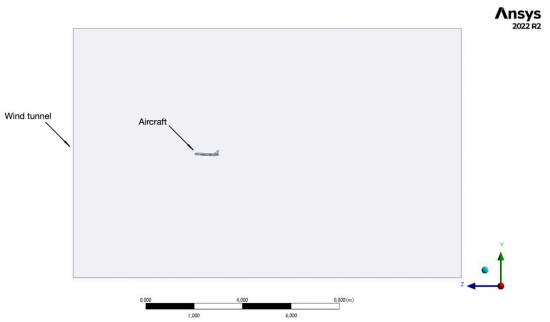

Figure 5.4: Wind tunnel (enclosure) definition

Using a Boolean operation, the aircraft is subtracted from the fluid, leaving the fluid domain completely defined.

The last step is to define a symmetry plane on the YZ axis to perform the simulation on half of the model, which will reduce the computational effort and speed up the simulation.

2. Mesh definition

One of the most important aspects needed to obtain an accurate and reliable CFD simulation is to define an appropriate mesh. Meshing refers to dividing the geometry into discrete elements on which equations will be solved numerically.

When defining the mesh, one of the most important aspects which needs special attention is that there are enough elements to capture all surfaces and shapes without having highly deformed elements forming the mesh. Ansys Fluent offers a variety of tools to define the quality of the mesh, such as maximum element size definition, curvature capture and “sizing”, which allows to define specific mesh conditions for specific geometric bodies (shapes, edges, bodies, etc). This is specially useful to put extra emphasis on relevant bodies or parts of the geometry.

For this specific project, there are several zones of interest in the aircraft which mesh will be refined to ensure an accurate result: the fuselage nose and tail, the wings, the flying boom and the aerial refueling wing pods. Note that an appropriate quality mesh will be defined on the rest of the aircraft surface too, but special emphasis is put on the mentioned zones as they will produce the majority of the drag produced by the aircraft. In Figure 5.5, the defined mesh is seen in a lateral view, where it is appreciated the refinement of it in the fuselage nose, tailcone and in the flying boom. In the same manner, Figure 5.6 shows the mesh of the main wing, the winglet, the wing root fairing and the aerial refueling wing pods.

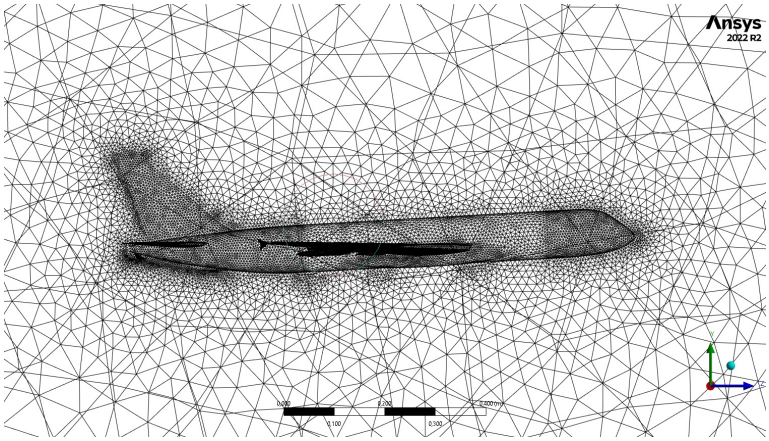

Figure 5.5: CFD simulation Mesh (side view)

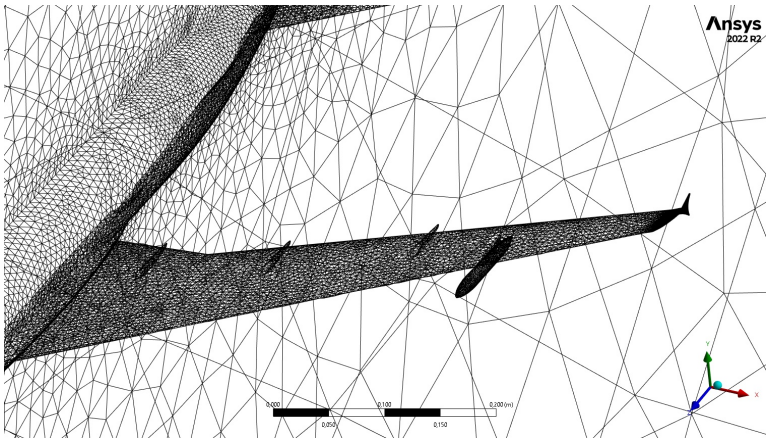

Figure 5.6: CFD Mesh (wing, aerial refueling wing pods and wing root fairing)

Before proceeding to the next step of the CFD analysis, it is important to verify the quality of the mesh. Ansys Fluent provides a tool to check each element's quality assigning each element values from 0 to 1. It also colors all the mesh elements depending on their shape (red meaning they are severely distorted or blue meaning they are a perfect tetrahedron). The mesh quality of the current CFD model shows a good resolution and smooth transitions, presenting a quality of 0'78-0'99 in the majority of the elements, as it is illustrated in Figure 5.7:

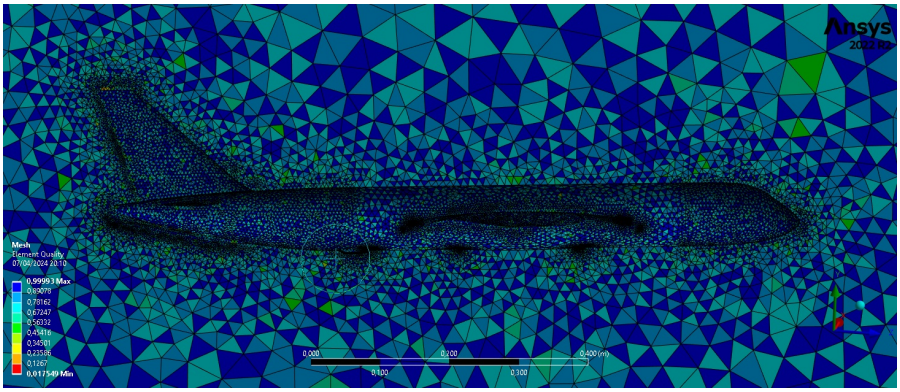

Figure 5.7: CFD Mesh elements quality

3. Boundary conditions and simulation setup

It is important to define the appropriate boundary conditions in the CFD simulation setup window to obtain accurate results with respect to the real ones during actual flight. It is going to be set the scenario of cruise flight (30,000 ft altitude, T=218'8 K and ρ=0'379597 kg/m^3) and an airspeed of M=0'8 (237'16 m/s with previous mentioned ISA conditions).

The same flow inlet conditions cannot be set, as the aircraft was scaled to 1:62'5 to perform the CFD simulation. To find the necessary flow conditions, the Buckingham Pi theorem is used, which can be applied to state that only two dimensionless similarity parameters (Reynolds [Re] and Mach [M] numbers) govern the flow and thus, relevant aerodynamic coefficients (such as C_L, C_D, C_M, etc) are only a function of (Re, M_∞). Hence, for the majority of aerodynamic applications, flows over geometrically similar bodies at the same Reynolds and Mach numbers are dynamically similar and Lift and Drag coefficients will be identical ([27], John Anderson, 2017, pp. 36-42).

Then both the Reynolds and Mach numbers should equal the ones which the real aircraft will have during cruise flight. Let the "R" and "W" subscripts denote the real and the wind-tunnel scaled model. To obtain identical Lift and Drag coefficients, the wind-tunnel flow must be dynamically similar:

$$Re_R = Re_W \text{ and } M_{\infty_R} = M_{\infty_W}$$

Assuming both the dynamic viscosity (μ) and the speed of sound (c) are proportional to $T^{1/2}$, the following statements can be defined:

$$M_{\infty_R} = \frac{V_R}{c_R} \propto \frac{V_R}{\sqrt{T_R}} \text{ and } M_{\infty_W} = \frac{V_W}{c_W} \propto \frac{V_W}{\sqrt{T_W}}$$

It is defined the wind tunnel temperature to be T_W = 15 ºC = 288 K.

Then, equaling both Mach numbers, the wind tunnel's inlet flow speed can be calculated:

$$M_{\infty_R} = M_{\infty_W} \; ; \; \frac{V_R}{\sqrt{T_R}} = \frac{V_W}{\sqrt{T_W}}; \; V_W = \frac{V_R}{\sqrt{T_R}} \cdot \sqrt{T_W} = \frac{237'16}{\sqrt{218'8}} \cdot \sqrt{288} = 272'09 \; m/s$$

Let the same approach be applied to Reynolds numbers to calculate the air density inside the wind tunnel:

$$Re_R = \frac{\rho_R \cdot V_R \cdot L_R}{\mu_R} \propto \frac{\rho_R \cdot V_R \cdot L_R}{\sqrt{T_R}} \text{ and } Re_W = \frac{\rho_W \cdot V_W \cdot L_W}{\mu_W} \propto \frac{\rho_W \cdot V_W \cdot L_W}{\sqrt{T_W}}$$

$$Re_R = Re_W \; ; \; \frac{\rho_R \cdot V_R \cdot L_R}{\sqrt{T_R}} = \frac{\rho_W \cdot V_W \cdot L_W}{\sqrt{T_W}} \; ; \; \frac{\rho_W}{\rho_R} = \frac{V_R \cdot L_R}{V_W \cdot L_W} \cdot \frac{\sqrt{T_W}}{\sqrt{T_R}} = \frac{237'16 \cdot 62'5}{272'09 \cdot 1} \cdot \frac{\sqrt{288}}{\sqrt{218'8}} = 62'5$$

Applying the equation of state for ideal gasses (Equation 5.1), the necessary wind tunnel pressure can be calculated, knowing that at cruise altitude, atmospheric pressure is P_R = 30,089'6 Pa.

$$P = \rho \cdot R \cdot T \; ; \; \frac{P_W}{P_R} = \frac{\rho_W \cdot R \cdot T_W}{\rho_R \cdot R \cdot T_R} = 62'5 \cdot \frac{288}{218'8} = 82'27$$

Equation 5.1: Equation of state for ideal gasses

$$P_W = 82'27 \cdot P_R = 82'27 \cdot 30{,}089'6 = 2{,}474{,}378'43 \; Pa = 24'43 \; atm$$

The wind tunnel must be pressurized to 24'43 atm (2,474,378'43 Pa) to obtain the necessary air density and hence, accurate and real Lift and Drag coefficients.

The setup tool is ran afterwards to define the boundary conditions before running the simulation. The most relevant setup conditions which are set are listed below:

- The fluid is defined to be air and the aircraft's model material is defined to be aluminum.
- The wind tunnel inlet airspeed is set to 272'09 m/s and the air density is set to vary as an ideal gas, to consider compressibility effects.
- The wind tunnel operating pressure is set to 2,474,378'43 Pa.
- The viscous model selected is k-omega, which is more suitable for complex flows involving pressure gradients, separation and strong curvature on streamlines ([47], Kristaq Hazizi, 2022).

4. Post-CFD and results

After 130 iterations approximately, the drag and lift force values stabilize noticeably as residuals are reduced (to the order of 10^{-4}). Using the post-CFD tool provided by Ansys Fluent, several plots and parameters can be defined and calculated.

Lift and Drag can be calculated using the "Function calculator", which will compute and calculate the total force exerted on the fluid by the aircraft in any selected direction. To calculate Drag, the Z direction is defined (downstream direction) and to calculate Lift, the Y direction is defined (perpendicular to the wind tunnel inlet velocity). These functions are parametrized as outputs, so they can be calculated when other parameters are modified (in this case, the only input parameter which was defined is the angle of attack). Figures 5.8 and 5.9 show the functions definition in Ansys Fluent post-CFD.

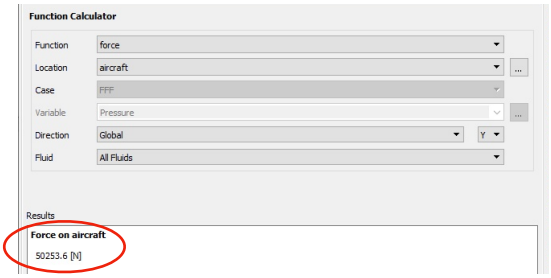

Figure 5.8: Lift function calculator

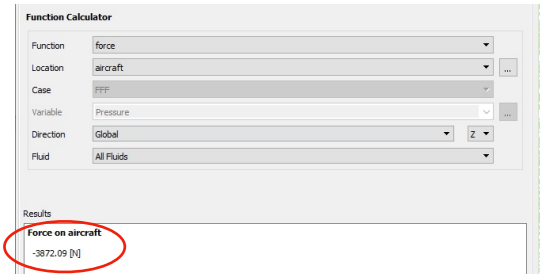

Figure 5.9: Drag function calculator

The aircraft scaled model produces 50,253'6 N of Lift at the angle of attack which was calculated for steady level flight at cruise conditions (α=3'25º) at the aircraft flight design gross weight. A total amount of 3,872'1 N of Drag are produced at these conditions.

Dimensionless aerodynamic coefficients (C_L, C_D) can be then calculated using the wind tunnel conditions and the wing reference area of the scaled model, calculated dividing the aircraft's wing area by the square of the scale factor ($415/(62'5)^2$ = 0'106 m^2).

$$L_{AC} = \frac{1}{2} \cdot C_{L_{AC}} \cdot S \cdot \rho_\infty \cdot u_\infty^2 \; ; \; C_{L_{AC}} = \frac{2 \cdot L_{AC}}{S \cdot \rho_\infty \cdot u_\infty^2} = \frac{2 \cdot 50{,}254}{0'106 \cdot 0'379597 \cdot 62'5 \cdot 272'09^2} = 0'5398$$

Equation 5.2: Aircraft's lift coefficient calculation at cruise conditions

$$D_{AC} = \frac{1}{2} \cdot C_{D_{AC}} \cdot S \cdot \rho_\infty \cdot u_\infty^2 \; ; \; C_{D_{AC}} = \frac{2 \cdot D_{AC}}{S \cdot \rho_\infty \cdot u_\infty^2} = \frac{2 \cdot 3{,}872}{0'106 \cdot 0'379597 \cdot 62'5 \cdot 272'09^2} = 0'0416$$

Equation 5.3: Aircraft's lift coefficient calculation at cruise conditions

The aircraft achieves successfully the required Lift coefficient for steady level flight during cruise.

The simulation is repeated varying the angle of attack (from -5º to 15º) and parametrizing again the Lift and Drag forces. Results are shown in Figure 5.10:

Table of Design Points

	A	B	C	D	E
1	Name	Update Order	P1 - Angle of Attack	P2 - Lift force	P3 - Drag force
2	Units		degree	N	N
3	DP 1	0	-5	-21994	2638,6
4	DP 2	1	0	22641	1875,3
5	DP 0 (Current)	2	3,25	50254	3872,1
6	DP 3	3	5	62568	5994,2
7	DP 4	4	10	73848	13091
8	DP 5	5	15	71313	19715

Figure 5.10: Lift and Drag results for different α

The most relevant graphs are built then with the results which the software calculates for each different scenario. Initially, a table is built to define and collect all data:

Angle of Attack (º)	Lift (N)	C_L	Drag (N)	C_D	L/D
-5º	-21,994	-0'2362	2,638'6	0,0283	-8'3354
0	22,641	0'2432	1,857'3	0,0199	12'1903
3'25	50,254	0'5398	3,872'1	0,0416	12'9785
5	62,568	0'6721	5,994'2	0,0644	10'4381
10	73,848	0'7932	13,091	0,1406	5'6411
15	71,313	0'7660	19,715	0'2118	3'6172

C_L-α and C_D-α graphs for the whole aircraft are plotted using Microsoft Excel, illustrated in Figures 5.11 and 5.12.

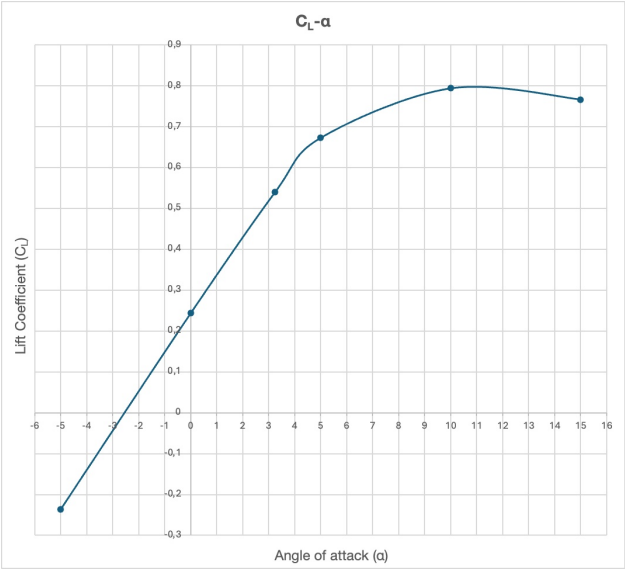

Figure 5.11: Aircraft's C_L-α graph

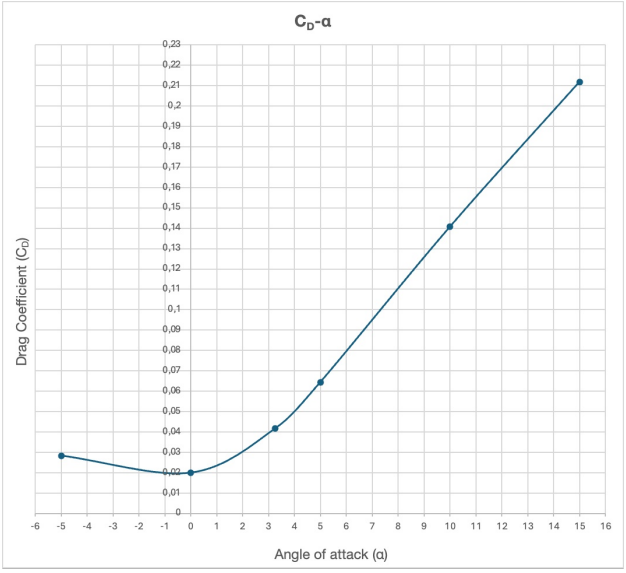

Figure 5.12: Aircraft's C_D-α graph

According to CFD simulations, the required angle of attack to achieve the necessary C_L to maintain steady level flight at the aircraft flight design gross weight (218,500 kg) is α=2'5º, slightly lower than that which was calculated by the software Aeolus ASP during the main wing design process.

Additionally, the aerodynamic efficiency can be plotted too for the whole aircraft at different angles of attack (seen in Figure 5.13). Maximum aerodynamic efficiency is located at an angle of attack of α=1'5º approximately, where a maximum value of 13'5 is achieved.

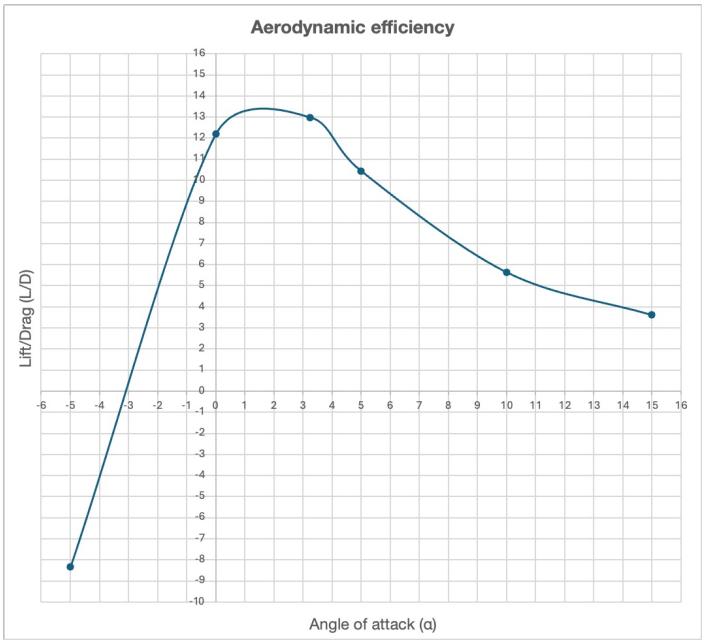

Figure 5.13: Aircraft's aerodynamic efficiency as a function of α

Making use of Ansys Fluent post-CFD tool, streamlines can be plotted at different locations and planes of the aircraft. Figure 5.14 illustrates the airflow over the main wings at an angle of attack of α=3'25º, where it is appreciated how the flow significantly accelerates and reaches much higher velocities at the upper surface of the wing (the extrados) compared to the lower surface (the intrados).

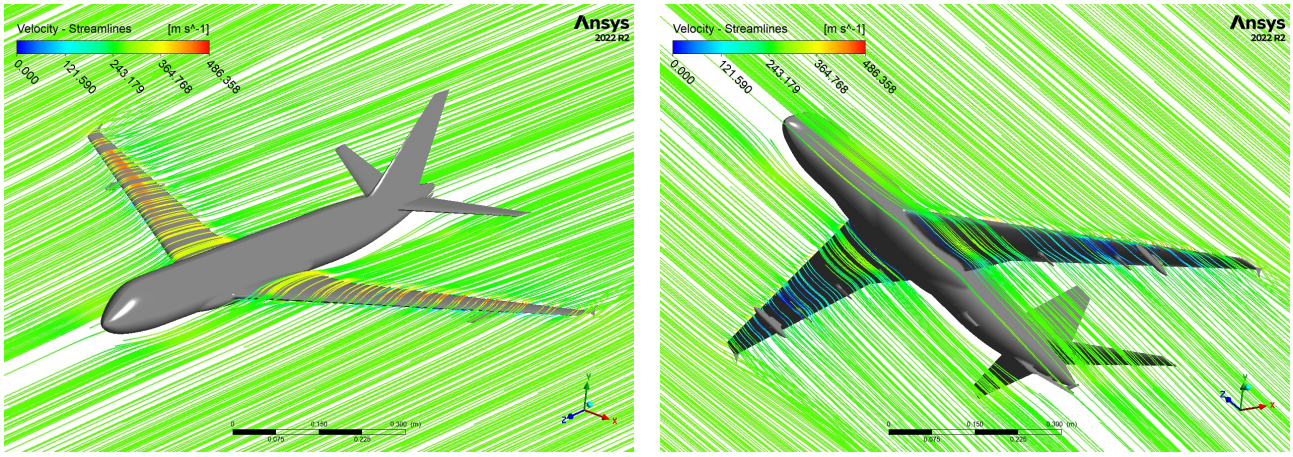

Figure 5.14: Streamlines over the main wings

Streamlines over the aircraft's symmetry axis show uniform alignment and demonstrate smooth continuity throughout the fuselage. Even though there is no significant flow separation, minor flow separation bubbles are generated behind the boom cam and at the upper surface of the fuselage (mainly produced by changes in the aircraft's fuselage geometry). As expected, flow velocity is significantly reduced at areas which face the flow directly, such as the nose or the Boomcam.

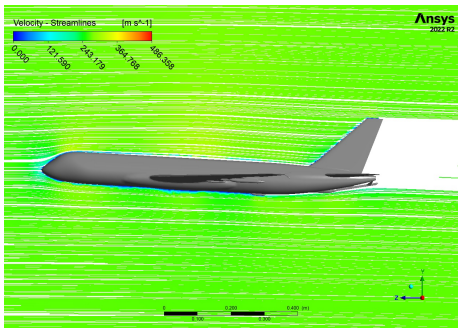

Figure 5.15: Streamlines over the aircraft symmetry axis

Figure 5.16 shows the downwash, the upwash and the trailing tip vortices when the streamlines over the wing are seen from a rearward view.

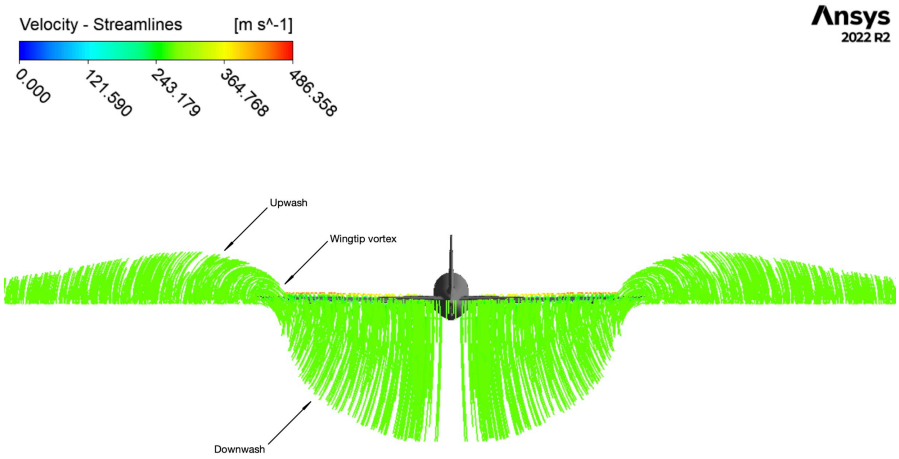

Figure 5.16: Streamlines over the aircraft main wings (rearward view)

Figure 5.17 shows the streamlines at the stall condition due to flow separation (α=11º):

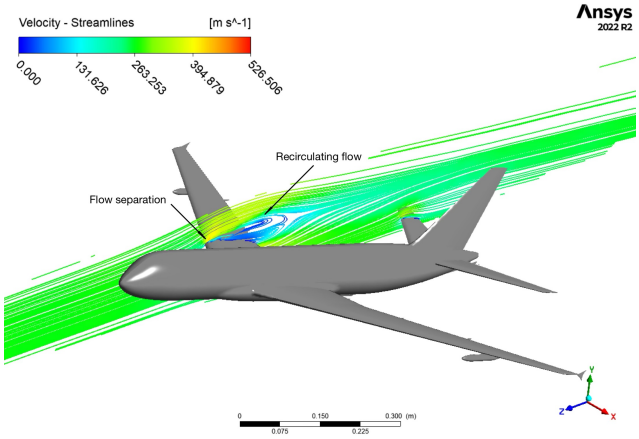

Figure 5.17: Stall condition

To conclude, Figure 5.18 shows the pressure contour over the aircraft's surface. As expected, pressure is much higher at the lower surface of the wings compared to the upper one. Maximum aerodynamic pressure is achieved at stagnation points, which are located mainly at the aircraft nose, at the leading edge of the wings and at the nose of the aerial refueling wing pods.

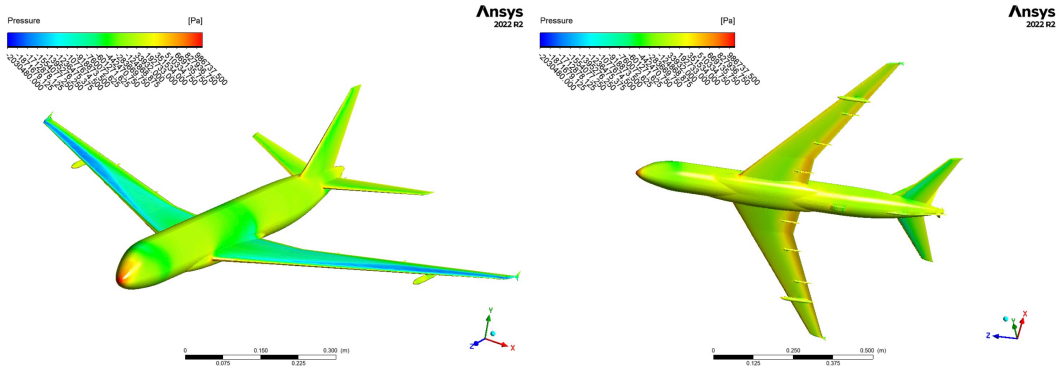

Figure 5.18: Pressure contour on aircraft surface

5.2 Powerplant selection

Required thrust can be calculated at the start and end of cruise, assuming always steady level flight. Again, calculations will be performed on the mission scenario purposed in section 3.1 of the project (70,000 kg of fuel + 40,000 kg of payload), setting an amount of 5% of fuel burnt during the takeoff and climb phases and leaving 5% of reserve fuel. Weights at the start and end of cruise are calculated according to Equation 5.4:

$$W_{START\ CRUISE} = 107{,}800 + 40{,}000 + 0'95 \cdot 70{,}000 = 214{,}300\ kg = 2{,}102{,}283\ N$$
$$W_{END\ CRUISE} = 214{,}300 - 0'9 \cdot 70{,}000 = 151{,}300\ kg = 1{,}484{,}253\ N$$

Equation 5.4: Aircraft's weight calculation at the start and end of cruise

Forces are balanced due to steady level flight:

$$\begin{cases} T_{REQ} = D \\ L = W \end{cases}$$

Equation 5.5: Aircraft's force balance at steady level flight

Thrust required can be then calculated at the start and end of cruise:

$$\frac{D}{D} = \frac{L}{L} \; ; \; D = D \cdot \frac{L}{L} \; ; \; T_{REQ} = \frac{L \cdot D}{L} = L \cdot \frac{D}{L} = L \cdot \frac{1}{L/D} = W \cdot \frac{1}{L/D}$$

At the beginning of cruise (approximately at the aircraft flight design gross weight), the aircraft needs to fly at an angle of attack of α=2'5º. L/D has a value of 13'4. At the end of cruise, the required C_L to maintain steady level flight is calculated too according to Equation 5.6.

$$C_{L\ END\ CRUISE} = \frac{2 \cdot L}{S \cdot \rho_\infty \cdot u_\infty^2} = \frac{2 \cdot 1{,}484{,}253}{415 \cdot 0'379597 \cdot 237'16^2} = 0'335$$

Equation 5.6: Aircraft's required C_L at the end of cruise

A C_L of 0'335 is achieved at an angle of attack of α=1°, angle at which L/D has a value of 13'4 too. The values of required thrust at the start and end of cruise are finally calculated.

$$T_{REQ\ START\ CRUISE} = W_{START\ CRUISE} \cdot \frac{1}{L/D} = 2{,}102{,}283 \cdot \frac{1}{13'4} = 156{,}886'79\ N = 156'89\ kN$$

$$T_{REQ\ END\ CRUISE} = W_{END\ CRUISE} \cdot \frac{1}{L/D} = 1{,}484{,}253 \cdot \frac{1}{13'4} = = 110{,}765'15\ N = 110'77\ kN$$

Equation 5.7: Thrust required for steady level flight at the start and end of cruise

To select an appropriate engine which complies with powerplant certification and performance requirements, operating data of similar wide-body operating aircraft will be used as a reference. The main limiting factor for the powerplant selection is takeoff, the main reason why the takeoff thrust to weight ratio is used as the main indicator for the engine selection.

Analyzing and comparing this set of data for Airbus A350-900, Airbus A330-200, Boeing 787-8 and Boeing 777-200, the take-off thrust-to-MTOW ratio is calculated for each one of them, resulting in very similar values: 2'72, 2'65, 2'78 and 2'58 respectively ([14], Boeing, 2022) ([15], Boeing, 2023) ([17], Airbus, 2023) ([29], Airbus, 2021).

The average value (2'68) is used to determine the maximum take-off thrust in Equation 5.8, using the aircraft's MTOW which was estimated previously:

$$\frac{T_{TO}}{MTOW} \approx 2'68 \; ; \; T_{TO} = MTOW \cdot 2'68 = 2'68 \cdot 230{,}000 \cdot = 616{,}400\ N = 616'4\ kN$$

Equation 5.8: Thrust required for take-off

Turbofan engines are selected to power the aircraft. These type of engines are the most suitable and efficient for the aircraft's flight envelope (speed-altitude flight regime) ([25], Jan Roskam, 1985, p. 124). The number of engines selected is 2 (which need to produce a take-off thrust [T_{TO}] of 308,200 N each approximately), which will reduce significantly the costs, maintenance tasks and weight compared to 4 of them.

There are currently several revolutionary high-bypass efficient turbofan engines in development which will propel some of the latest airliners (General Electrics GE9X or Rolls-Royce UltraFran, for example), but operational and performance data is still not available as they are still not mounted in any operative aircraft. The most relevant, advanced and efficient turbofan engines which propel the latest wide-body airliners are mainly Rolls-Royce Trent XWB, Rolls-Royce Trent 1000 and General Electric GEnx.

Basing on LT-018 thrust requirements which were estimated, Rolls-Royce Trent 1000-A is selected as the main powerplant of the aircraft, as these are the ones which better adjust to the amount of thrust which the aircraft needs. As mentioned before, these are one of the most efficient aircraft engines in service at the moment. In fact, they are 20% more efficient than its previous generation. The engine is seen in Figure 5.19 and the most relevant performance features of it are listed too ([48], EASA, 2024).

- Dry engine weight = 6,114 kg
- Fan diameter = 285 cm
- Number of blades = 20
- Bypass ratio = 10:1
- Take-off net thrust = 307,800 kN
- Thrust Specific Fuel Consumption at cruise = 14'3 g/kN·s ([49], Aviation Week, 2008)

- Ultra-efficient swept fan, 3D bladed compressors, contra-rotation, modulated high pressure air system
- Three-shaft turbofan engine
- Low, Intermediate and High pressure compressors
- Low, Intermediate and High pressure turbines

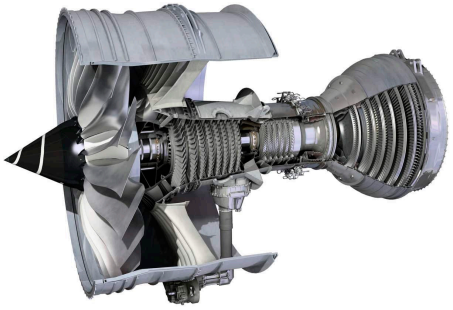

Figure 5.19: Rolls-Royce Trent 1000 (AeroExpo, 2024)

Another relevant feature which Rolls-Royce Trent-1000 engines present is full compatibility with SAF (Sustainable Aviation Fuels), having been the first engines which were used in a cross-Atlantic flight powered completely with this type of sustainable and low-pollutant fuel ([50], Rolls-Royce Inc. 2023). This would permit LT-018 to operate with Sustainable Aviation Fuel reducing considerably its CO_2 emissions once the aviation industry establishes a worldwide supply chain.

5.3 Nacelle and Pylon design

Nacelles are mainly streamlined covers used to locate the engine and its main components. The main functions of the nacelles are to protect the engines against foreign objects and to improve the overall aerodynamic efficiency of the aircraft. A round shape is used, trying to minimize the wetted area as much as possible but being large enough to accommodate the engines. The most relevant limiting dimensions for its design are the fan diameter and the engine's length. Strakes are installed on the nacelle too, a common technique employed in modern turbofan-powered aircraft to generate vortices which help to control the flow separation on the aircraft's wing decreasing the nacelle upwash and inducing downwash on the wing's upper surface. Additionally, chevrons are defined at the trailing edge of the engine nozzle to smooth the hot and cold air mixture and reduce the turbulence that creates noise ([51], Ravindra Krishnamurthy, 2021) ([52], NASA, 2010).

The nacelle design is shown in Figures 5.20 and 5.21, where the most relevant dimensions of it are also indicated.

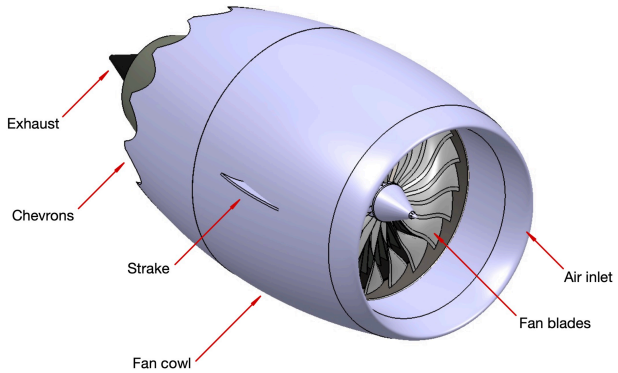

Figure 5.20: Nacelle components

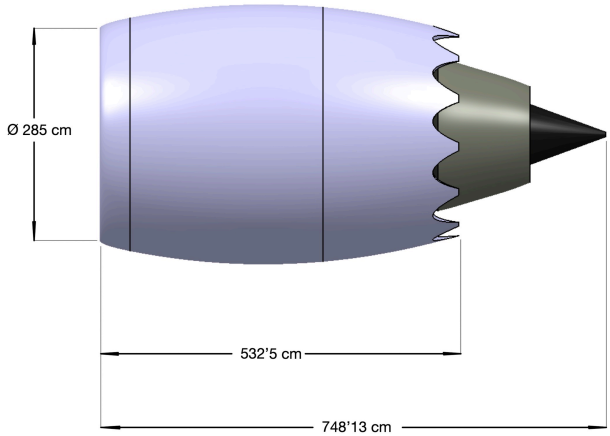

Figure 5.21: Nacelle dimensions

Engine pylons are the main structural element which connects both engines with the wings, being the mean through which the thrust force is transferred to the whole airframe. Moreover, they host the main fuel, oil and hydraulic lines. Besides the structural function, they must also provide a safety distance between the engines and the wings in case of engine fire.

A triangular trussed titanium welded structure is selected, which is connected to the aircraft wing structural elements by means of fuse pins, designed to break due to shear at a certain load in case of emergency landing or ground impact. Figures 5.22 illustrates a cross section of the wing, engine pylon, nacelle and engine assembly.

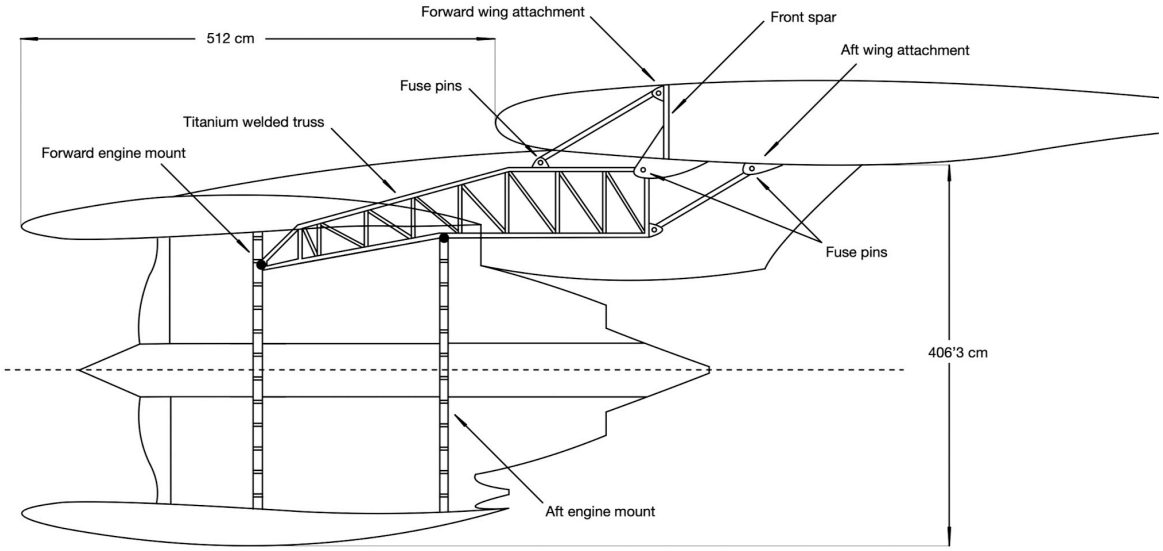

Figure 5.22: Engine pylon structural arrangement (cross-section)

Additionally, Figure 5.23 shows the engine assembly on the aircraft 3D model in Catia V5:

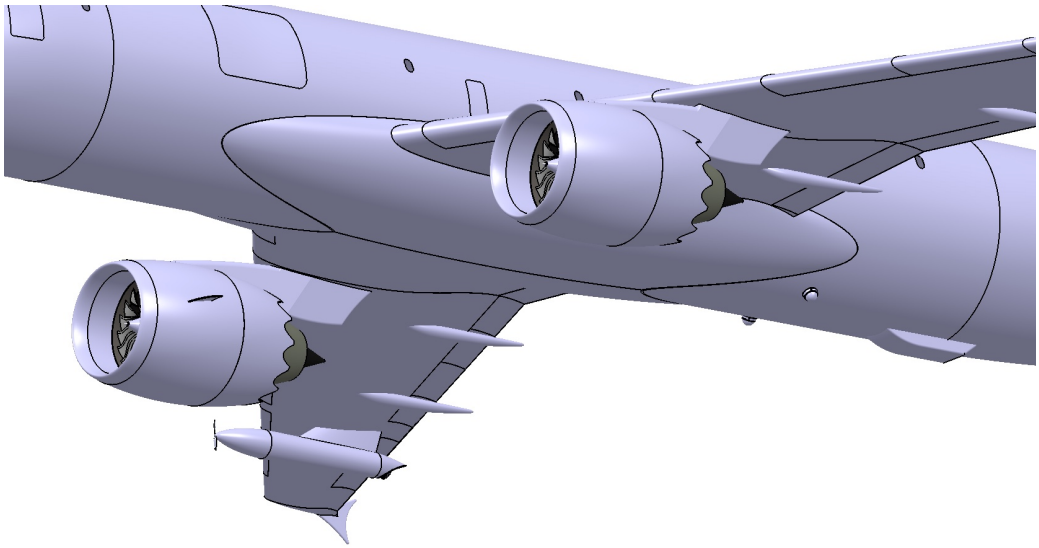

Figure 5.23: Rolls-Royce Trent 1000-A engines mounted on the aircraft

5.4 Auxiliary Power Unit

The APU is a small gas turbine which does not provide propulsion, but electrical and pneumatic energy when support is needed or in emergency scenarios. It can start up the aircraft's main engines, supply electrical energy and run the air conditioning system. Having an auxiliary power unit is crucial for LT-018, as one of its main missions is aeromedical and passengers or troops evacuation, where it may land and take-off in remote airports where no external ground source of energy is available, making it completely independent ([53], Aertec, 2024).

To select an appropriate APU, it is necessary to analyze the one which equip similar aircraft which mount two Rolls-Royce Trent 1000 engines. In this case, Boeing 787, which equips the Pratt & Whitney APS5000 APU (shown in Figure 5.24), the first auxiliary power unit for large aircraft which operates all-electric, is able to generate 450 kVA of electrical power at mean sea level and can operate at a maximum altitude of 43,100 ft ([54], Pratt & Whitney, 2024).

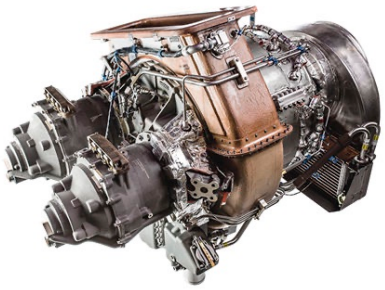

Figure 5.24: Pratt & Whitney APS5000 (Pratt & Whitney, 2024)

In LT-018, the Auxiliary Power Unit is located at the tail of the aircraft's fuselage, behind the horizontal stabilizer's center wingbox, making use of the end of the fuselage tailcone to expel the combustion gasses. When the APU operates, a small door is opened in the upper part of the fuselage to clear the air intake (next to the vertical stabilizer). In Figure 5.25, the main layout of the auxiliary power unit's components are shown:

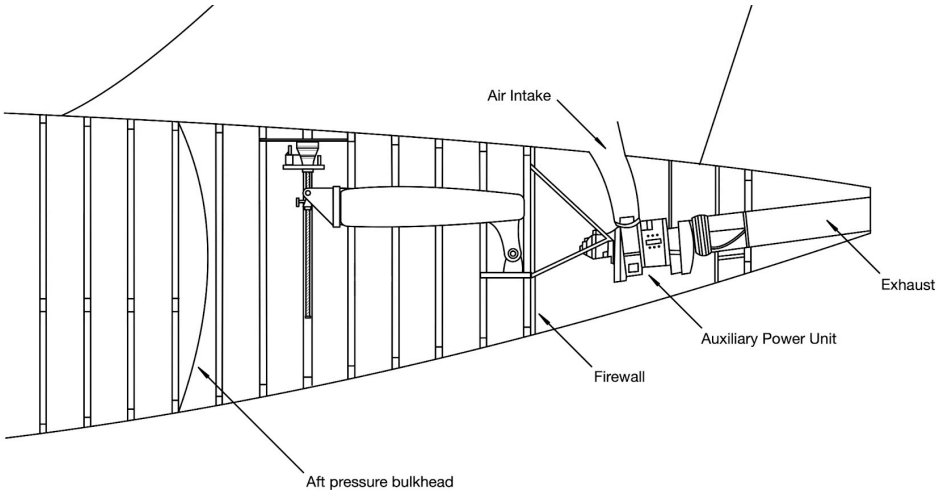

Figure 5.25: APU location and components

5.5 Maximum range calculation

It can be calculated the aircraft's maximum range using the aircraft design and performance data. Breguet equation for jet aircraft is used for this purpose, which is stated in Equation 5.9:

$$R = \frac{V}{SFC} \cdot \frac{C_L}{C_D} \cdot \ln\left(\frac{W_{START\ CRUISE}}{W_{END\ CRUISE}}\right)$$

Equation 5.9: Breguet range equation for jet aircraft

The most relevant parameters which affect the aircraft's maximum range are the cruise speed (V), the specific fuel consumption (SFC), the aerodynamic efficiency (C_L/C_D) and the difference between the initial and the final weight at cruise.

Specific Fuel Consumption of Rolls-Royce Trent 1000 engines is calculated initially in metric units:

$$SFC = 14'3\ \frac{g}{kN \cdot s} \cdot 10^{-3}\ \frac{kg}{g} \cdot 9'81\ \frac{N}{kg} \cdot \frac{1}{10^3} \cdot \frac{1}{\frac{N}{kN \cdot s}} = 0'000140283\ \frac{N}{N \cdot s} = 1'40283 \cdot 10^{-4}\ \frac{N}{N \cdot s}$$

Equation 5.10: Specific fuel consumption calculation

Different scenarios will be exemplified for calculations depending on the mission which the aircraft is going to carry out:

- **Aerial refueling mission**: the aircraft operates completely as a tanker for aerial refueling, taking off at its MTOW with the fuel tanks completely full and flying at cruise speed until all fuel is burnt to return to a military base or airport. Even though finding sources of reliable military aircraft data is a difficult task, fighter jets such as F-18 Hornet can accommodate around 13,000 kg of jet fuel ([55], Amfuel, 2024). Eurofighter Typhoon carries approximately 7,600 kg of fuel ([56], Eurofighter, 2024).

  Setting up the case where 3 F-18 Hornet and 3 Eurofighter Typhoon fighter jets are refueled 3/4 of their whole fuel tanks capacity, the aircraft will transfer a total amount of 46,350 kg of jet fuel.

  The weight at the start and end of cruise are then calculated (note that transferred fuel is not accounted):

  $$W_{START\ CRUISE} = 107{,}800 + 0'95 \cdot (120{,}688 - 46{,}350) = 178{,}421'1\ kg$$
  $$W_{END\ CRUISE} = 178{,}421'1 - 0'9 \cdot (120{,}688 - 46{,}350) = 111{,}516'9\ kg$$

  $$R = \frac{237'16}{1'40283 \cdot 10^{-4}} \cdot 13'4 \cdot \ln\left(\frac{178{,}421'1}{111{,}516'9}\right) = 10{,}646{,}617'3\ m = 10{,}646'61\ km = 5{,}749'17\ nmi$$

  For this specific scenario, LT-018 would remain approximately 12 hours flying at cruise speed while carrying out aerial refueling.

- **Passenger evacuation mission**: scenario in which the aircraft performs an evacuation mission, making use of its special configuration where 312 passengers are accommodated. Assuming an average weight of 100 kg per passenger (including minimum luggage), the payload weight would be 31,200 kg.

  Setting the case in which 75,000 kg of fuel are carried in the fuel tanks, the range calculation is performed:

  $$W_{START\ CRUISE} = 107{,}800 + 312 \cdot 100 + 0'95 \cdot 75{,}000 = 210{,}250\ kg$$
  $$W_{END\ CRUISE} = 210{,}250 - 0'9 \cdot 75{,}000 = 142{,}750\ kg$$

  $$R = \frac{237'16}{1'40283 \cdot 10^{-4}} \cdot 13'4 \cdot \ln\left(\frac{210{,}250}{142{,}750}\right) = 8{,}771{,}609'56\ m = 8{,}771'61\ km = 4{,}736'29\ nmi$$

  Some examples of long-haul routes which LT-018 could perform at its maximum passenger capacity are Kyiv - Washington DC, Baghdad - Madrid or Canberra - Pekin, to mention a few.

- **Military transporter**: exemplified scenario in which the aircraft presents a mixed configuration carrying two High mobility Multipurpose Wheeled Vehicles (3,600 kg each approximately), 14 pallets of passengers (126 in total) and 8 stretcher pallets (32 stretchers, assuming a total weight of 120 kg per patient including medical equipment).

  Again, setting the case in which 75,000 kg of fuel are carried in the fuel tanks, the range calculation is performed:

  $$W_{START\ CRUISE} = 107{,}800 + 3{,}600 \cdot 2 + 126 \cdot 100 + 32 \cdot 120 + 0'95 \cdot 75{,}000 = 202{,}690\ kg$$
  $$W_{END\ CRUISE} = 202{,}690 - 0'9 \cdot 75{,}000 = 135{,}190\ kg$$

  $$R = \frac{237'16}{1'40283 \cdot 10^{-4}} \cdot 13'4 \cdot \ln\left(\frac{202{,}690}{135{,}190}\right) = 9{,}174{,}713'02\ m = 9{,}174'71\ km = 4{,}953'95\ nmi$$

- **Ferry range**: the last example of mission scenario studied, in which the flies with the maximum fuel amount and the minimum equipment and no payload (maximum range). Repeating the process, the ferry range is calculated:

  $$W_{START\ CRUISE} = 107{,}800 + 120{,}688 = 228{,}488\ kg$$
  $$W_{END\ CRUISE} = 107{,}800\ kg$$

  $$R = \frac{237'16}{1'40283 \cdot 10^{-4}} \cdot 13'4 \cdot \ln\left(\frac{228{,}488}{107{,}800}\right) = 17{,}017{,}676'47\ m = 17{,}017'68\ km = 9{,}188'8\ nmi$$

Chapter 6: Landing gear and other relevant systems

This chapter of the project covers the layout design of the landing gear, as well as other relevant aircraft systems which have not still be defined, such as the communications or the hydraulic system layout.

6.1 Landing gear design

The first member of the landing gear to be designed is the main one (located in the wing root fairing), as it is critical to determine the necessary height with respect to the ground that it will provide to the aircraft when it is deployed, ensuring a proper ground clearance for a 5º bank angle. The first step is to determine the length of it, tanking into consideration the angle which has been explained and the expected location of the main landing gear. Note that this was already decided in the wing design chapter, to be more specific, the main location of the support beams was shown in Figure 2.15.

Considering this limiting factors and making use of a front and side view of the aircraft, the height of the main landing gear height when it is completely deployed is determined. Afterwards, to ensure that the aircraft remains completely parallel to the ground (mainly to ensure a safe environment to load, place and secure the cargo and to avoid any possible slope), the front landing gear is designed.

Figure 6.1 illustrates the main dimensions and the most important components of the aircraft landing gear system. Moreover, it can be also appreciated its two different positions (deployed and retracted), demonstrating that the lower deck of the fuselage is able to accommodate them when the takeoff or landing configurations are not active.

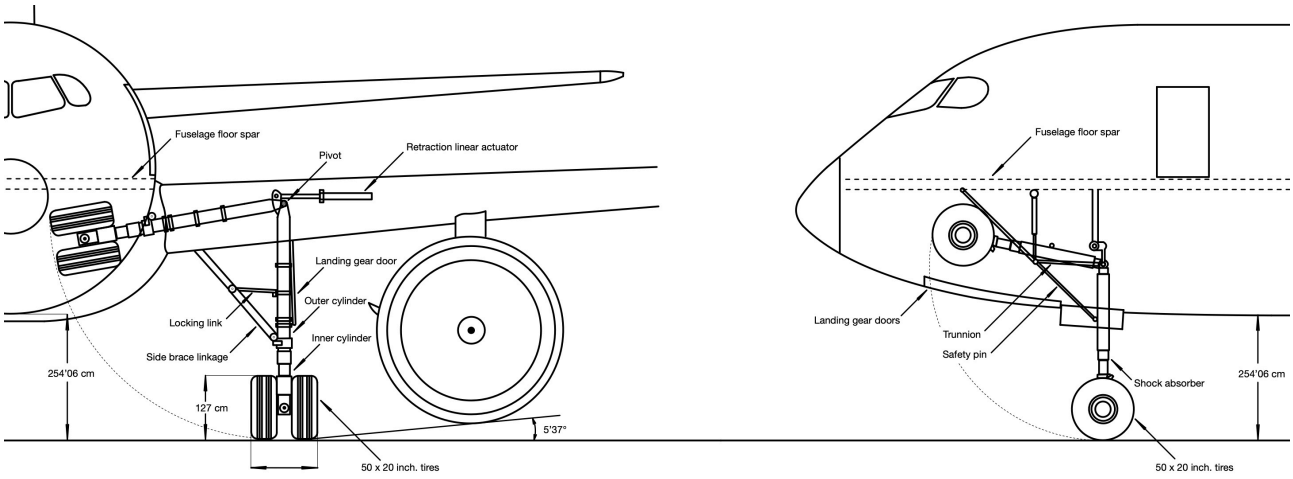

Figure 6.1: Landing gear system layout

The landing and the taxiing shocks are absorbed by several members, mainly composed of an oleo-pneumatic strut which is made of an inner and outer cylinder filled with oil and nitrogen. The size of the tires selected for the whole landing gear system is 50 x 22 ” (127 x 50 cm), which is the most suitable to be properly accommodated inside the landing gear bays.

A double-axle bogie is selected for the main landing gear. To retract the main landing gear, a linear actuator is used, which pushes and pulls the oleo-pneumatic strut by means of an attachment.

The two main doors which give access to the main landing gear bay are located in the wing root fairing and attached to the main strut. Note that the wing root fairing doors remain closed when the landing gear is either retracted or deployed and are only opened during the transition process.

In the case of the nose landing gear, there is also a linear actuator which deploys and retracts it, attached to the trunnion and to the safety pin, so it remains completely locked when it is deployed. Regarding the doors, two different types are also used. The front ones only are opened during the transition from retracted to deployed or vice versa. The other ones, located behind them, will remain opened when the nose landing gear is deployed to allow the oleo-pneumatic strut to emerge.

With this design of the landing gear, the fuselage is located at a distance of 254'06 cm above the ground. The following figures illustrate the landing gear system assembled to the complete aircraft model.

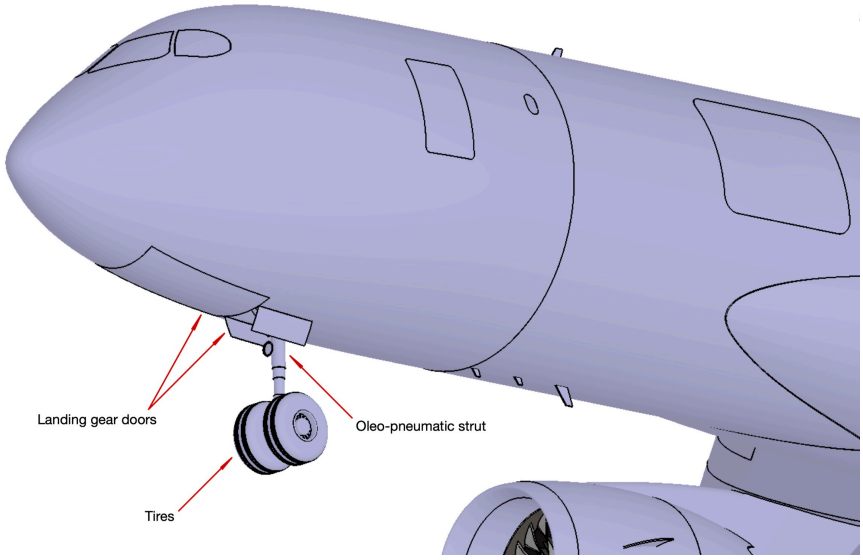

Figure 6.2: Nose landing gear (deployed)

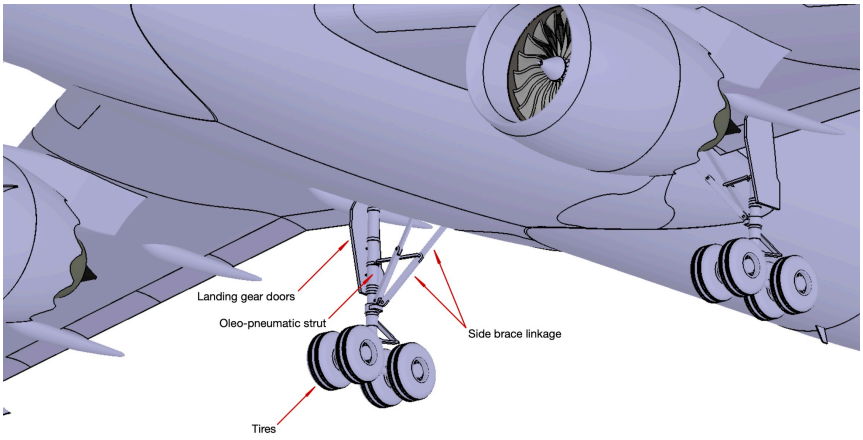

Figure 6.3: Main landing gear (deployed)

Figures 6.4 and 6.5 show the nose and the main landing gear (colored in red) inside its respective bays when they are retracted:

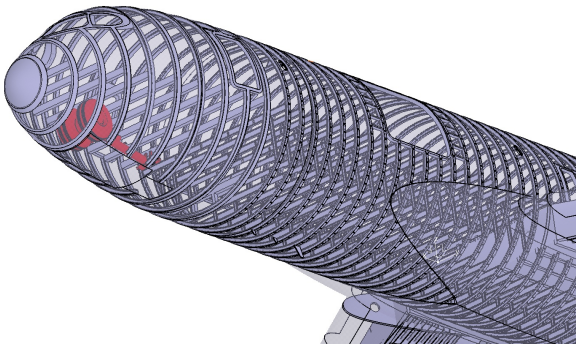

Figure 6.4: Nose landing gear (retracted)

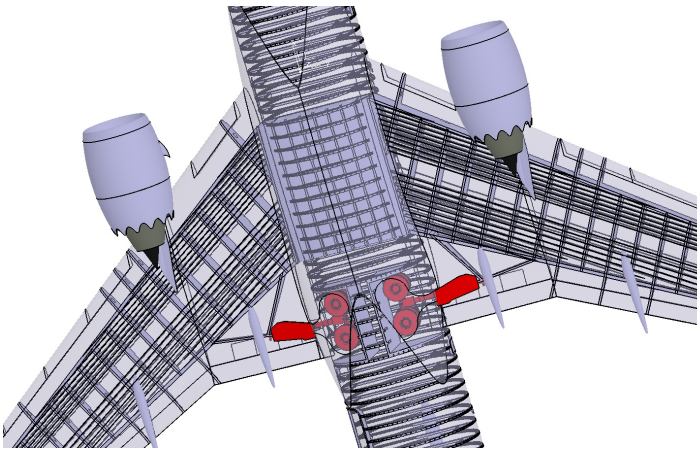

Figure 6.5: Main landing gear (retracted)

6.2 Communications

Several systems (mainly antennas) must be placed in the outer part of the fuselage to establish communications between the aircraft and the ground stations, as well as other possible allied aircraft.

For redundancy purposes and to avoid any possible screening events, several **VHF (Very High Frequency) antennas** are installed in the aircraft for this purpose. Two of them are located in the lower part of the fuselage and one of them in the upper part of it.

In the same manner, two **DME (Distance Measurement Equipment) antennas** are located in the lower part of the fuselage, as they will communicate mainly with ground stations to determine and reveal the aircraft position.

A **SATCOM (Satellite Communication) antenna** is located in the upper part of the fuselage too, to communicate with civil and military satellite networks.

Lastly, two **GPS (Global Positioning System) antennas** are installed in the upper part of the fuselage too, to communicate with GPS satellites for navigation and mission coordination. All mentioned communication systems are shown in Figure 6.6:

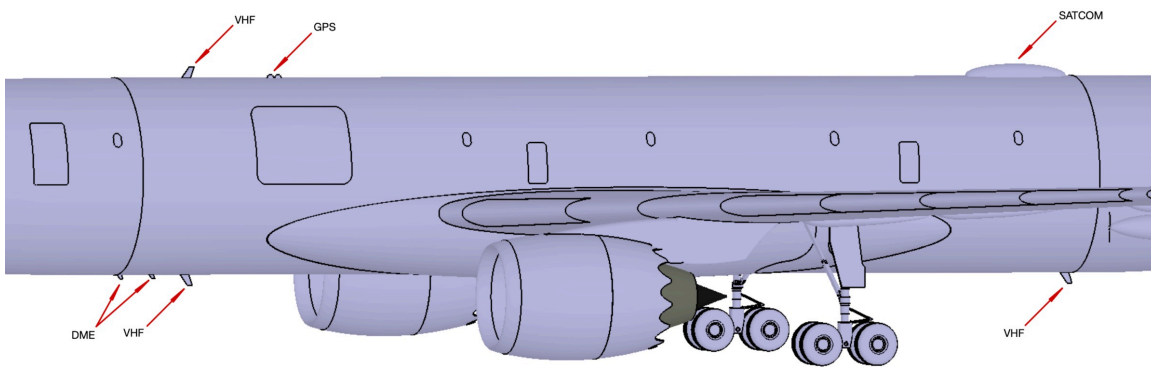

Figure 6.6: Aircraft communication systems

6.3 Hydraulic system

To perform essential operations during flight such as the control surfaces' deflection, the landing gear deployment, the thrust reversers or the high-lift systems' deployment, hydraulic actuators are used, which need constant pressure from the aircraft's hydraulic system.

For safe operations in any case of emergency or attack that the aircraft may suffer, three independent hydraulic systems are used (A, B and C), where each one has independent reservoirs, pipe lines, pumps and valves.

Hydraulic system A is pressurized by an engine-driven pump located in the left engine. It is responsible for the flaps, left elevator, left aileron, rudder and extendable boom actuators' functioning, as well as the upper deck cargo door.

Hydraulic system B is pressurized by an engine-driven pump too, located in the right engine. It is responsible for the slats, spoilers, landing gear deployment, right elevator, right aileron and rudder actuators' functioning.

Hydraulic systems A and B are interconnected by the PTU (Power Transfer Unit), which enables both hydraulic systems to pressurize each other in case of failure of any engine-driven pump.

All actuators can function solely with Hydraulic system C, which can be either pressurized completely by an electric-driven pump or in case of emergency, by the RAT (Ram Air Turbine).

Figure 6.7 shows the general arrangement of the three different hydraulic systems, where the main pipelines, reservoirs, power transfer unit and systems which they affect are indicated.

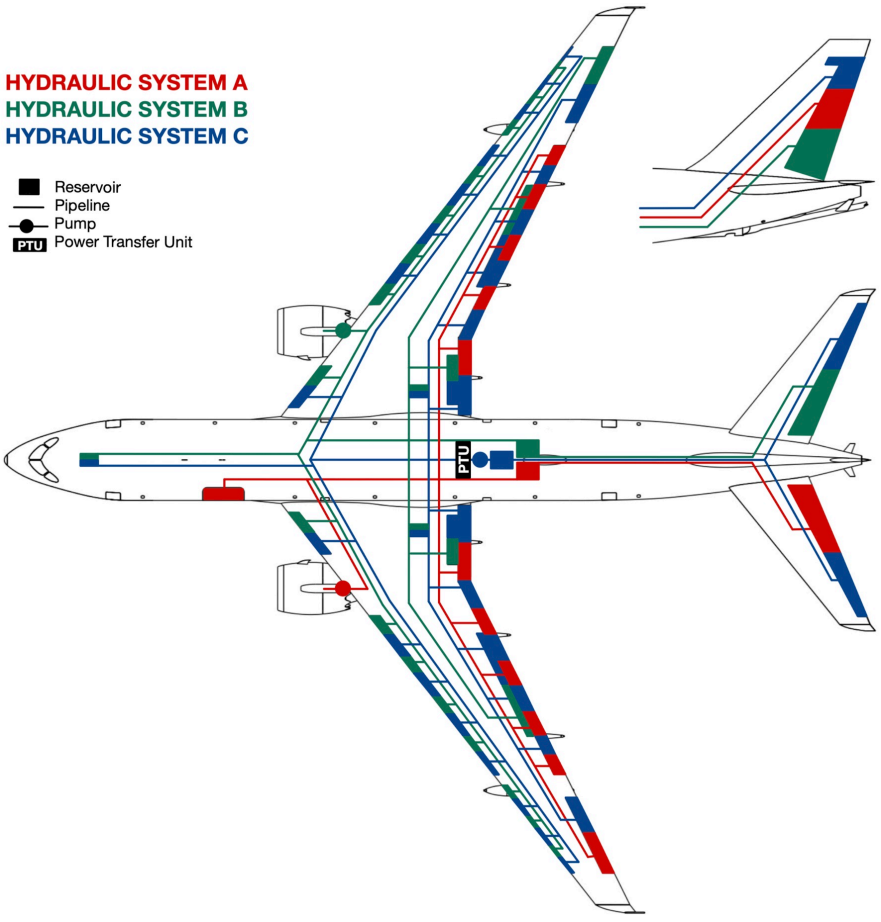

Figure 6.7: Hydraulic system arrangement

Chapter 7: Manufacturing and materials

7.1 Construction materials

This chapter covers mainly the selection of materials employed to manufacture the different components of the aircraft which have been designed throughout the project. Two main types of materials will be used to manufacture the airframe of LT-018: metallic alloys and composite materials.

There are several advantageous reasons to combine traditional metallic alloys with composite materials in aircraft manufacturing. Besides presenting excellent fatigue resistance, the most relevant reason is probably the weight reduction that can be achieved if composite materials are used properly. This is due to the fact that composite materials and CFRP (Carbon Fiber Reinforced Plastic) in particular (which is the most used composite material in aircraft structural members) present a much lower density than metallic alloys. For example, aluminum alloy 2024 (Al2024), widely used in aviation, has a density of 2,780 kg/m^3, much higher than CFRP density, which has a value of approximately 1,550 kg/m^3 ([57], ASM Aerospace Specification Metals, 2024).

Having a lighter airframe translates in more usable payload weight (considering structural limitations), but there are more reasons why LT-018 can benefit from being manufactured partially with composite materials. For example, being more resistant to rust and corrosion than traditional metallic materials (if proper resins and reinforcements are used to create the composite material itself) ([58], Composites Lab, 2024).

Aluminum alloy is selected as the main metallic material to form the airframe. The whole skin of the fuselage, wings, vertical and horizontal stabilizers, the flying boom and the nacelles' leading edge are manufactured with aluminum alloy panels to avoid additional manufacturing complexity and costs, due to the fact that installing an additional external metallic mesh would be necessary if these components were manufactured in composite materials (mainly for lightning strike protections, as CFRP is not a conductive material).

Steel and titanium alloys are used for structural components which demand high structural loads, as they presents exceptional mechanical properties while being light at the same time. Steel is used mainly for the landing gear structure. Titanium alloys are used to manufacture the engine pylons' structure.

Fiberglass composite material is selected to manufacture non-structural components (mainly fairings) or panels which cover communication systems. This material, besides being light and inexpensive, is a dielectric material and allows radio frequency signals to pass through it. The wing root fairing, the flap track fairings, the flying boom gimbal fairing, the antennas and the radome (radar dome which covers the weather radar, located next to the front pressure bulkhead) are manufactured in fiberglass.

CFRP (Carbon Fiber Reinforced Plastic) is used to manufacture the rest of the structural components. The fuselage frames, the floor spar, the stringers, the floor struts, the pressure bulkheads and the wings and stabilizers' spars, ribs and stringers are designed to be manufactured using this material, as well as the nacelles' main body.

Two approaches are used to manufacture the different composite material components depending on their function and location (fiberglass and CFRP). All the fairings, including the radome, the flap track fairings and the wing root one are manufactured using a wet lay-up process, which basically consists in combining material sheets with resin using a mandrel with the component shape.

Structural members which withstand flight loads are manufactured using a resin infusion process and attached mechanically if they cannot be co-cured, which can result to be expensive and is more complex but provides a high dimensional accuracy, allows the creation of complex geometries, can integrate different components and presents a higher uniformity and consistency.

Moreover, resin infusion or RTM (Resin Transfer Moulding) does not require an autoclave to cure the composite material components and thus, manufacturing costs would be significantly reduced ([59], Composite Integration, 2024).

Figures 7.1 and 7.2 show all the major aircraft components which are intended to be manufactured in the materials mentioned previously:

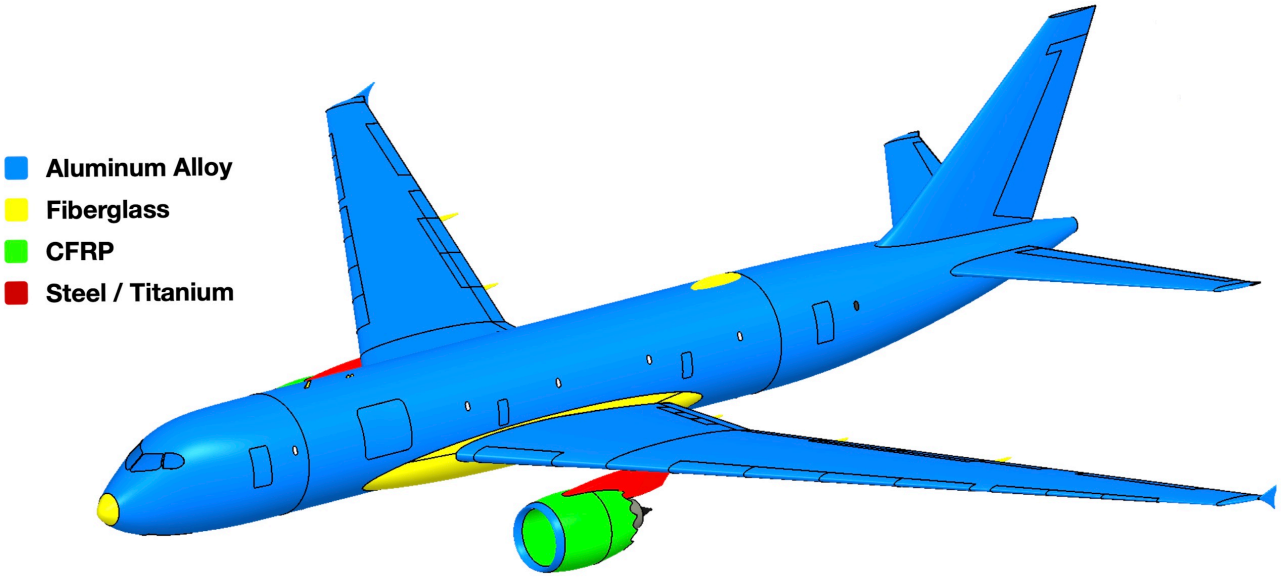

Figure 7.1: Aircraft construction materials (skin, nacelles and pylons)

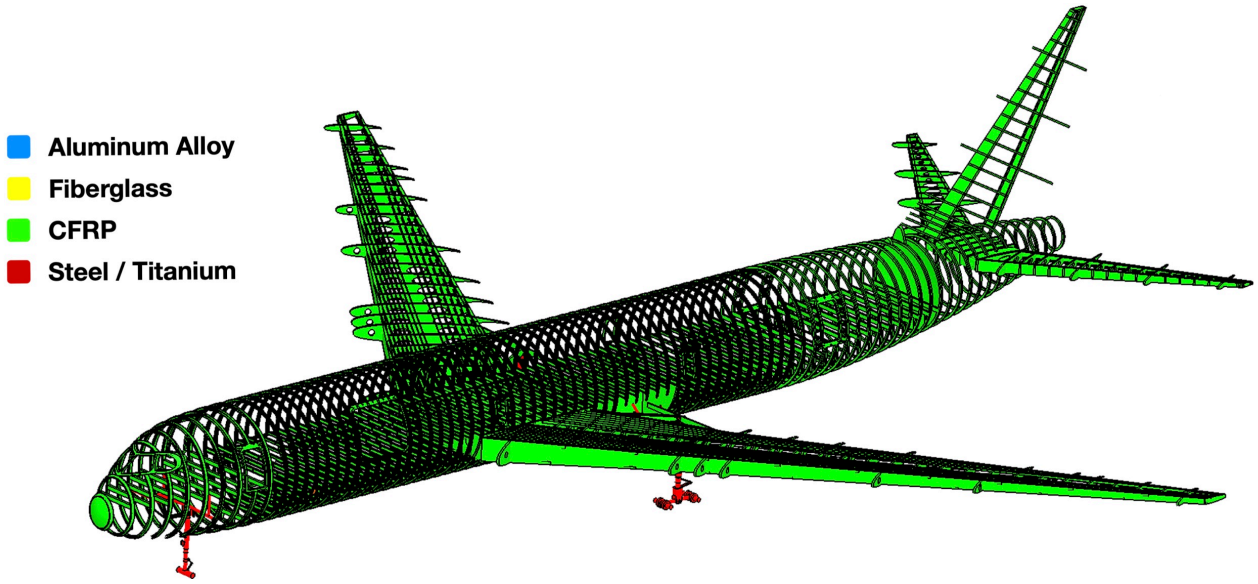

Figure 7.2: Aircraft construction materials (structural components)

Chapter 8: General dimensions and final design

This chapter describes the aircraft general dimensions, operating drawings, secondary figures, comparisons and other additional design features (such as the paint job, for example).

8.1 Paint job

Contrary to commercial aircraft, which are painted with the airline's logo or different advertisements, military aircraft usually aim to go unnoticed when they fly. For this purpose, they are usually painted in different tones of gray color, which can be properly camouflaged at high altitudes flying though different atmospheric conditions (either it is cloudy, clear, foggy, etc).

The name of the aircraft is also painted on the fuselage. The following figure shows the left and right views of the aircraft, where the paint job is appreciated:

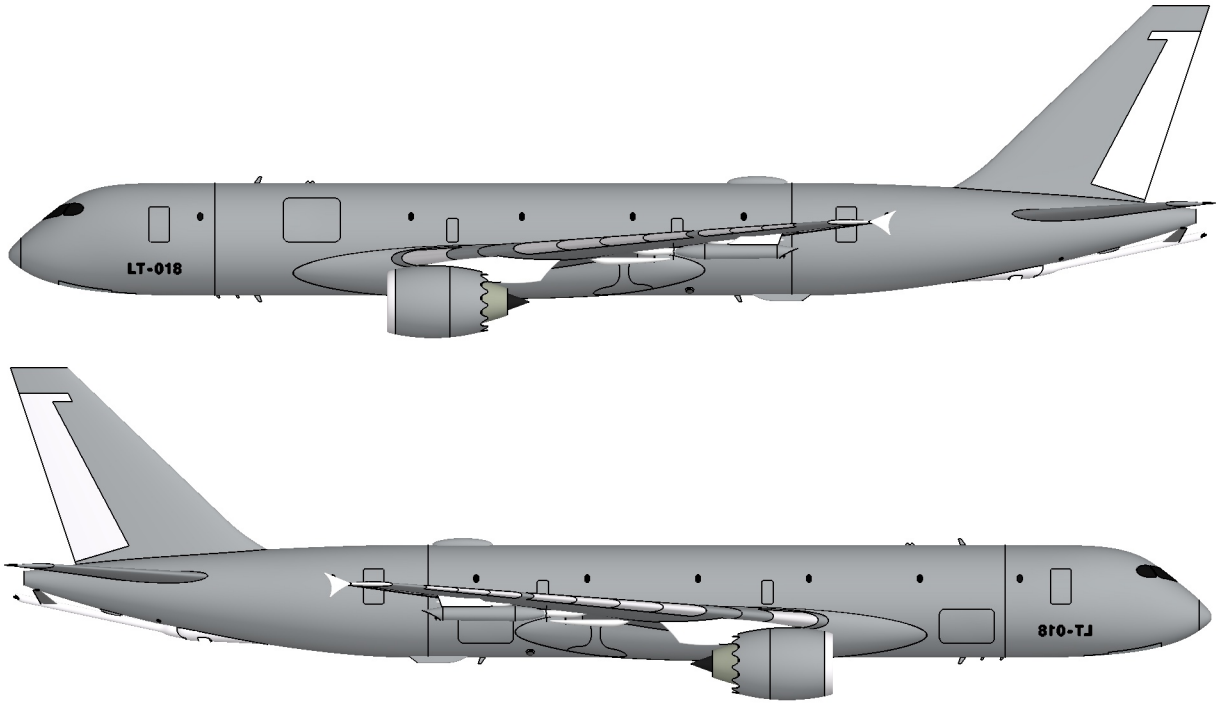

Figure 8.1: LT-018 Archangel paint job

8.2 LT-018 Archangel: General Dimensions

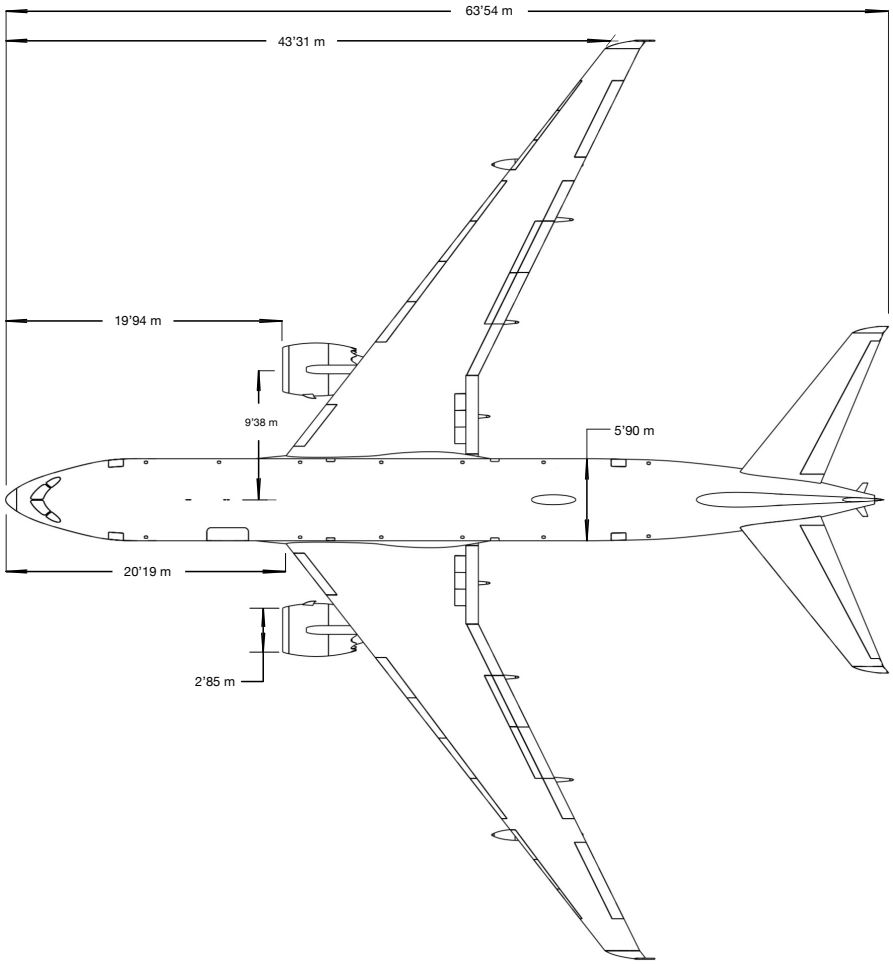

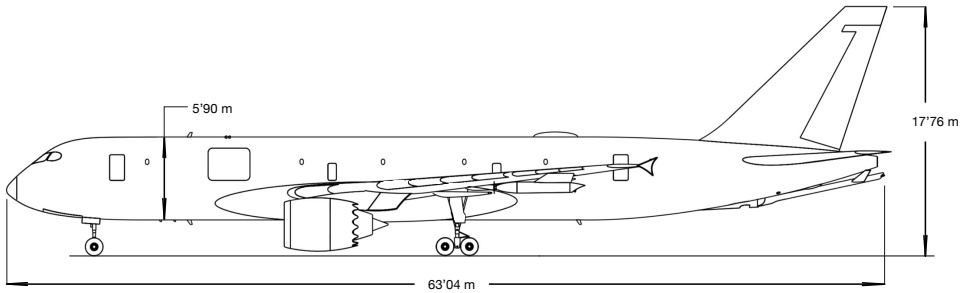

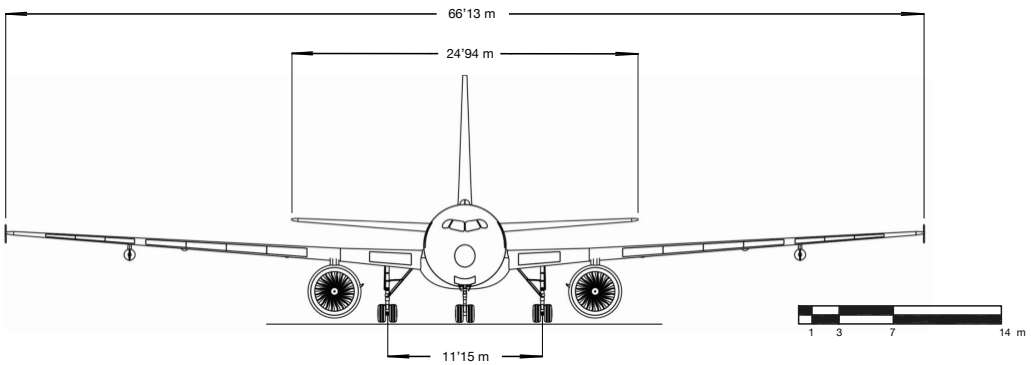

8.3 Ground servicing arrangement

The following figure shows the layout and arrangement of the different ground services which the aircraft may need to use before performing a mission:

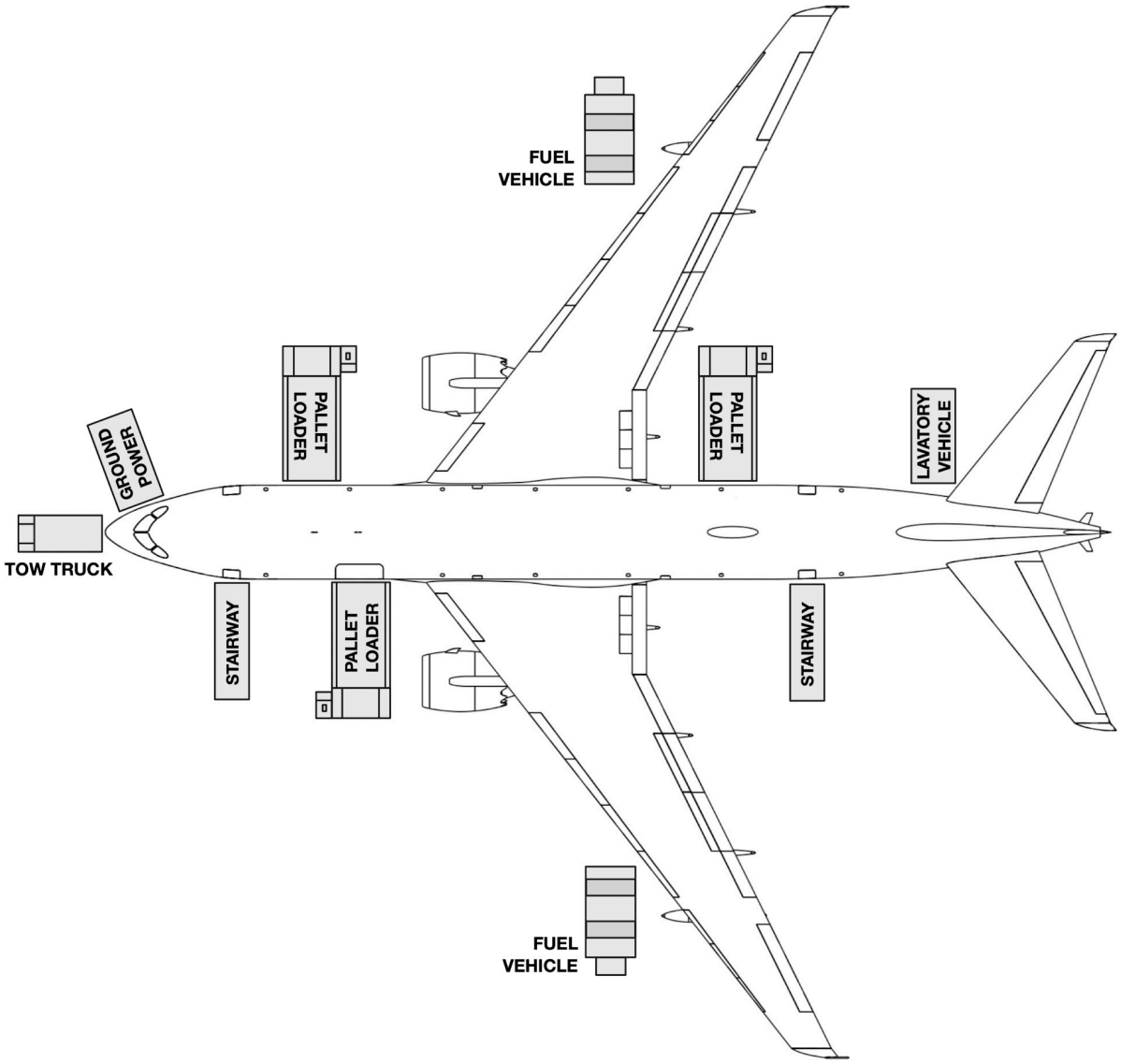

Figure 8.1: Ground servicing arrangement

8.4 Tailstrike angle

Being limited by the flying boom attachment, the critical tailstrike angle results to be 9º :

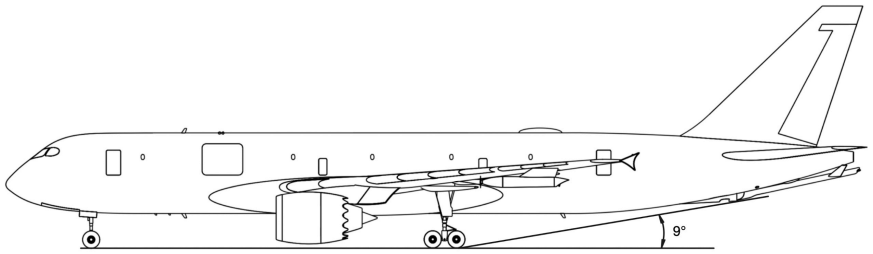

Figure 8.2: Critical tailstrike angle

8.5 Similar aircraft comparison

Figure 8.3 compares LT-018 Archangel to different wide-body military tankers and commercial aircraft:

Figure 8.3: Similar wide-body aircraft comparison

8.6 Operational images

The figures shown in this section illustrate aerial refueling scenarios which may take place in those missions for which the aircraft is designed.

Figure 8.4 shows LT-018 Archangel refueling a Fairchild Republic A-10 Thunderbolt II attack aircraft by means of the flying boom:

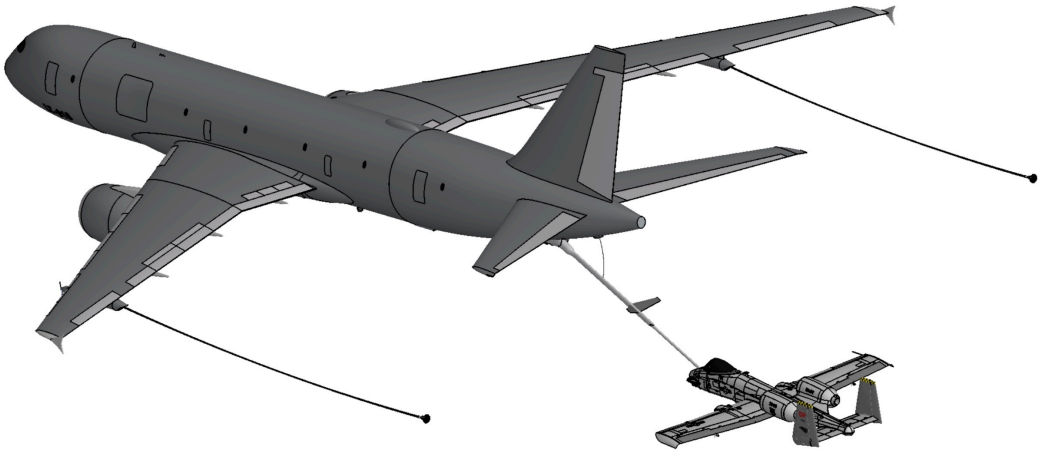

Figure 8.4: A-10 Thunderbolt II performing aerial refueling through the flying boom

It is common that long range bombers also perform aerial refueling using the flying boom system, as it is illustrated in Figure 8.5 with Northrop Grumman B-2 Spirit:

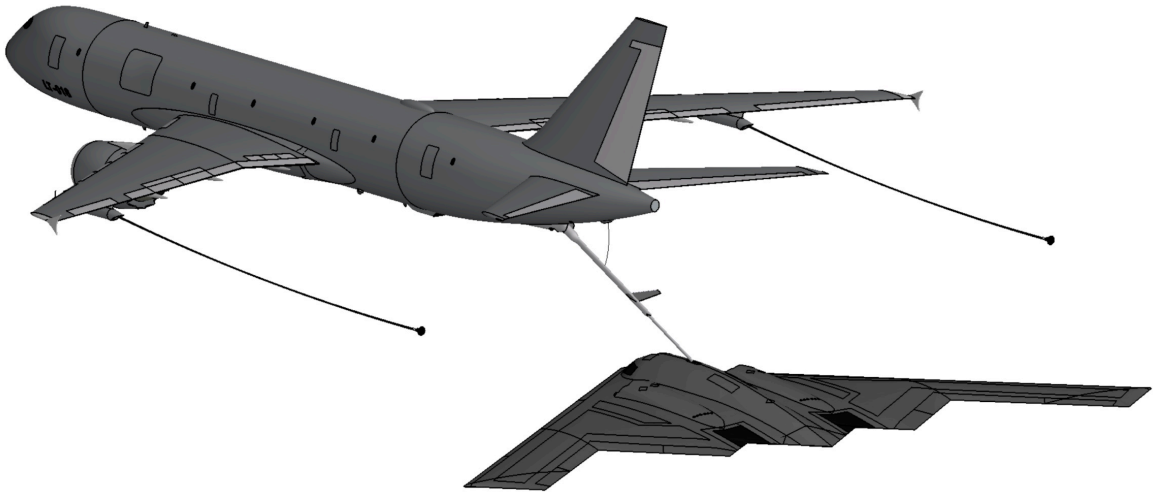

Figure 8.5: B-2 Spirit bomber performing aerial refueling through the flying boom

The following figures show the probe and drogue aerial refueling system. In Figure 8.6, two Eurofighter Typhoon fighter jets are being refueled simultaneously from the wing pods using the probe and drogue system:

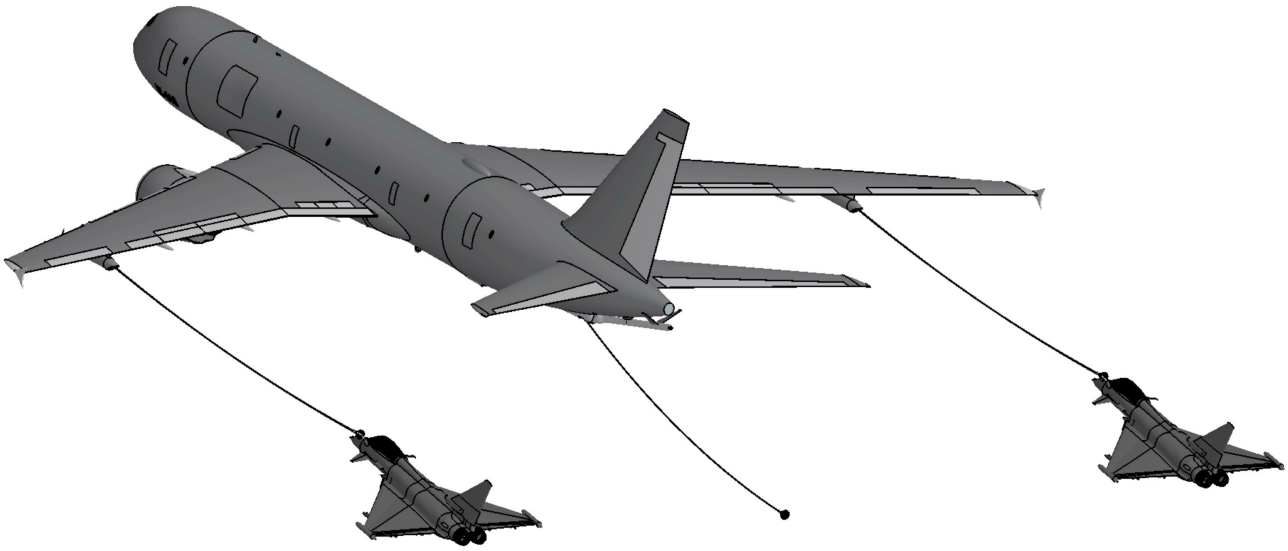

Figure 8.6: Eurofighter Typhoon fighter jets refueling simultaneously from the wing pods

Lastly, Figure 8.7 shows an Eurofighter Typhoon too, refueling using the centerline drogue:

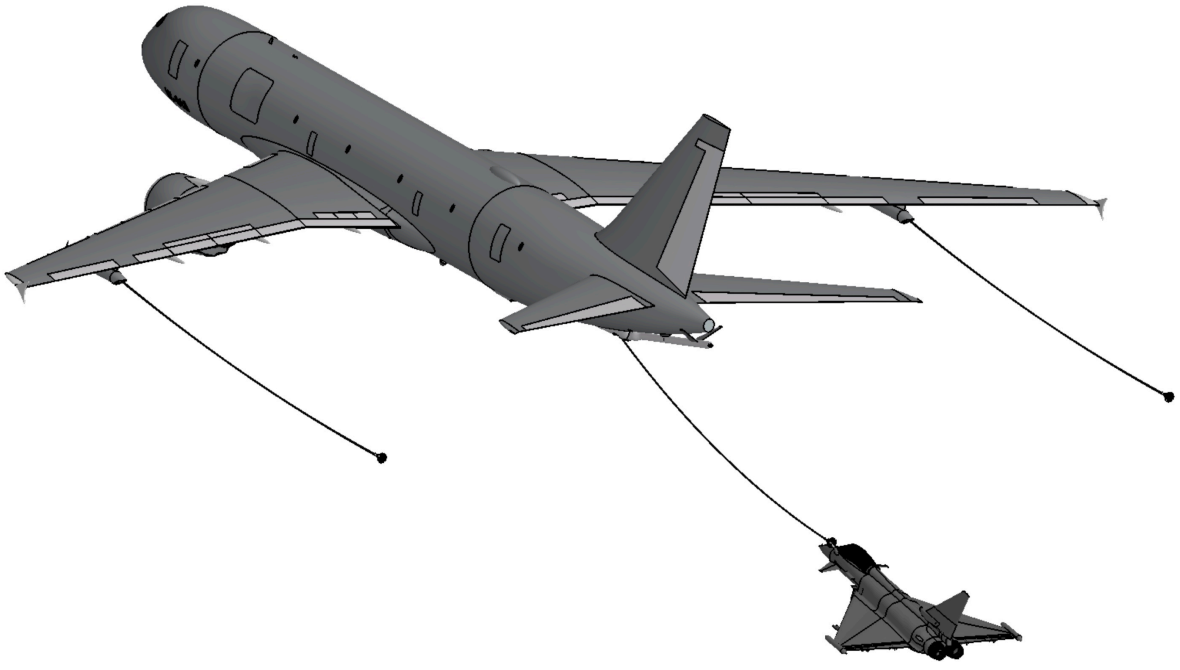

Figure 8.7: Eurofighter Typhoon fighter jet refueling from the centerline drogue

8.7 Market analysis

This section illustrates different figures with graphs which compare different operational aspects of LT-018 Archangel with different civil and military aircraft. Figure 8.8 compares the maximum fuel capacity of different military tanker aircraft.

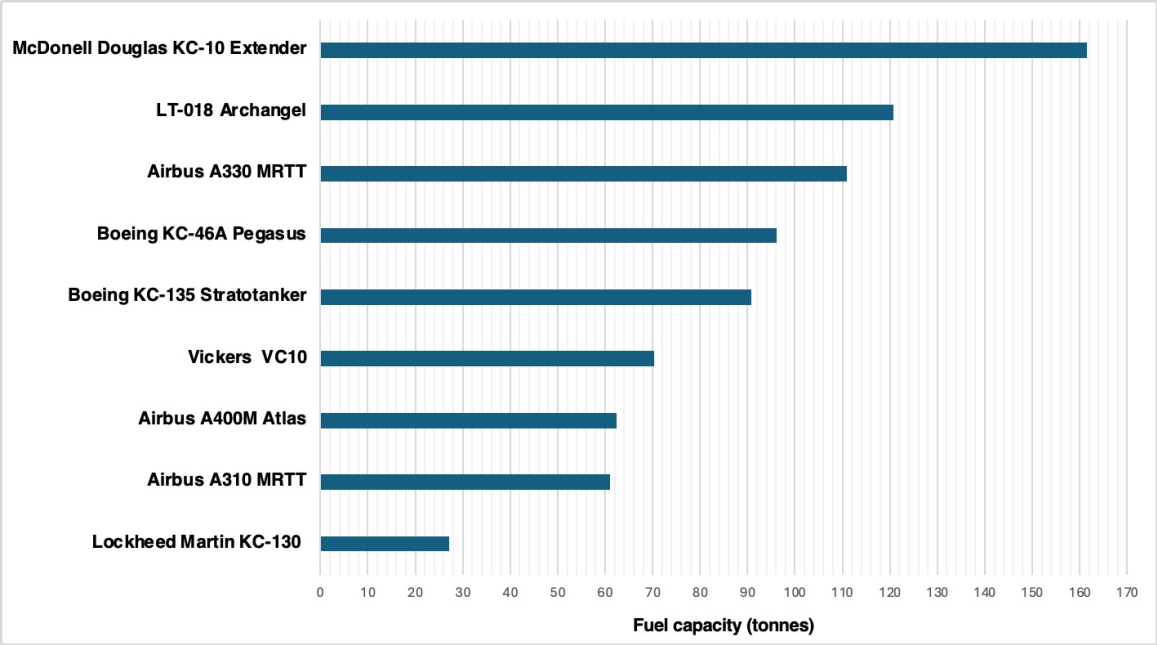

Figure 8.8: Maximum fuel capacity for different military tanker aircraft

Figure 8.9 compares both the maximum amount of passengers and the maximum range that different aircraft can achieve:

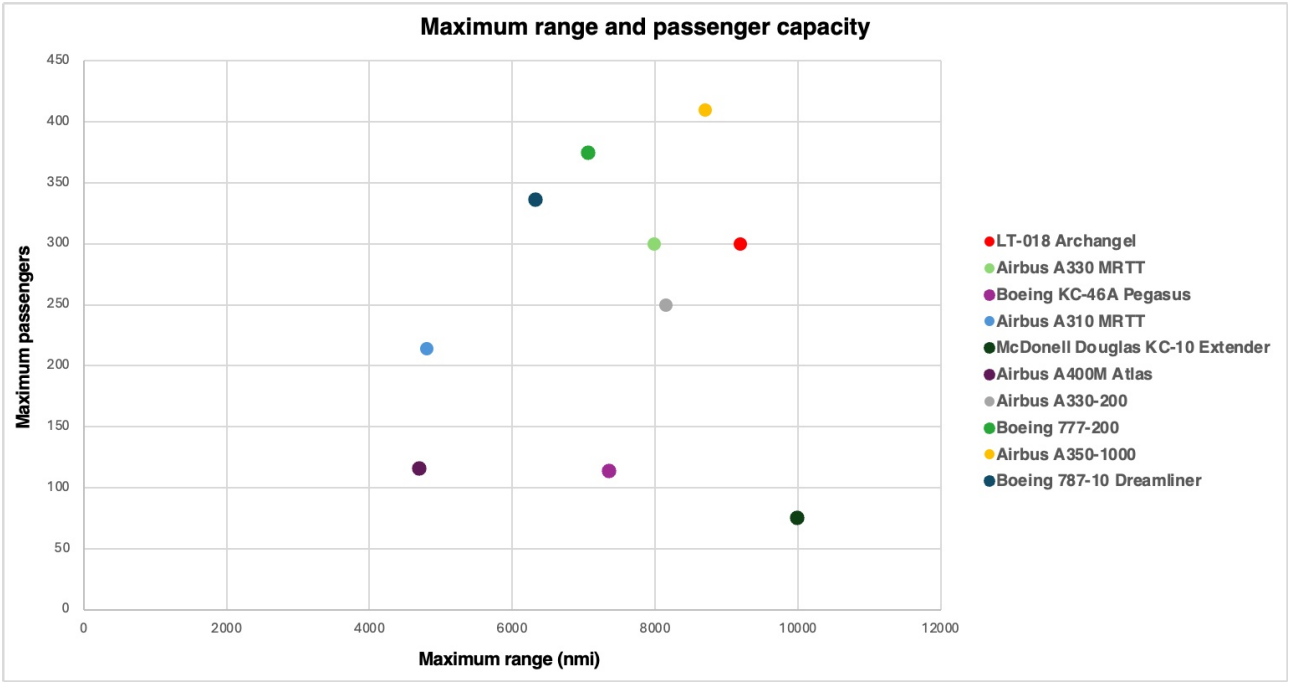

Figure 8.9: Maximum range and passenger capacity for different aircraft

Chapter 9: Conclusions and Future Works

9.1 Findings

After the preliminary design process of the aircraft has been concluded, it can be stated that the main objectives mentioned in the introduction of the report have been achieved:

- It has been designed a multirole tanker aircraft for military use which can accommodate a high amount of fuel (120'69 tonnes).
- The aircraft has been designed to be highly versatile thanks to its military pallet handling system, which allows the transport of a wide variety and a high amount of payload (military vehicles, standard LD3 containers, passengers, medical stretchers, etc).
- Some of the best performance and operational features which modern tankers and commercial aircraft present have been combined to design LT-018 Archangel, such as the variety of aerial refueling systems, the high fuel capacity, the aerodynamic and thrust efficiency, the possibility of using sustainable aviation fuels, the pallet handling system to transport different types of payloads or the use of advanced materials for its construction.
- Despite this fact, it has been also understood why tanker aircraft are manufactured from conversion processes of airliners, since the development of a tanker aircraft solely for this purpose is a tedious process that does not differ significantly from that of a commercial aircraft.

9.2 Significance of the project

It is important for air forces to have state-of-the-art advanced aircraft which can carry out pure combat missions (fighter jets, bombers and spy planes), but special attention must be payed also to all the infrastructure which supports the deployment, operation and maintenance of these.

Tankers and military transporters, as it was mentioned in the introduction, are one of the most important pillars of any air force and it is important to take care of this type of aircraft fleet for the proper execution of any military operation and maneuver.

Moreover, as bombers and fighter jets make great advancements and achieve superior performance and operational capabilities, it is important that those previously mentioned tankers and military transporters also develop to keep up and not slow down the development of military operations. For that specific reason, it is probable that in the following years, new military multirole transport tankers are developed or manufactured from the latest airliners.

Lastly, integrating and combining the latest advancements in composite materials, aerodynamics, powerplants and advanced aerial refueling systems definitely demonstrates the potential for improvements in tanker aircraft efficiency and performance.

9.3 Implications for the particular field of study

The development of this project has required to apply and further develop many of the concepts and knowledge acquired throughout the degree. The complexity of developing a preliminary aircraft design has been understood, where all the different disciplines involved in this task (aerodynamics, aircraft design, aircraft propulsion, structures, materials, etc) must be properly interlinked and depend on each other.

Furthermore, this project has been a great opportunity to learn and understand the functioning of several engineering design and analysis software which have been mentioned several times throughout the degree and which have a high relevance in the current aviation industry, such as Catia V5, Ansys or Aeolus ASP, to mention a few.

9.4 Future works

Due to the lack of time and the brevity of the document, only the most relevant aspects of the preliminary aircraft design and flight performance have been studied. Some details, further research and a deeper analysis is intended to be done on the majority of the topics covered in this project, listed below:

- **Aerodynamic optimization on the shape of the fuselage nose and tailcone**: based on the knowledge acquired in Ansys Fluent, the most critical components of the fuselage regarding the aerodynamic performance will be optimized. Different nose and tailcone geometries will be created in Catia V5 modifying the most relevant design aspects of them (the length, the shape, the parabolas' radius, L_{FC}/d_F, etc) with the purpose of performing the same aerodynamic simulations on all of them and creating a database to select those which have the best aerodynamic performance (lower drag).

- **Topology structural optimization and cross-section design of the structural components**: once the main structural arrangement of the different components has been done, there are currently different software which can optimize a defined structural arrangement modifying both the number of elements and the placement on them on the airframe. Moreover, topology optimization applications are able to define the most suitable, lighter and stronger cross-sectional shape that a structural element should have to withstand the defined loads.

  This process can also be done using Ansys, interconnecting the different modules which the software provides (for example, Ansys Fluent with Ansys Structural) to analyze in detail a structure with the loads directly obtained from an aerodynamic analysis. This process is tedious and requires an exhaustive research and study on all the different load cases considering all maneuvers, the load factor, the flight envelope and emergency scenarios which may arise.

- **Aerodynamic analysis on the high-lift devices and control surfaces**: the CFD Ansys aerodynamic simulation performed on this project has proven to be crucial to determine essential performance data such as the main aerodynamic coefficients or the aircraft components which contribute the most to the reduction in the overall aerodynamic performance.

  Control surfaces and high-lift devices have been sized using real statistical data on military transporters, but their performance could be studied in detail defining all the control surfaces and high-lift devices which the aircraft presents and parametrizing their rotation angle as it was done with the aircraft's angle of attack in section 5.1. Afterwards, a database could be created analyzing the pitching, rolling and yawing moments and the lift-increasing effectiveness of these systems separately and combined.

- **CFD validation with empirical data**: to validate CFD Ansys results and to obtain a comparison or relation between aerodynamic simulations and real data, it is interesting to benefit from the resources available at university. This empirical data could be obtained by 3D printing a scaled model of the aircraft and by using the wind tunnel available at university. After calculating both Reynolds and Mach numbers by measuring airspeed, temperature, humidity, pressure, etc, the tests could be replicated in Ansys fluent to perform a comparative task between both the real and the CFD simulation data.

It is worth mentioning that there are several matters which have a significant importance on the aircraft performance, such as aeroelastic effects, controllability, lateral stability, etc, but this final project has focused mostly on both the design and performance analysis of the tanker aircraft.

Sources Consulted and References

- [1]: Official United States Air Force Website - Air Force Historical Support Division. (2023). 1923 - The Beginnings of Inflight Refueling. https://www.afhistory.af.mil/FAQs/Fact-Sheets/Article/458986/1923-the-beginnings-of-inflight-refueling/

- [2]: © AirTanker 2021. (July 15, 2023). Aerial Lifelines: Tracing the History of Air-to-Air Refuelling. https://www.airtanker.co.uk/media/news/airtanker-news/history-of-air-to-air-refuelling#

- [3]: US Centennial of flight commission - Dwayne A. Day. (2023). Aerial Refueling. https://www.centennialofflight.net/essay/Evolution_of_Technology/refueling/Tech22.htm

- [4]: ARSAG - AERIAL REFUELING SYSTEMS ADVISORY GROUP. (October 15, 2018). ARSAG Document No. 04-06-18 - Aerial Refueling Probe/Drogue System. https://apps.dtic.mil/sti/pdfs/AD1064517.pdf

- [5]: Official United States Air Force Website. (2023). KC-10 Extender. https://www.af.mil/About-Us/Fact-Sheets/Display/Article/104520/kc-10-extender/

- [6]: Boeing. (2023). KC-46A Pegasus: The World's Most Advanced Multi-Mission Aerial Refueling Aircraft. https://www.boeing.com/defense/kc-46a-pegasus-tanker/#stories

- [7]: Boeing. (2023). KC-46A Pegasus - Technical specifications. https://www.boeing.com/content/dam/boeing/boeingdotcom/defense/kc-46a_pegasus_tanker/images/kc46_key_features_960.jpg

- [8]: Official United States Air Force Website. (2023). KC-46A Pegasus. https://www.af.mil/About-Us/Fact-Sheets/Display/Article/104537/kc-46a-pegasus/

- [9]: Airforce Technology. (June 11, 2000). Airbus A310 MRTT Multi-Role Tanker Transport. https://www.airforce-technology.com/projects/mrtt/?cf-view

- [10]: Airbus. (2023). A330 MRTT. https://www.airbus.com/en/products-services/defence/military-aircraft/a330-mrtt

- [11]: Airbus. (2023). A330 MRTT Technical information. https://www.airbus.com/en/products-services/defence/military-aircraft/a330-mrtt/a330-mrtt-technical-information

- [12]: Airbus. (2023). A400M. https://www.airbus.com/en/products-services/defence/military-aircraft/a400m

- [13]: Lockheed Martin. (2023). KC-130J Tanker. https://www.lockheedmartin.com/en-us/products/c130/kc-130j-tanker.html

- [14]: Boeing. (December, 2022). 777-200LR / -300ER / -Freighter - Airplane Characteristics for Airport Planning. p. 2-4. https://www.boeing.com/content/dam/boeing/boeingdotcom/commercial/airports/acaps/777_2lr_3er_f.pdf

- [15]: Boeing. (February, 2023). 787 Airplane Characteristics for Airport Planning. p. 2-5. https://www.boeing.com/content/dam/boeing/boeingdotcom/commercial/airports/acaps/787.pdf

- [16]: Airbus. (July 1, 2021). A340-500/-600 - AIRCRAFT CHARACTERISTICS AIRPORT AND MAINTENANCE PLANNING. p. 2-2-0. https://www.airbus.com/sites/g/files/jlcbta136/files/2021-11/Airbus-Commercial-Aircraft-AC-A340-500_600.pdf

- [17]: Airbus. (July 1, 2023). A350 - AIRCRAFT CHARACTERISTICS AIRPORT AND MAINTENANCE PLANNING. p. 2-2-0. https://www.airbus.com/sites/g/files/jlcbta136/files/2021-11/Airbus-Commercial-Aircraft-AC-A350-900-1000.pdf

- [18]: Globid Inc. (2023). 463L Pallets. http://www.463lpallet.com/

- [19]: Air Europa. (2024). Travel in maximum comfort - Maximise your comfort by selecting the seat that's right for your trip. https://www.aireuropa.com/es/en/aea/aexperience/services/seats.html

- [20]: EASA. (2024). CS-25 SUBPART D – DESIGN AND CONSTRUCTION, CS 25.807 (section g) - Emergency exits. https://www.easa.europa.eu/en/document-library/easy-access-rules/online-publications/easy-access-rules-large-aeroplanes-cs-25?page=27

- [21]: EASA. (2024). CS-25 SUBPART D – DESIGN AND CONSTRUCTION, CS 25.807 (section f - 4) - Emergency exits. https://www.easa.europa.eu/en/document-library/easy-access-rules/online-publications/easy-access-rules-large-aeroplanes-cs-25?page=27

- [22]: Jan Roskam. (1986). Airplane Design - Part III: Layout Design of Cockpit, Fuselage, Wing and Empennage: Cutaways and Inboard Profiles.

- [23]: Aditya Rajan Iyer, Anjali Pant - International Research Journal of Engineering and Technology. (August, 2020). A review on nose cone designs for different flight regimes. p. 3549. https://www.irjet.net/archives/V7/i8/IRJET-V7I8605.pdf

- [24]: Federal Aviation Administration. (September 1, 1993). Pilot Compartment View Design Considerations - AC No: 25.773-1. https://www.faa.gov/documentlibrary/media/advisory_circular/ac_25_773-1.pdf

- [25]: Jan Roskam. (1985). Airplane Design - Part II: Preliminary Configuration Design and Integration of the Propulsion System.

- [26]: T.H.G. Megson. (2007). Aircraft Structures for engineering students - Fourth Edition.

- [27]: John Anderson. (2017). Fundamentals of Aerodynamics - Sixth Edition.

- [28]: Ejército del Aire y del Espacio. (2023). Airbus A330 (T.24/TK.24) - Datos. https://ejercitodelaire.defensa.gob.es/EA/ejercitodelaire/es/aeronaves/avion/Airbus-A330-T.24-TK.24/

- [29]: Airbus. (2021). A330 - AIRCRAFT CHARACTERISTICS AIRPORT AND MAINTENANCE PLANNING. https://www.airbus.com/sites/g/files/jlcbta136/files/2021-11/Airbus-Commercial-Aircraft-AC-A330.pdf

- [30]: Jan Roskam. (1985). Airplane Design - Part I: Preliminary Sizing of Airplanes.

- [31]: AMME, University of Sydney. (2006). International Standard Atmosphere Calculator. http://www-mdp.eng.cam.ac.uk/web/library/enginfo/aerothermal_dvd_only/aero/atmos/atmos.html

- [32]: Federal Aviation Administration. (August 6, 2007). Area Navigation (RNAV) and Miscellaneous Amendments. https://www.federalregister.gov/documents/2007/06/07/E7-10609/area-navigation-rnav-and-miscellaneous-amendments

- [33]: NATO - OTAN. (2016). MAJOR BOOST TO NATO'S AERIAL REFUELLING CAPABILITY. https://shape.nato.int/2016/major-boost-to-natos-aerial-refuelling-capability

- [34]: ICAO. (2024). DATAPLUS - Conversion factors. https://data.icao.int/newDataPlus/content/docs/glossary.pdf

- [35]: Nikola N. Gavrilović, Boško P. Rašuo, George S. Dulikravich, Vladimir B. Parezanović. (July, 2014). Commercial Aircraft Performance Improvement Using Winglets. https://www.mas.bg.ac.rs/_media/istrazivanje/fme/vol43/1/1_ngavrilovic.pdf

- [36]: Daniel P. Raymer. (2006). Aircraft Design: A Conceptual Approach, 4th edition.

- [37]: Jan Roskam. (1985). Airplane Design - Part V: Component Weight Estimation.
- [38]: Warren F. Phillips. (2004). Mechanics of Flight.
- [39]: Boeing. (July, 2021). 767 Airplane Characteristics for Airport Planning. https://www.boeing.com/content/dam/boeing/boeingdotcom/commercial/airports/acaps/767.pdf
- [40]: Lewis Boyd. (2008). Active Valve & Pump Technology: Modelling and Control of Variable-Speed Trim Transfer Pump in Aircraft Fuel Systems.
- [41]: Collins Aerospace. (2024). Ram Air Turbine. https://www.collinsaerospace.com/what-we-do/industries/commercial-aviation/power-controls-actuation/turbine-systems/ram-air-turbine
- [42]: Christopher Bolckom - Foreign Affairs, Defense, and Trade Division. (June 5, 2006). Air Force Aerial Refueling Methods: Flying Boom versus Hose-and-Drogue - CRS Report for Congress. https://sgp.fas.org/crs/weapons/RL32910.pdf
- [43]: Northridge pumps. (September 13, 2019). What Are Vane Pumps? https://www.northridgepumps.com/article-93_what-are-vane-pumps
- [44]: Air Force Reserve Command - USAF. (2024). Boeing KC-135R Stratotanker Fact Sheet. https://peetz.us/kc135.htm
- [45]: MR-CFD Co. (2024). Introduction to ANSYS Fluent: A beginner's guide to CFD simulation. https://www.mr-cfd.com/introduction-to-ansys-fluent-a-beginners-guide/#:~:text=How does ANSYS Fluent work,interconnected control volumes or cells.
- [46]: Ansys Innovative Space - Learning Forum. (September 19, 2018). https://forum.ansys.com/forums/topic/optimum-domain-size-for-fluid-flow-problems/
- [47]: Kristaq Hazizi - Coventry University, Research Gate. (November 25, 2022) What is difference between standard,Realizable k-ε and k-omega turbulence models in CFD? https://www.researchgate.net/post/What_is_difference_between_standard_Realizable_k-e_and_k-omega_turbulence_models_in_CFD
- [48]: EASA. (April 2, 2024). Type-Certificate data sheet for Trent 1000 series engines. https://www.easa.europa.eu/en/downloads/7733/en
- [49]: Aviation Week. (January 28, 2008). Gas Turbine Engines. https://web.archive.org/web/20181106021310/http://www.geocities.jp/nomonomo2007/AircraftDatabase/AWdata/AviationWeekPages/GTEnginesAWJan2008.pdf
- [50]: Rolls-Royce Inc. (November 28, 2023). Rolls-Royce Trent 1000 engines power Virgin Atlantic's world first 100% Sustainable Aviation Fuel flight from London Heathrow to New York JFK. https://www.rolls-royce.com/media/our-stories/discover/2023/poweroftrent-rr-trent-1000-engines-power-virgin-atlantics-world-first-100-sustainable-aviation.aspx
- [51]: Ravindra Krishnamurthy. (October 14, 2021). Aircraft Vortex Generators – The Nacelle Strakes. https://blog.gridpro.com/aircraft-vortex-generators-the-nacelle-strakes/
- [52]: NASA. (December 13, 2010). NASA Helps Create a More Silent Night. https://www.nasa.gov/aeronautics/nasa-helps-create-a-more-silent-night/
- [53]: AERTEC. (2024). The APU and its benefits. https://aertecsolutions.com/en/2015/05/11/the-apu-and-its-benefits/
- [54]: Pratt & Whitney. (2024). Auxiliary Power Units (APU). https://www.prattwhitney.com/en/products/auxiliary-power-units
- [55]: Amfuel. (2024). F-18 Hornet Boeing. https://www.amfuel.com/defense-f-18-hornet-boeing

- [56]: Eurofighter. (2024). Eurofighter Typhoon. https://www.eurofighter.com/the-aircraft/features
- [57]: ASM Aerospace Specification Metals. (2024). https://asm.matweb.com/search/SpecificMaterial.asp?bassnum=ma2024t4
- [58]: Composites Lab. (2024). Corrosion Resistance. https://compositeslab.com/benefits-of-composites/corrosion-resistance/index.html
- [59]: Composite Integration. (2024). Resin Transfer Moulding. https://composite-integration.co.uk/resin-transfer-moulding/

Figure References

Note: non-referenced figures, images and drawings are own-made

- Figure I.1: Marines. (April 18, 2016). A Spanish Air Force F/A-18 Hornet with 462 Squadron receives fuel from a U.S. Marine Corps KC-130J with Marine Aerial Refueler Transport Squadron 252, Special-Purpose Marine Air-Ground Task Force-Crisis Response- Africa during an aerial refuel mission, Gran Canaria, Spain. [Image]. https://www.marines.mil/Photos/igphoto/2001516562/

- Figure I.2: Aviation Stack Exchange. Why are flying-boom tankers restricted to a single boom? [Image]. https://aviation.stackexchange.com/questions/51692/why-are-flying-boom-tankers-restricted-to-a-single-boom

- Figure I.3: Infodefensa. (March 27, 2023). Boeing hace frente a otro recargo por más problemas en sus aviones cisterna KC-46A. [Image]. https://www.infodefensa.com/texto-diario/mostrar/4226703/boeing-hace-frente-otro-recargo-problemas-aviones-cisterna-kc-46a

- Figure I.4: Flynews. (March 7, 2024). Singapur compra el Airbus A330 MRTT. [Image]. https://flynews.es/aviacion-comercial/aviones/singapur-compra-el-airbus-a330-mrtt/

- Figure 1.1: Don Phillips. (February 6, 2023). Aviation Pallet (463L Master Pallet) [3D Model]. https://grabcad.com/library/aviation-pallet-463l-master-pallet-1

- Figure 4.1: Charles D. Harris - NASA. (1990). NASA Supercritical Airfoils - A Matrix of Family-Related Airfoils. [Image]. https://ntrs.nasa.gov/api/citations/19900007394/downloads/19900007394.pdf

- Figure 2.26: Sebastian Sowa. (March 4, 2024). YR-AGA photos. [Image]. https://www.jetphotos.com/photo/11257157

- Figure 6.1: Raunak Kunde - IDRW. (October 27, 2022). [Image]. https://idrw.org/drdo-to-develop-next-gen-air-to-air-refueling-pods-for-tanker-program/

- Figure 6.8: Yonhap News Agency. (January 30, 2019). Air Force holds ceremony introducing 1st aerial tanker. [Image]. https://en.yna.co.kr/view/PYH20190130168000315

- Figure 6.17: Rapid City Journal. (May 20, 2019). KC-135 Refueling B1. [Image]. https://rapidcityjournal.com/news/local/photos-kc-135-and-crew-from-fairchild-air-force-base-train-for-air-refueling-with/collection_1dc602ea-7989-5270-88b6-8eefe1d1337c.html

- Figure 6.18: NARA & DVIDS Public Domain Archive. (March 27, 1987). A boom operator directs the refueling boom from his station under the rear fuselage of a Utah Air National Guard KC-135 Stratotanker aircraft during an aerial refueling operation for 79th Tactical Fighter Squadron F-111E aircraft. [Image]. https://nara.getarchive.net/media/a-boom-operator-directs-the-refueling-boom-from-his-station-under-the-rear-41e96f

- Figure 6.19: United States Air Force. (September 25, 2015). KC-46A Air Refueling Operator Station Demonstrator visiting McConnell. [Image]. https://www.931arw.afrc.af.mil/News/Article-Display/Article/677598/kc-46a-air-refueling-operator-station-demonstrator-visiting-mcconnell/